Stockholm University

Master Thesis

one year

Degree Project in Geology 30 hp

Characterization of an REE-enriched black substance in fractured bedrock in the Ytterby Mine

Susanne Sjöberg

Stockholm 2014

Department of Geological Sciences
Stockholm University
SE-106 91 Stockholm
Sweden

ABSTRACT

A black substance seeping from fractured bedrock was observed in tunnels leading to the main shaft of the Ytterby mine on Resarö, Sweden. These are dry tunnels at shallow depth, +5 m above sea level and 29 m below ground surface, resulting from the reconstruction of the mine into a fuel deposit for the Swedish Armed Forces during the Cold War era. To keep the tunnels dry, the groundwater level is forced below its natural level which has resulted in oxidizing conditions in a previously anoxic environment. Thus, the deposition of this substance occurs in a dark and moist environment which has been exposed to changing redox conditions. Geochemical analysis and scanning electron microscopy (SEM) analyses show that this is a Mn- and Ca-bearing substance highly enriched in rare earth elements (REE) with concentrations being one to two orders of magnitude higher than the surrounding rocks. A minor phase that includes fluorine is also present. The organic content is low. Based on X-ray diffraction patterns, the mineral assemblage is suggested to primarily consist of poorly crystalline birnessite, vernadite and pyrolusite. The high calcium concentration of these manganese oxides-hydroxides implies a terrestrial origin. If they were marine then they would be enriched in magnesium. Scanning electron microscopy revealed three different manganese microstructures in the dried matter: dendritic or shrub-like, microspherolitic/botryoidal and wad-like spheres frequently covered by filaments of varying thickness. The observed internal lamination of one of these manganese oxides implies an iterative change in production.

Despite the well documented mineralogy of the Ytterby pegmatite, there are no manganese minerals reported from the area, but there are a number of minerals in which manganese likely constitutes a minor component. Previous results show that the REE occurrences in Ytterby are found in the quarry pegmatite and that they are highly localized within it. It is therefore suggested that manganese colloids, suspended in the local groundwater, work as metal traps and likely contribute to the mobility of the REEs. The black substance acts thus as a sink for these metals in the Ytterby mine area. The marine influence on the investigated substance is visible in the $\delta^{13}C$ signature, the carbon to nitrogen ratio and to a certain extent in the identified lipids. Even though the organic carbon content is low, the influence of microorganisms in the accumulation of manganese oxides appears to be important. Lipid biomarkers provide evidence of bacterial presence and also suggest that that this presence is caused by *in situ* production of light independent eubacteria. An electron paramagnetic resonance (EPR) analysis was done in an attempt to distinguish between abiotically and biotically precipitated manganese. Results imply a two, or multiple, component substance where at least one part has a biogenic signature.

TABLE OF CONTENTS

1. INTRODUCTION

This is a study of the geology, biogeochemistry and hydrochemistry associated of a jet black rare earth element (REE) enriched substance observed in the Ytterby mine tunnels. The mine is located on Resarö in the Stockholm archipelago. Historically mainly feldspar but also quartz was quarried in Ytterby. The quartz is thought to have been used in glass and iron works while the feldspar provided the rising porcelain industry with material (Nordenskjöld, 1904; Lööf, 1981). The mine is also well known for the discovery of yttrium (Y), scandium (Sc) and five rare earth elements in the periodic table: ytterbium (Yb), erbium (Er), terbium (Tb), holmium (Ho) and thulium (Tm) (Enghag, 1999). As the type locality of these rare earth elements, the Ytterby mine gave its name to yttrium, ytterbium, erbium and terbium. Furthermore, the mine has also contributed to the discovery of tantalum (Ta) and niobium (Nb), elements found in a mineral that has become known as yttrotantalite (Nordenskjöld, 1904). Examples of minerals containing rare earth elements are Gadolinite, Yttrotantalite, Fergusonite, Anderbergite and Xenotime. Many of these rare minerals contain the radioactive elements uranium and thorium (Nordenskjöld, 1910).

In 1933 the mine was closed down (Lööf, 1981) but in the beginning of the 1950s it was back in use. This was the Cold War era and the Ytterby mine, just like many other mines in Sweden, was used as a fuel deposit for the Swedish Armed Forces. Three different petroleum products have been stored in the mine-shaft over a period that totals about 35-40 years. During the 1950s and for approximately 25 years afterwards, jet fuel MC-77 was stored in the mine shaft and more recently two types of diesel (Lindgren & Lundmark, 2012); (J&W Energi och Miljö, Kemakta Konsult AB, 2001). The reconstruction of the mine into a fuel deposit involved blasting away rock to give room for 500-600 m tunnels linking the old mine with a newly constructed quay to the northeast of the quarry (Fig.3). The mine opening was sealed with a concrete vault covered by a 15 m thick layer of boulders left from the blasting. These boulders were then covered with a blast protective mantle (J&W Energi och Miljö, Kemakta Konsult AB, 2001). In 1995 the storage of petroleum products in the Ytterby mine was brought to an end and it was emptied from diesel and closed down. Since 1999, the mine has been managed by the Swedish Fortifications Agency (Fortifikationsverket) and the work involved with the decommissioning is still in progress (Lindgren & Lundmark, 2012).

The REE enriched black substance seeps from fractured bedrock in tunnels leading to the main shaft of the mine. This is a dry tunnel at shallow depth, +5 m above sea level and 29 m below the ground surface, resulting from the reconstruction of the mine in the 1950s. To keep the tunnels dry, the groundwater level is forced below its natural level which has resulted in oxidizing conditions in a previously anoxic environment. Thus, the deposition of this substance, which from hereon will be referred to as the Ytterby black substance (YBS), occurs in a dark and moist environment which has been exposed to changing redox conditions. A number of minor leakages from bedrock fractures are observed in the dry tunnels, but the investigated fracture represents the largest one. The YBS is observed in association with a lithified beige-coloured precipitate which forms 2-3 mm thick blankets covering the rocks which also coincide with locations of water leakage. However, the beige precipitate is observed without involvement of the YBS. The heavier the water leakage, the thicker the substance precipitate appears. The beige-coloured precipitate and to a certain extent also the underlying bedrock are slightly disintegrated at the investigated site. This is particularly the case for the relatively more mafic rock while the granitoid appears more resistant. Whether this is due to mechanical weathering or a result of chemical interaction with the YBS is not known. The YBS surface has a greyish-bluish metallic type of luster while the inner part is jet black. The smell resembles that of soil and occasionally there are bubbles in varying sizes developed on the surface (Fig.1).

No previous studies describing this substance have been found. However, in an article dated 1904, Nordenskjöld reported that the shallow lenses of feldspar in the Ytterby quarry had a darker colour relative to the feldspar located at a greater depth of the mine. Apparently this darkness disappeared during combustion. Since iron concentrations were insignificant he suggested that the observed darker colour was due to some sort of bituminous substance (Nordenskjöld, 1904). Also Sundius (1948) describes how small droplets of what he calls *bergbeck* were observed during the quarrying period. Moreover, in an article on carbonaceous matter in pegmatites, the Ytterby mine is mentioned as a locality where hardened carbonaceous matter enriched in uranium is observed in association with rare minerals such as yttrotantalite, gadolinte, fergusonite and xenotime (Chukanov et al., 2009). However, this observation is not made by the authors of the article but rather refers to Fersman (1931) which in turn refers to sources not found (Nordenskiöld, 1893).

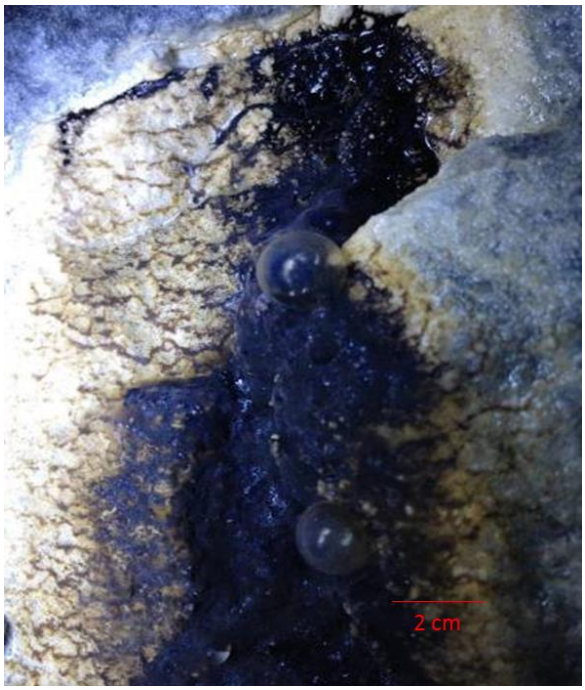

Fig.1: Gas bubbles on the surface of the Ytterby black substance (YBS)

Observations of organic matter as fracture fillings have been made at many locations and are common in Bergslagen and Uppland mines (see complete list of sources in Sandström et al., 2006). They occur both as hardened aggregates and as viscous substances that readily seep out of rock fractures in mine drifts, most probably because of the pressure from surrounding rocks (Sandström et al. 2009; Chukanov et al., 2009). Isotopic analyses imply that the organic material originates from Cambrium alum shales from the sea floor of the Baltic Proper and the Botnia Bay, squeezed in to fractures in the Precambrian bedrock (Sandström et al., 2006). Occasionally carbonaceous matter is uranium- and thorium- bearing and then named carburan and thucholite after its constituents: thorium, uranium, carbon, hydrogen and oxygen (Chukanov et al., 2009; Welin, 1966). In an environment, as REE enriched as Ytterby, it is plausible that a similar matter also contains REEs.

1.1. Aim

The aim of this study is to characterize a REE enriched black substance seeping from fractured bedrock in tunnels leading to the main shaft of the Ytterby mine and to understand if it originates from the surrounding bedrock, from the groundwater, from the mine shaft or from elsewhere. This will be achieved by biogeochemical, petrological and hydrochemical analyses of YBS samples, fractured bedrock and water from the mine shaft.

2. GEOLOGICAL SETTING

The Ytterby mine is located in the south-eastern part of Resarö in the Stockholm archipelago. Put into a larger regional-geological context, the rocks in this area belong to the Proterozoic Svecofennian domain which covers most of the northern and central part of Sweden, the western part of Finland and part of the Kola Peninsula in Russia. The rocks belonging to the Svecofennian domain are grouped as synorogenic, late orogenic, post orogenic or anorogenic according to the extent to which they are affected to the main folding stage of the Svecocarelian orogeny which occurred approximately 1850 m.y.ago. (Lindström et al., 2000). Isotopic age determination has dated the Ytterby pegmatite, i.e the mined rock type, to be approximately 1795 m.y.old (Welin, 1992) which suggests that it is late to post orogenic (Lindström et al., 2000).

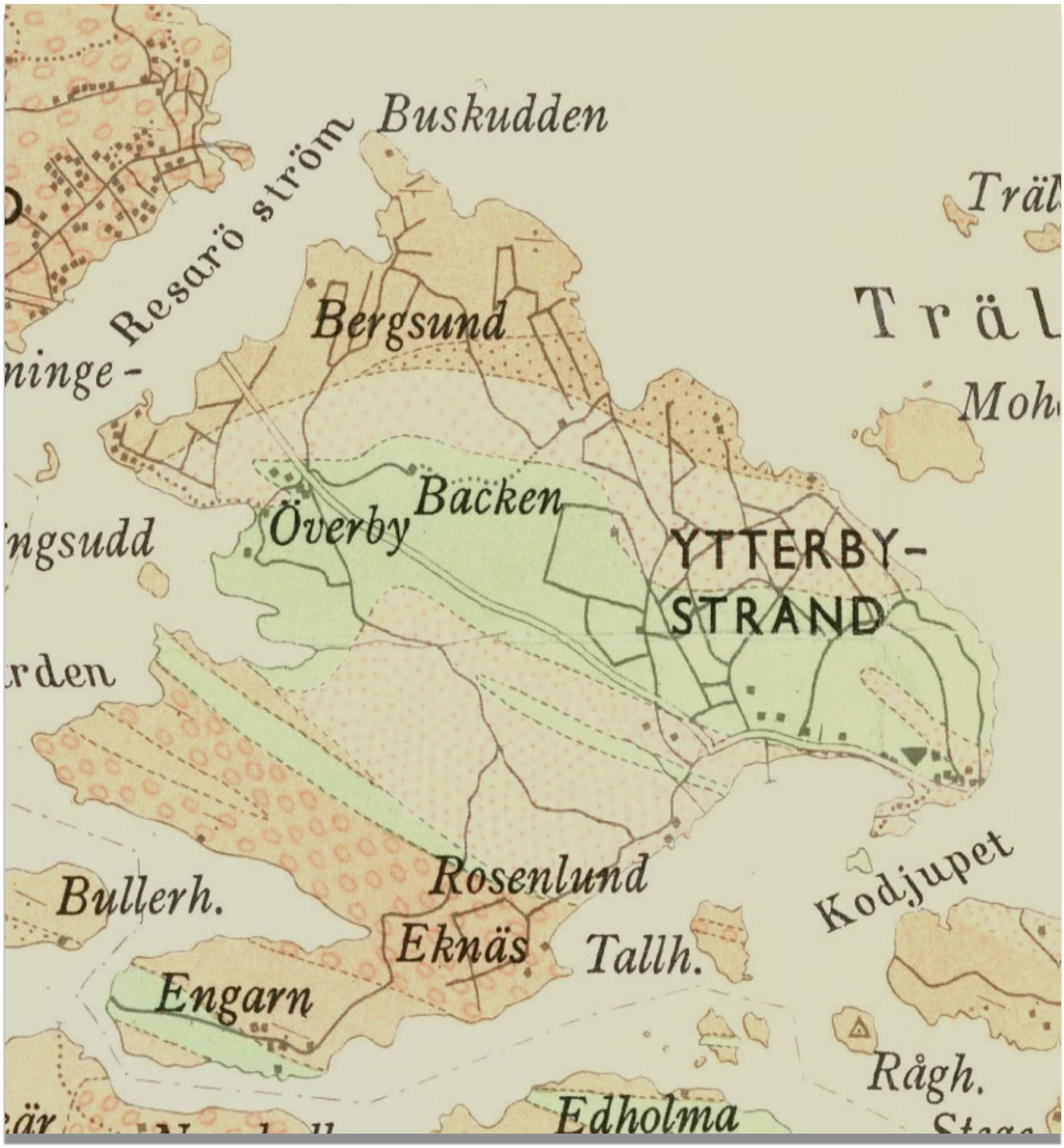

Figure 2: Geological map of the Resarö area (Sundius, 1948). The Ytterby pegmatite is situated in the south-eastern corner of the map and is marked with an upside down triangle. The green band which extends across the whole island, WNW-ESE, is described by Sundius (1948), as gabbroic greenstone. Greenstone is a generic term and in this case the interpretation is that it refers to mafic rocks with varying chemical composition and metamorphic grade, which are given a greenish colour by their mineral content. The surrounding rocks are all described as various types of gneiss-granite.

The pegmatite, i.e. the mined rock, is a planar structure trending NNE-SSW and according to Nordenskjöld (1904), the length and width is approximately 15 respectively 12 m at the surface and decreases with depth. The pegmatite dips at 60 degrees west and borders two different rock types; amphibolites, i.e part of the greenstone mentioned above, in the NW hanging wall and gneiss in the SE (Nordenskjöld, 1904).

The most widely used classification system of pegmatites today is that of Černý (1991); (revised by Černý & Ercit, 2005). This system classifies pegmatites primarily by their emplacement depth. They are then divided into families, subclasses, types and subtypes based on geochemical features, mineral assemblages and structural features that reflect the pressure and temperature conditions during solidification. The rare element class which reflects low temperature and pressure is subdivided into two main pegmatite families: the LCT-family which is enriched in lithium (Li), cesium (Ce) and tantalum (Ta) and the NYF-family which is enriched in niobium (Nb), yttrium (Y) and fluorine (F) (Černý & Ercit, 2005; Simmons & Webber, 2008). The Ytterby pegmatite belongs to the NYF-family (Lindström et al., 2000). Another characteristic of the NYF-pegmatites is that they are enriched in heavy rare earth elements (HREE), Be, Ti, Sc and Zr (London, 2008). There is also a predominance of niobium (Nb) over tantalum (Ta) and they are depleted in phoshorus (P) (London, 2008). The NYF-family is then subdivided into subclasses distinguished by their specific rare-element association and further into types and subtypes by rare-element mineralogy (Černý & Ercit, 2005; London, 2008). According to Černý (1992), based on the work of Nordenskjöld (1910), the Ytterby pegmatite is associated with the rare earth element type and the gadolinite subtype.

The pegmatite body mainly consists of quartz, red microcline (K-feldspar), grey-white oligoclase (Na-Ca feldspar) and biotite (dark mica) but there is also a considerable number of other minerals (Lindqvist, 1989). For a full listing see appendix 1.

3. HYDROLOGICAL DATA

The mean hydraulic conductivity in the rocks around the mine was calculated in a previous study (J&W Energi och Miljö, Kemakta Konsult AB, 2001) and was estimated to be $3*10^{-8}$ m/s. The same study measured the mean daily inflow of water to the shaft to be $9m^3$/day. This inflow is due to groundwater formation from infiltrating precipitation in the proximity of the mine. The groundwater divide in the area is situated on high ground north of the mine shaft and thus limits the area of inflow upstream. The inflow area is calculated by the same study to be 100 000 m^2 (J&W Energi och Miljö, Kemakta Konsult AB, 2001). The groundwater levels in and around the mine shaft correspond to artificial levels. In this area the groundwater level is lowered below its natural level and these artificial levels have been kept relatively constant since the mine became a fuel deposit up to the present. During the mining period, the inflow of groundwater to the shaft was very sparse and during the last years of quarrying it only took a barrel to keep the mine dry and no pumping arrangement was needed (Sundius, 1948). This implies that the mined rock was relatively impermeable.

4. MATERIALS AND METHODS

4.1. Sampling and sampling sites

The Ytterby mine tunnels link the old shaft with the more recently constructed quay located approximately 300-400 m northeast of the quarry (Fig.3). The YBS seeps from fractured bedrock in a dry tunnel at shallow depth, +5 m above sea level and 29 m below ground surface.

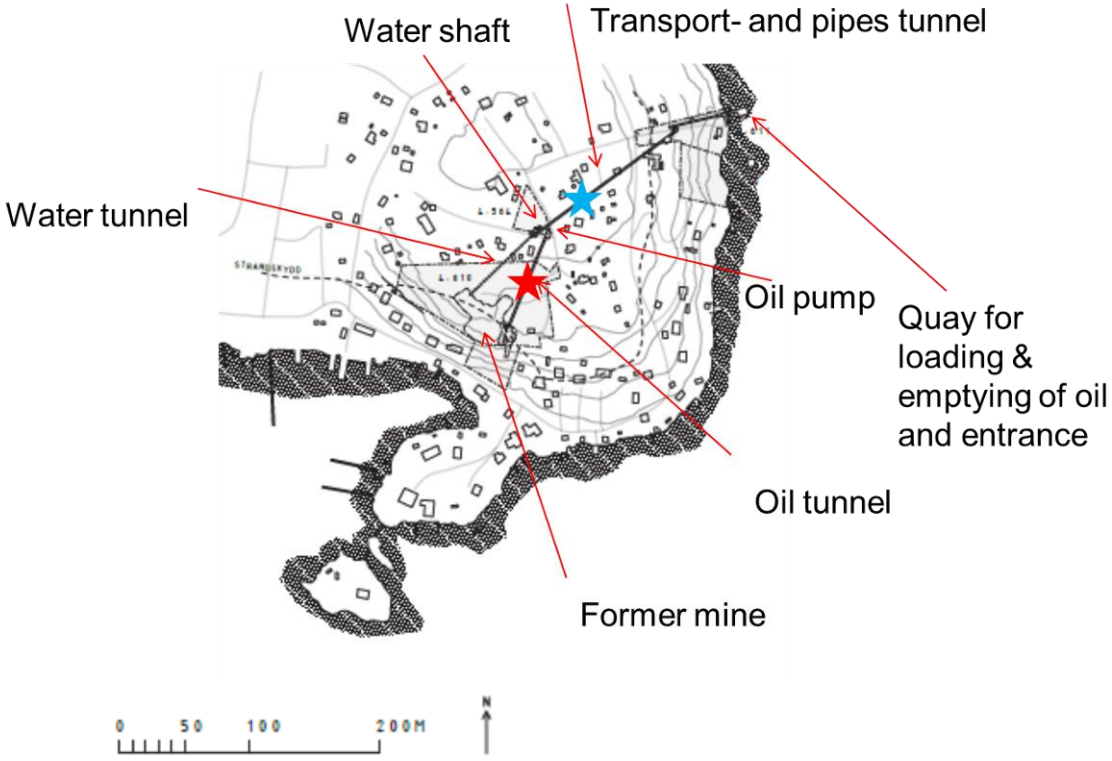

Figure 3: Base map of integrated underground structures. As the mine is inclined towards the NW, the bold continuous line (former mine) describes the propagation of the mine projected on ground level. Modified after The Swedish Fortifications Agency (2012).

★ Ytterby black substance (YBS) seeping from fractured bedrock in dry tunnel

★ Nodular outgrowths in previously water-filled tunnel.

4:610 – Quarry
4:611 – Quay & entrance to the underground space

Ytterby black substance (YBS)

The YBS was collected at two different occasions; the first batch was collected in pre-combusted glass bottles and immediately placed in the freezer while the second batch was collected in a glass bottle and placed in the fridge. The second batch was then divided in two: i) rinsed in 420 ml ultrapure water using a nitrile cellulose membrane filter, 0.2 µm ø 47 mm, and vacuumed. Thereafter dried at 60°C for 48h; ii) not rinsed, but dried in 60°C for 48h.

Fig.4: Ytterby black substance (YBS) seeping from fractured bedrock in tunnels leading to the main shaft of the Ytterby mine.

Rocks

A first set of rock samples was collected to obtain information about different rock compositions in the proximity of the seeping fracture. A second set of samples was collected at a later stage of the study in order to obtain additional information about REE mobility in the two rock types in immediate contact with the fracture.

Groundwater

Groundwater samples were collected from five locations*;* i) the mine tunnel, dripping from fractured bedrock where the major leaching occurs,14-YB-W01, ii) sample separated from the YBS through centrifugation, 14-YB-W02, iii) the mine shaft, at 1.3m depth, 14-YB-W03, iv) the mine shaft, at 0.5m depth, 14-YB-04, iv) the water shaft, at 1.0m, depth 14-YB-05). The sampling procedure was adjusted to the circumstances of each sample location. The water feeding the fracture was collected directly from dripping water while water from the mine- and water shaft was collected in a plastic tube before it was poured into the sample bottles. To minimize the risk for contamination all bottles were pre-rinsed with sample water.

4.2. Wetness and Loss On Ignition (LOI)

The loss on ignition method was used to estimate the wetness, organic matter and carbonate content in the YBS and was calculated as follows: The weight of the empty crucible was recorded, followed by the weight of the crucible plus moist sample, i.e. sample directly from the sampling site. Then the sample was dried at 80°C for 17 hours to constant weight. The wetness was noted and the sample was left at 450°C for 8 hours in the muffle furnace. The crucible was removed from the furnace and re-weighed. Then the weight loss of the dry sample at 450°C was noted. Additional results for wetness were recorded by using another subsample which was dried in a fume cupboard before drying it in 80°C for one week. The wetness was noted as the weight difference between the first and second drying occasions. Results for loss on ignition at 1050°C was provided by Activation Laboratories, Canada.

4.3. Chemical analyses

4.3.1. Ytterby black substance and rocks

In total 16 rock samples were grinded into fine powders in a Retch Vibratory Disc Mill, type RS200 at the Stockholm University. All samples were milled for 30 seconds at 1500 RPM. About 2 mg of each rock sample and the two samples of dried YBS (see section 4.1) were sent to an external laboratory, Activation Laboratories Ltd, Canada for analyses of major- and trace elements. The package ordered is named WRA (Whole Rock Analysis) + trace 4lithoresearch (Actlab website, 2014). Samples were diluted and analyzed by Perkin Elmer Sciex ELAN 6000, 6100 or 9000 ICP/MS. A combination of lithium metaborate/tetraborate fusion ICP whole rock and trace element ICP/MS analyses was made on each sample.

Results for REEs are presented separately for the reason that Ytterby is the type locality for these elements. To facilitate comparisons with other data, the REE concentrations of the Ytterby samples are normalized to standard reference values of chondrites (Boynton, 1984).

4.3.2. Groundwater

Inductively Coupled Plasma Optical Emission Spectrometry (ICP-OES)

ICP-OES is a technique that is used for determining what elements are present in a sample and at what concentrations. Elements screened for in this analysis are marked blue in the periodic table shown in Fig.5.

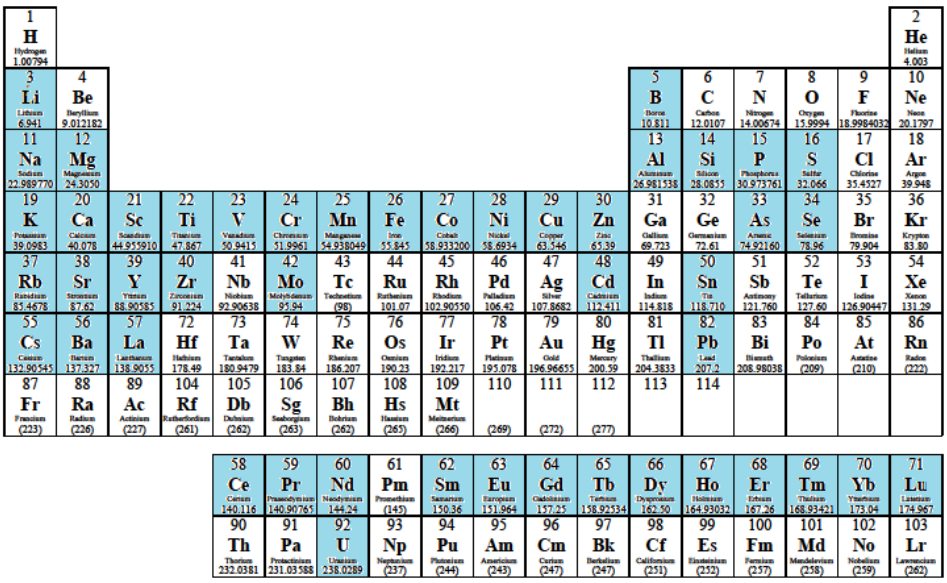

Figure 5: Elements screened for in the ICP-OES are marked blue in the periodic table.

The samples were prepared for ICP-OES analysis by filtration (0.45 µm) into test tubes which were pre-rinsed with sample water. All water samples except for the 14-YB-W5 were filtered directly from the sampling tubes into ICP test tubes. Sample 14-YB-W5, i.e. water separated from the YBS, was obtained by centrifugation of the YBS at 1500 RPM at 4ºC for five minutes

and thereafter filtrated into ICP test tubes. The instrument was calibrated using standard solutions and a blank. Each sample was injected into the instrument as a stream of liquid and then converted to aerosols, i.e. particles suspended in gas. These aerosols were transported to the plasma where the solvent was removed from the samples and the resultant dry sample particles were broken down into a gas of sample molecules. This sample gas was dissociated into free atoms and excited and/or ionized by the plasma. The excited atoms and ions emitted their characteristic radiation which was turned into electronic signals that were converted into concentration information. (Boss & Fredeen, 1997).

4.4. Preparation of thin sections and microscopy

4.4.1. Preparation of thin sections

Thin sections of both rinsed and unrinsed dried YBS were prepared in three different thicknesses at the Department of Geological Sciences at Stockholm University. In addition to these thin sections, one puck each for the rinsed and unrinsed dried YBS were made to observe the whole grains. In total 17 rock samples were prepared for becoming thin sections; 11 of these rock blocks were sent to Vancouver Petrographics Ltd. for preparation of polished thin sections 30 µm. The remaining 6 samples, which were considered to need special care, were prepared into thin sections at Stockholm University. As the study proceeded, it became clear that only two of the rock thin sections prepared were of direct importance and since time did not allow for analysis of them all, focus is on these two.

4.4.2. Microscopy

Microscopy studies were carried out partly to obtain an optical image of the YBS and adjacent rock structures and partly to understand their superficial composition. These studies were done using a standard polarizing microscope and a Quanta environmental scanning electron microscope (ESEM) with a field emission gun (FEG 650). An energy dispersive X-ray spectrometer (EDS) was used with the SEM for compositional information. All analyses have been made at the Department of Geological Sciences at Stockholm University.

Information obtained from SEM analyses are primarily a function of the type of detector used but also the preparation of the sample. In this work I have chosen to study the dried YBS in polished thin sections and as a powder sprinkled on stubs covered by copper tape. The copper tape was chosen to obtain information about carbon concentrations in the sample. Thin sections were made in three different thicknesses to make sure that even the smallest particles were visible. In addition to this, all analyses were made on both rinsed and unrinsed powder. Two different detectors were used during the SEM analyses: a large-field detector (LFD) providing topographic images and a circular backscatter detector (CBS) primarily providing information about elemental composition through image contrast. The heavier the element, the brighter the image contrast (Materials Evaluation and Engineering, Inc, 2014). Thus the SEM analyses have not only provided information on the composition and structure of the YBS but also served as an indicator of which areas to look closer into and make further investigations.

4.5. X-ray powder diffraction analysis (XRD)

Analytical technique
The finely mortled powder sample was prepared by back loading the PANalytical sample holder, with a 27 mm diameter area. The sample was measured with a PANalytical X'Pert-Pro diffractometer, using CuKa radiation. The XRD measurements were carried out using a step size of 0.010° 2theta from 5° - 70° 2theta at 40mA and 45kV with a spinning sample holder. The diffraction pattern was smoothed and the peaks were determined using PANalytical HighScore software.

Identification of minerals

A manual search-match approach was used for the recognition of mineral phases in the dried YBS. The sample diffraction pattern was primarily compared to diffraction patterns of known minerals in the American Mineralogist crystal structure database (American Mineralogist website, 2014) and to d-spacing values in a search manual for X-ray identification (Brindley and Brown, 1980).The mineralogy and locality database (Mindat website, 2014; Webmineral website, 2014) as well as previously published articles on x-ray diffraction patterns were also used as complementary sources of information. Satisfactory criteria for identification of phases is that at least three peak positions and adherent relative intensities fit. To note is that reference mineralogy analyses display high variability and thus make comparisons difficult.

4.6. Infrared spectrum (IR-spectrum)

Infrared spectroscopy provide information about chemical bonds in compounds and in particular so in organic systems. With this type of analysis it may for example be possible to see if bonds show an aliphatic or aromatic character or if a metal is linked to an acid. The infrared spectrum was achieved using a Perkin Elmer Fourier infrared Spectrum Two (FT-IR). The analysis was done on a dry sample (drying procedure is described in section 4.1).

4.7. $\delta^{13}C$, $\delta^{15}N$ and $\delta^{34}S$ isotopic signatures

Analyses of isotopic compositions were made using a Finnigan MAT Delta V mass spectrometer at the Department of Geosciences at the Stockholm University. The mortared sample powder (about 1-2 mg) was placed into a tin capsule and thereafter combusted using a Carlo Erba NC2500 elemental analyzer, connected via a split interface to reduce the gas volume, to the mass spectrometer. Concentrations of total carbon (TC), total organic carbon (TOC) and total nitrogen (TN) were determined simultaneously and carbon analyses were performed with and without acid to determine if the sample contained carbonates or not. The reproducibility of these measurements was calculated to be better than $0.15^{0}/_{00}$ for both $\delta^{13}C$ and $\delta^{15}N$ and the relative error was <1% for both measurements. Concentrations of sulphur (S) were determined separately and the reproducibility was calculated to be better than $0.2\ ^{0}/_{00.}$ To understand whether this was a possibly heterogeneous sample, the analysis was run twice using different portions of the sample. Results are presented as per-mil deviation from a standard (Pee Dee Belemnite, PDB, for C, AIR for N and Cañon Diablo Troilite for S**)** and denoted $\delta^{13}C$, $\delta^{15}N$ and $\delta^{34}S$ (equation 1, 2 and 3).

$$\delta^{13}C = \frac{^{13}C/^{12}C\ Sample}{^{13}C/^{12}C\ Standard} * 1000 \qquad \textit{(Equation 1)}$$

$$\delta^{15}N = \frac{^{15}N/^{14}N\ Sample}{^{15}N/^{14}N\ Standard} * 1000 \qquad \textit{(Equation 2)}$$

$$\delta^{34}S = \frac{^{34}S/^{32}S\ Sample}{^{34}S/^{32}S\ Standard} * 1000 \qquad \textit{(Equation 3)}$$

4.8. Lipid analysis

A lipid analysis was made partly to understand if there is microbial presence in the YBS and partly to obtain information about the origins of the organic components. This was accomplished by extraction of lipids from the frozen material, analysis using the GCMS and by identification of molecules or fragmented molecules associated with certain biological specimens. For the lipid extraction, three solvents having different polarity were used and duplicates of each fraction were made to ensure repetitive series (Table 1). The lipid extraction procedure is shown in detail in the text below. Identification of the lipids present in each fraction was made by comparing each peak to reference material on lipid spectra detailing molecular fragmentation. In addition, the similarity search offered by the GCMS software was consulted. To help identify the most complex lipid signals, a $\delta^{13}C$ analysis was made on the extracted lipids.

	Sample id.	Duplicate	Solvents arranged in order of increasing polarity
Fraction 1	**A:1**	**B:1**	**Hexane**
Fraction 2	**A:2**	**B:2**	**Hexane/DCM (1:1)**
Fraction 3	**A:3**	**B:3**	**DCM/MeOH (1:1)**

Table 1: Lipid analysis sample setup.

Total lipid extraction using ultrasonic extraction and methylation

Extraction procedure
The frozen sample material, approximately 109 g, was passed through a 500µm strainer and then equally distributed into four pre-combusted glass vials. The sample was then submersed in a mixture of two organic solvents: DCM:MeOH (2:1) (dichloromethane and methanol). These solvents have different polarity; DCM being less polar than MeOH. Thereafter the sample was placed into an ultrasonic bath for 10 minutes and subsequently centrifuged at 1500 RPM at 4ºC for five minutes. The supernatant was removed and collected in four glass vials. This procedure was repeated four more times and the supernatant from each extraction round was combined and kept. The combined extract was placed in a vacuum centrifuge to remove the solvent and to leave the lipid residue.

Separating total lipid extract into fractions of different polarity
Two pipette columns were washed with hexane and plugged at the bottom with pre-extracted cotton. The columns were then loaded to 2/3 of their volume with 5% deactivated silica gel.
The extract was collected and distributed into the three different fractions having different polarities described in table 1. Four column volumes were used for each fraction, i.e. the pipette column volume is 1 ml. Each fraction was dried using a sand bath fitted to a nitrogen gas. Hexane was added to Fraction 1 and Fraction 2 and analysed using GCMS. Fraction 3 was derivatized via methylation and sylilation.

Methylation (trans esterification) of Fraction 3
Methylation was made to prolong retention time and to make the sample less reactive. $NaCO_3$ (base) is used to neutralize the solution (acid) and also functions to remove water. The lipid extract was re-dissolved in 0.2 ml DCM. Thereafter 1.50 ml of MeOH and 0.30 ml of a diluted HCl solution was added. The tubes, i.e. sample A:3 and B:3, were vortexed and incubated at 70°C four hours. Approximately 0.5 mg of pre-combusted Na_2CO_3 was added to absorb the water. Then 1 ml of hexane and 1 ml of back extracted water were added to the samples for extraction of Fatty Acids Methyl Esters (FAME). Tubes were vortexed then the hexane separates as the top layer which can be pipetted off. The samples were dried using sand bath and nitrogen gas. Finally 1 ml of hexane was added to the residue and vortexed to ensure that all residue was dissolved.

Derivatization by Sylilation of Fraction 3

The process of silylation replaces various kinds of groups (e.g. alcohols, carboxylic acids, phosphates etc.) with a trimethylsilyl group ($SiMe_3$). The lipid fractions were transferred to GC vials used for analysis. Then 20 µl of pyridine was added and then 20 µl of N,O-Bis(trimethylsilyl)trifluoroacetamide (BSTFA) to the dried fractions in the vials. BSTFA was in the oven for 20 minutes. After the samples had cooled to room temperature hexane was added.

GCMS (Gas Chromatography Mass Spectrometry)

GCMS analyses were made using is a Shimadzu GCMS QP2010 Ultra fitted with an AOC-20i auto injector. Analyses were made at the Department of Geosciences at the Stockholm University. The liquid samples were inserted into the GCMS injector which vaporized and mixed them with the carrier gas at the top of the column. This gas mixture then moved through the column until the outlet where it passed through a detector which gave the retention time. Spectra were constructed for peaks being a minimum of three times the baseline to ensure that the peaks were really peaks and not only disturbances.

4.9. Electron paramagnetic resonance (EPR) spectroscopy

This last of methods was added as a complementary analysis at a late stage of the work. At this point, it was determined that the YBS consists of manganese oxides-hydroxides and that there are distinct signs of bacterial presence. EPR is a technique than can be used to obtain structural information about the manganese complexes in a sample and more specifically it can be used to distinguish between biotically and abiotically precipitated compounds. The sample was measured with an X-Band Bruker E500 EPR (Bruker Bio-Spin GmbH, Rheinstetten, Germany) with a 4103 TM resonator at room temperature. Measurements were done using microwave power of 10 mW or 1mW for comparisons, 2 G modulation amplitude, 5.12 ms time constant, 20 s sweep time (three added sweeps). Spectra were fitted by superpositions of Gaussian lines and values for the best fitted lines were determined. Analyses were done the Department of Medicine and Health Sciences at Linköping University.

5. RESULTS

5.1. Wetness and loss on ignition (LOI)

The wetness of the substance was determined to 45 wt.% when pre-dried in a fume cupboard and to 80% when expressed as weight percent of wet sample. Results show a loss on ignition of 14 and 27 wt.% at 450°C and 1050°C respectively (expressed as weight percent of the dry substance). The weight loss at 450°C is mainly organic carbon oxidizing to CO_2 while the loss at 1050°C may include carbonates, volatile salts and structural water (Heiri et al., 2001). Wetness and loss on ignition data are listed in Table 2.

Water loss 80°C, one week, (wt.% of pre-dried sample).	**Water loss 80°C 17H (wt.% of wet sample)**	**LOI 450° 8h (wt.% of dry sample)**	**LOI 1050°C (wt.% of dry sample)**
45*	79.8**	14.5**	**27.5*** **

Table 2: Wetness and loss on ignition of the YBS.

**Man-Technology-Environment Research Centre (MTM), Örebro University*
***Department of Geological Sciences, Stockholm University*
**** Activation Laboratories, Canada*

5.2. Chemical analyses

5.2.1. Major elements of the Ytterby black substance

Two samples of the substance were analysed for major- and trace elements; one which was rinsed in ultrapure water (14-YB-Rinsed) and one which was not (14-YB-Unrinsed) (see section 4.1 for details). Results for major elements vary quite substantially between these samples and the most probable reason is that larger crystal grains were separated from the bulk material during the rinsing procedure. Results show lower wt.% values for all major elements except MnO in the rinsed sample compared to the unrinsed sample. My interpretation is that the rinsed sample gives the preferred information about the substance bulk material while the difference between the samples gives information about the constituents of the larger mineral grains. The major constituents of the black phase are therefore manganese (MnO 58.47 wt.%) and calcium (CaO 8.6 wt.%). If calculated as a proportion of the dry substance, i.e. substance remaining after LOI at 1050°C, the corresponding values for Mn and Ca are 84.43 wt.% and 12.42 wt.% respectively. Data of major elements in substance samples are listed in Table 3.

Major elements	Detection Limit	Analysis Method	14-YB-Rinsed (wt%)	14-YB-Unrinsed (wt%)
Na_2O	0,01	FUS-ICP	0,06	0,82
K_2O	0,01	FUS-ICP	0,1	0,53
MgO	0,01	FUS-ICP	0,62	0,77
CaO	0,01	FUS-ICP	8,6	15,07
Fe_2O_3	0,01	FUS-ICP	0,13	1,23
Al_2O_3	0,01	FUS-ICP	0,25	3,24
MnO*	0,001	FUS-ICP	58,47	36,55
TiO_2	0,001	FUS-ICP	0,012	0,125
P_20_5	0,01	FUS-ICP	0,07	0,08
SiO_2	0,01	FUS-ICP	0,94	12,31
LOI**			27,84	27,26
TOTAL			97,09	97,98

Table.3: Major elements of rinsed and unrinsed YBS samples.

**Manganese is assumed to be divalent in these results*
***Loss on ignition (LOI, determined at 1050º C*

5.2.2. REEs in the Ytterby black substance and adjacent rocks

The bedrock in this area mainly consist of granitic and mafic rocks of varying chemical composition and metamorphic grade. Two different rock types are in direct contact with the fracture: a metagranite and a relatively more mafic rock. Only data that appear to be relevant for this study are presented in this section. For more extended data the reader should consult appendix 2. The REE content of eight rock samples were compared to the REE content of the YBS in order to see if they have any common features. Rock descriptions are presented in Table 4.

Sample id	Location	Description
14-YB-R01	~60m from cut-off at the oil pump.* Rigth side of the tunnel, bordering the seeping fracture on its left side.	Metagranite
14-YB-R02-A	~60m from cut-off at the oil pump. Right side of the mine tunnel, 5 cm from seeping fracture on its left side. Sample part closest to the surface; the black coloured part.	Metagranite. Sample is divided in two; a black coloured part closest to the sample surface and a reddish more felsic part further away from the surface.
14-YB-R02-B	~60m from cut-off at the oil pump. Right side of the mine tunnel, 5 cm from seeping fracture on its left side. Sample part furthest away from the surface; the reddish more felsic part.	Metagranite. Sample is divided in two; a black coloured part closest to the sample surface and a reddish more felsic part further away from the surface.
14-YB-R03-A	~60m from cut-off at the oil pump. Right side of the mine tunnel, bordering the seeping fracture on its right side. Sample part closest to the surface.	More mafic relative to sample R01 and R02. Sample is divided in two; one part as close as possible to the edge which is covere in a beige precipitate and one part further away.
14-YB-R03-B	~60m from cut-off at the oil pump. Right side of the mine tunnel, bordering the seeping fracture on its right side. Sample part furthest away from the surface.	More mafic relative to sample R01 and R02. Sample R03 is divided in two; one part as close as possible to the edge which has some sort of beige precipitate on it and one part further away.
14-YB-R04	~57m from cut-off at the oil pump. Right side of the mine tunnel, ~3m from seeping fracture on its right side.	Pegmatitic granite
14-YB-R06	~75m from cut-off at the oil pump. Right side of the mine tunnel, ~15m from seeping fracture on its left side.	Border between two rock types, possibly a metagranite and an amphibolite.
14-YB-R09	~80m from cut-off at the oil pump. Sample taken in the mine roof.	Heavily altered amphibolite.
14-YB-R12	~15m from the western wall in the quarry, along the major vertical fault. of the western wall in the quarry 59° 25' 35'' N, 18° 21' 11'' E	
14-YB-R15	SW of major vertical fault in the quarry. 59° 25' 34'' N, 18° 21' 12'' E	Dark brick-red to black rock, no shine.

Table 4: Desccriptions of rock samples.

**Descriptions of sample locations start out from the oil pump marked in Fig.2 and are mapped from SW to NE.*

The absolute REE concentrations were normalised using average chondrite abundances according to Boynton (1984). Patterns are shown as log-normalised values versus increasing atomic numbers of the REEs (Fig.6). The patterns of the substance are almost identical to those of the felsic rock immediately to the left of the seeping fracture (14-YB-01 and 14-YB-R02); enrichment in LREEs and pronounced negative Eu-anomalies. The relatively more mafic rock bordering the fracture on its right side (14-YB-R03) also show enrichment in LREEs but rather a vague positive EU-anomaly. This is a pattern which is shared by the other mafic rock situated further away from the fracture (14-YB-R06) while the heavily altered amphibolite (14-YB-R09) only shows a weak negative Eu-anomaly. The tunnel pegmatite (14-YB-R04) is in contrast to all other samples enriched in HREEs relative to LREEs. These results fit well the description of the quarried Ytterby pegmatite which is suggested to belong to a family of pegmatites which partly is characterised by its enrichment in HREEs (London, 2008; Lindström et al., 2000). However, the most striking feature is the significantly higher REE concentrations in the substance compared to the rocks. Substance concentrations are one to two orders of magnitude higher than the rock values. Substance values were also compared to statistics of REE concentrations in European and Swedish samples of top soil, subsoil and stream sediments (Sadegi et al, 2013). The Ytterby substance values are higher than all maximum values reported in this study. Note that the surface sample of the metagranite (14-YB-R02a) is slightly enriched in all elements compared to the deeper part of the sample (14-YB-R02b) (Fig.6).

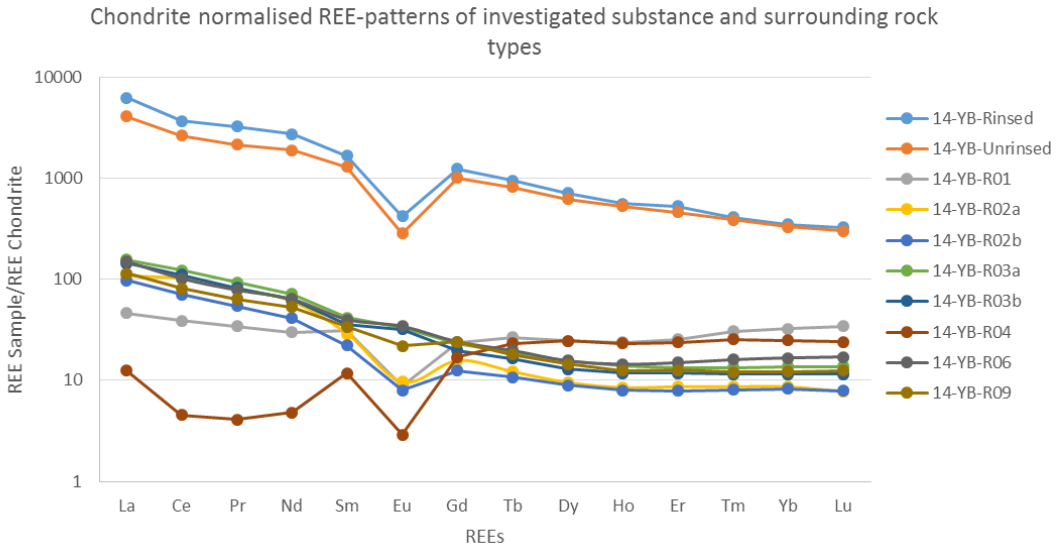

Fig 6: Chondrite normalized REE-patterns of investigated substance in Ytterby mine tunnels and of surrounding rock types. Patterns are shown as log-normalised values versus increasing atomic numbers of the REEs. Chondrite values from Boynton (1984).

In addition to the above presented chemical results, a complementary set of rock samples was collected in order to understand if the rock shows depletion or enrichment of REEs with distance to the seeping fracture. The 14-YB-R100 to 14-YB-R101 series correspond the metagranitic rock while the 14-YB-R200 and 14-YB-R202 series is the mafic equivalence. In Fig.7, chondrite normalized patterns for these samples are displayed and in Fig.8 and 9, elemental concentrations of the fresh and presumably altered rocks adjacent to the fracture are compared. This was done using the isocon method (Grant, 1986) assuming immobility of Al_2O_3. Al_2O_3 was used since concentrations in the two samples are almost identical and because it is likely to be immobile. Al_2O_3 defines a straight line through the origin of the diagram, the isocon. All elements or oxides plotting above the line are depleted in the altered rock compared to the fresh rock and elements below the line are enriched.

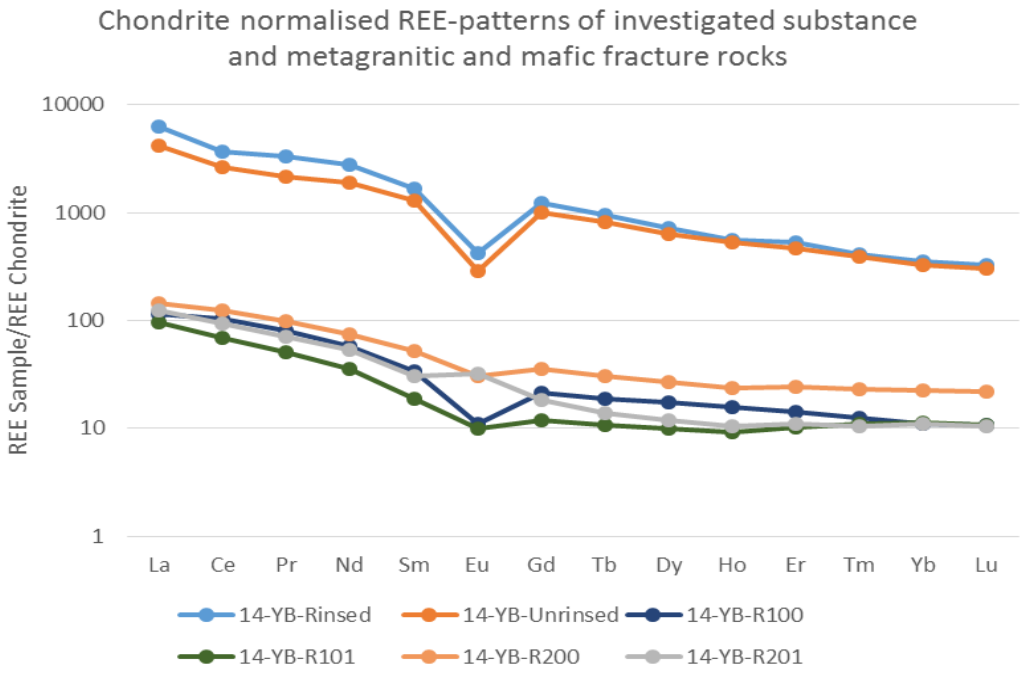

Fig 7: Chondrite normalized REE-patterns of investigated substance in Ytterby mine tunnels and of metagranitic and mafic fracture rock. The 14-YB-R100 to 14-YB-R101 series correspond to metagranite samles with increasing distance from the fracture while the 14-YB-R200 and 14-YB-R202 series is the mafic equivalence. Patterns are shown as log-normalised values versus increasing atomic numbers of the REEs. Chondrite values from Boynton (1984). Notably the pronounced EU-anomaly seen in the substance REE-pattern is also seen in the metagranite sample immediately adjacent to the fracture (14-YB-R100) but much less so in the sample taken at a greater distance from the fracture (14-YB-R101). This is also valid for the mafic rock samples where the sample closest to the fracture (14-YB-R200) shows a similar pattern to the metagranite while in contrast the sample further away shows a positive EU-anomaly. This likely relates to loss or gain of plagioclase

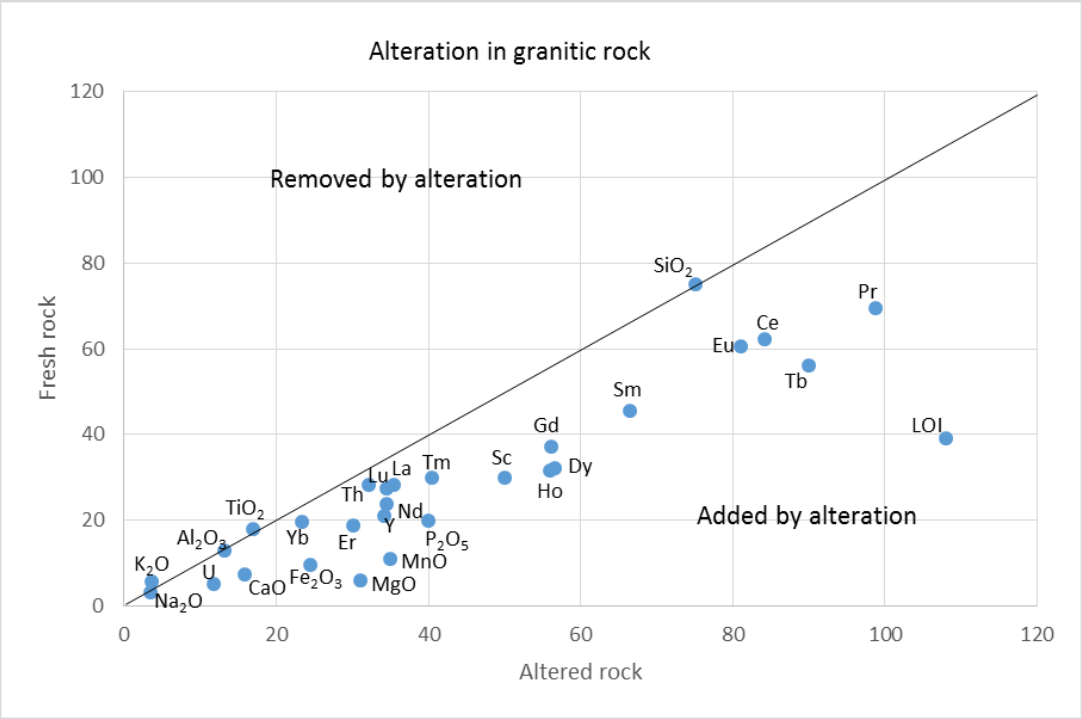

Fig.8: Isocon diagram (after Grant 1986) of elemental concentrations in fresh and altered granitic rock for elements of interest. The concentration of each element is multiplied by an arbitrary factor, here 1000, 100, 50,10, 1 or 0.1. This is done to make the elements fit on the same plot and the values represent relative magnitudes of the components not their absolute magnitude. All elements or oxides plotting above the line are depleted in the altered rock compared to the fresh rock and elements below the line are enriched. To construct the isocon diagram Al_2O_3 has been considered immobile. The altered rock is clearly enriched in all REEs, yttrium (Y), scandium (Sc), uranium (U) and thorium (Th). Note that it is also enriched in MnO, CaO and MgO.

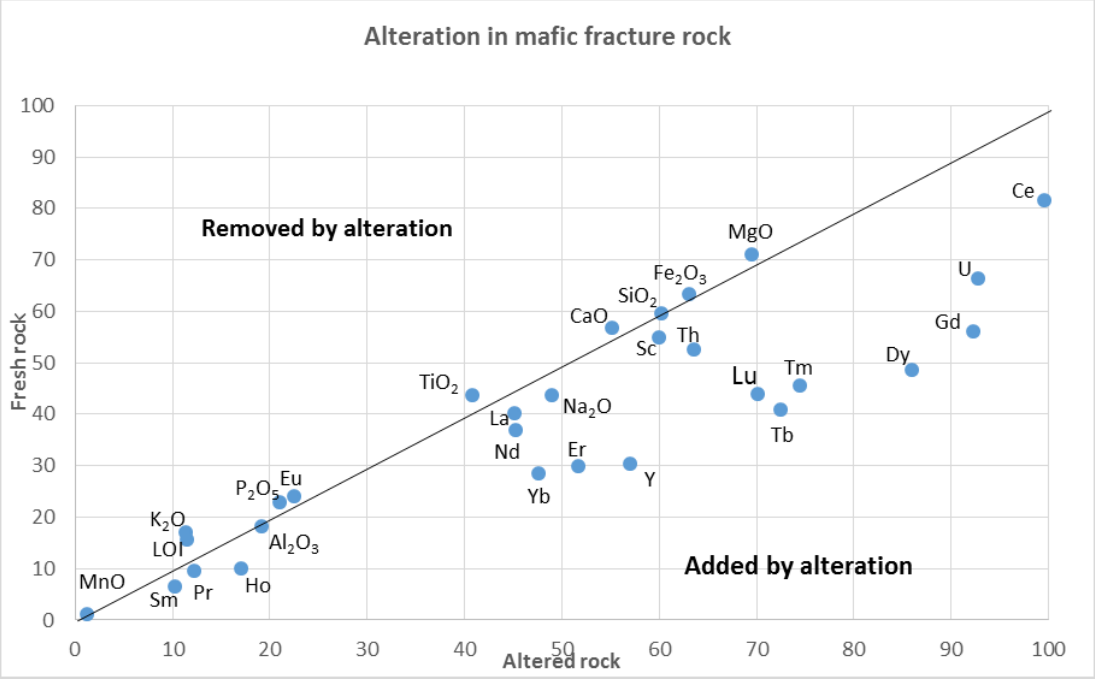

Fig.9: Isocon diagram (after Grant 1986) of elemental concentrations in fresh and altered mafic rock for elements of interest. The concentration of each element is multiplied by an arbitrary factor, here 1000, 100, 50,10, 1 or 0.1. This is done to make the elements fit on the same plot and the values represent relative magnitudes of the components not their absolute magnitude. All elements or oxides plotting above the line are depleted in the altered rock compared to the fresh rock and elements below the line are enriched. To construct the isocon diagram Al_2O_3 has been considered immobile. The altered rock is enriched in all REEs except for europium (Eu).

5.2.3. Groundwater

Only data that appear to be relevant for this study are presented in this section. For more extended data the reader should consult appendix 3. Ytterby groundwater data for Na, Ca, Mn, Fe and Mg are compared to reference values for the Uppland region. These reference values are given for water sources in bedrock environments as well as in soil environments (Fig.10). All water samples in this study have near neutral or slightly alkaline pH.

Mn concentrations in fracture water (14-YB-W01) are high compared to the other Ytterby samples. Contents of Mn in groundwater are more connected to prevailing redox conditions than to pH and the soluble form of manganese, Mn^{2+}, exists in oxygen poor environments whereas Mn^{3+} and Mn^{4+} are most common in well oxygenated environments (Bydén, 2003).

Seven REEs and Y are present in the sampled groundwater: lanthanum (La), neodymium (Nd), samarium (Sm), Terbium (Tb), dysprosium (Dy), erbium (Er) and ytterbium (Yb). The ΣREE content range from 13.3 to 30.1 µg/L. These values can be compared to median values of 6.7 µg/L and 52 µg/L reported for overburden groundwaters in Forsmark and Simpevarp, Eastern Sweden (Rönnback et al., 2008). Apparantly these values are considered high while the same study concluded that the REE content in bedrock groundwaters in the same localities were low (no values reported) (Rönback et al., 2008). This implies that the Ytterby samples, which are bedrock groundwater having similar REE-levels as overburden groundwaters, are high. Note also that the highest concentrations are found in the mine shaft water and that concentrations increase with depth. This is particularly true for Y. A REE depth profile of the mine shaft water would likely help in understanding their distribution in the local environment.

Data show that there are compositional differences in the Ytterby local water but without complementary data regarding anions it is not possible to discuss its origin and will therefore not be handled further.

Sample id.	Description
14-YB-W01	Water feeding the fracture
14-YB-W02	Water separated from YBS by centrifugation
14-YB-W03	Mine shaft at 1.3m depth
14-YB-W04	Mine shaft at 0.5m depth
14-YB-W05	Water shaft at 1.0m depth
U.Bedrock	Mean value for water sources in Uppland bedrock (SGU, 2013)
U.Soil	Mean value for water sources in Uppland soil environments (SGU, 2013)

Table 5: Description of water samples.

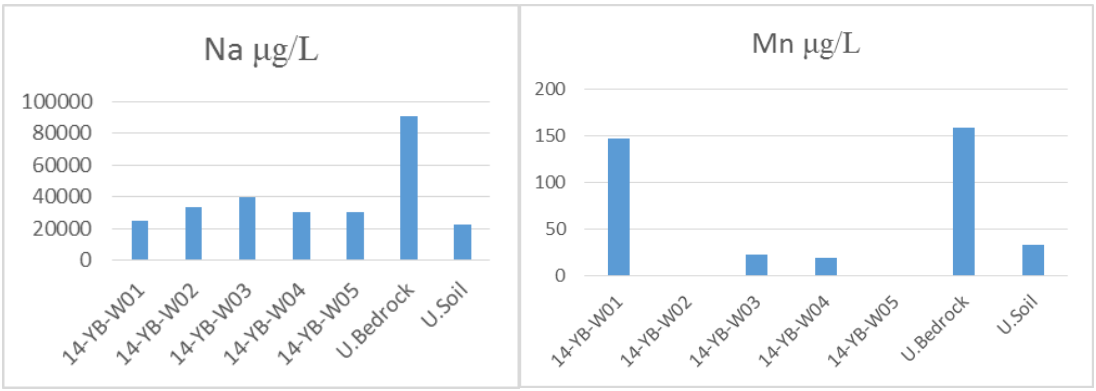

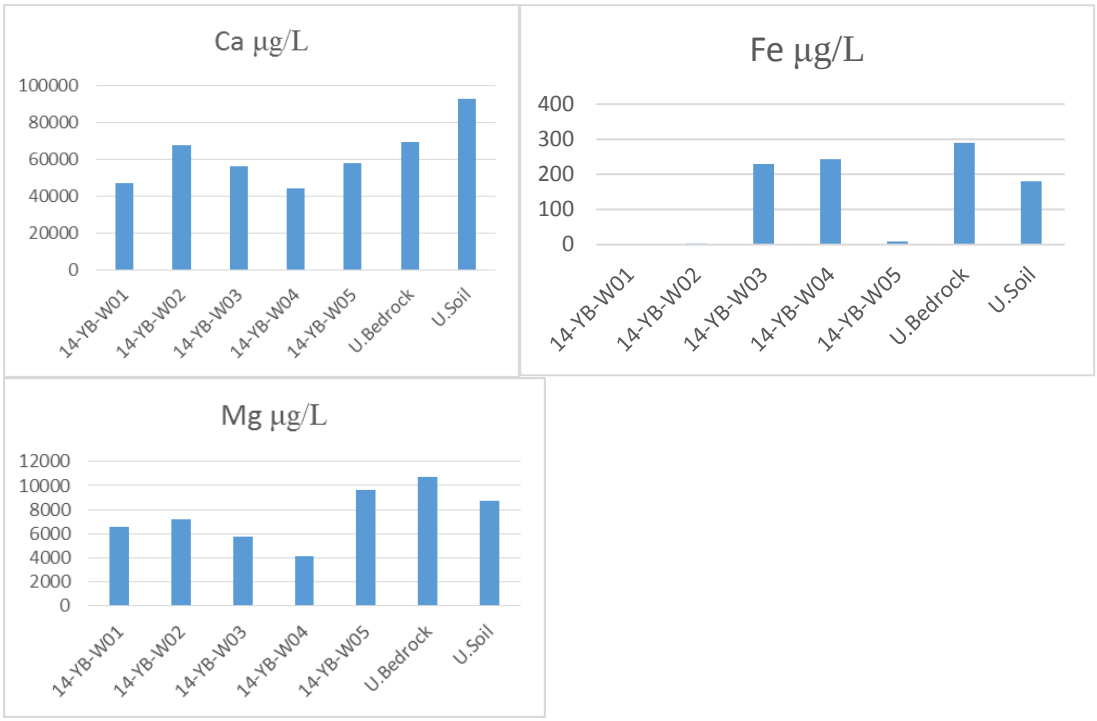

Fig.10: Elemental distributions in the Ytterby groundwater samples.

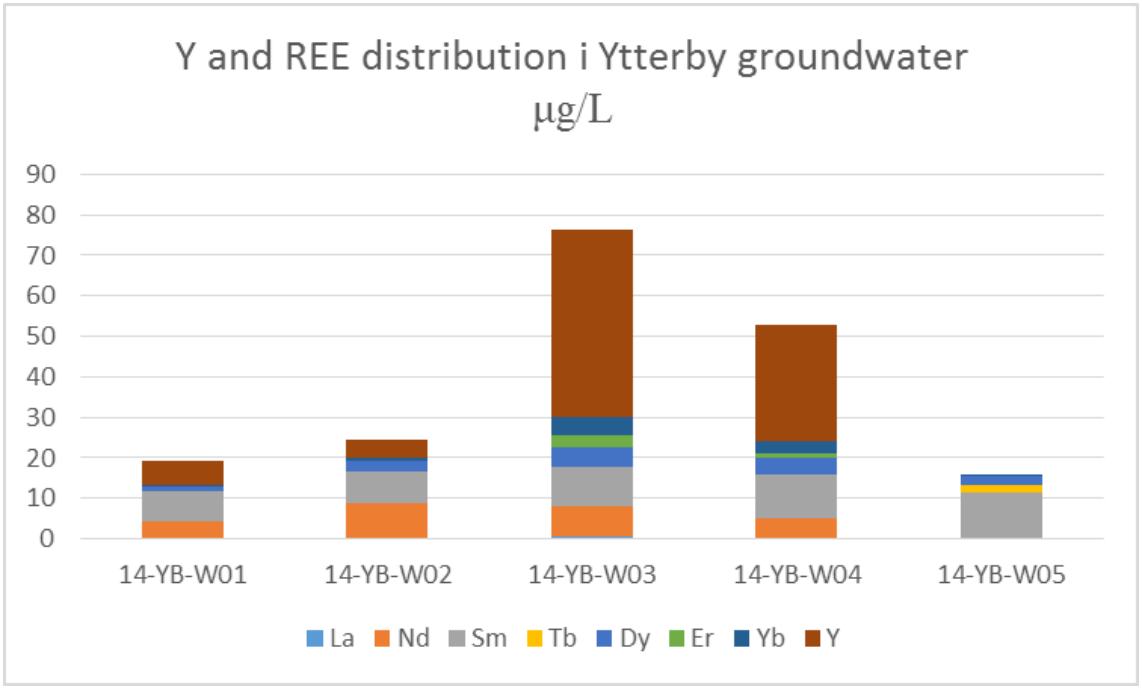

Fig.11: Y and REE distribution in the Ytterby groundwater samples.

5.3. Microscopy

5.3.1. Ytterby black substance

The bulk material of the YBS consists primarily of manganese and calcium in varying concentrations, but also a minor phase that includes fluorine. Within this manganese-bearing bulk, three different structures exist: dendritic or shrub-like (Fig.12:A & B), microspherolitic/botryoidal (Fig.12. C) and wad-like material frequently covered by filaments of varying thickness. The internal structure of the microsherolitic/botryoidal morphology shows lamination which implies an iterative change in production (Fig 13. A-D). So does also the shrub-like structures but less so and more randomly. Image C is showing a microspherolite/botryoidal texture in what likely is a calcium-rich manganese oxide-hydroxide. The wad-like material (light grey) attached to the surface of the microsperolites/botrydoids show similar Mn and Ca concentrations as the microsperolites, but also appear to include fluorine. The D image is showing wad-like Mn-Ca material covered by filaments of varying thickness. In this image, dried powder of the YBS is spread on a copper stub in order to observe the surface morphology of the components. Both the shrub-like and the spherolitic/botryoidal morphologies show a marked growth direction. The significance of the varying symmetry of shrubs, from highly irregular to regular geometric patterns, have been discussed in previously published articles and suggests a gradational relationship depending on the degree of bacterial involvement (Chafetz and Guidry, 1999).

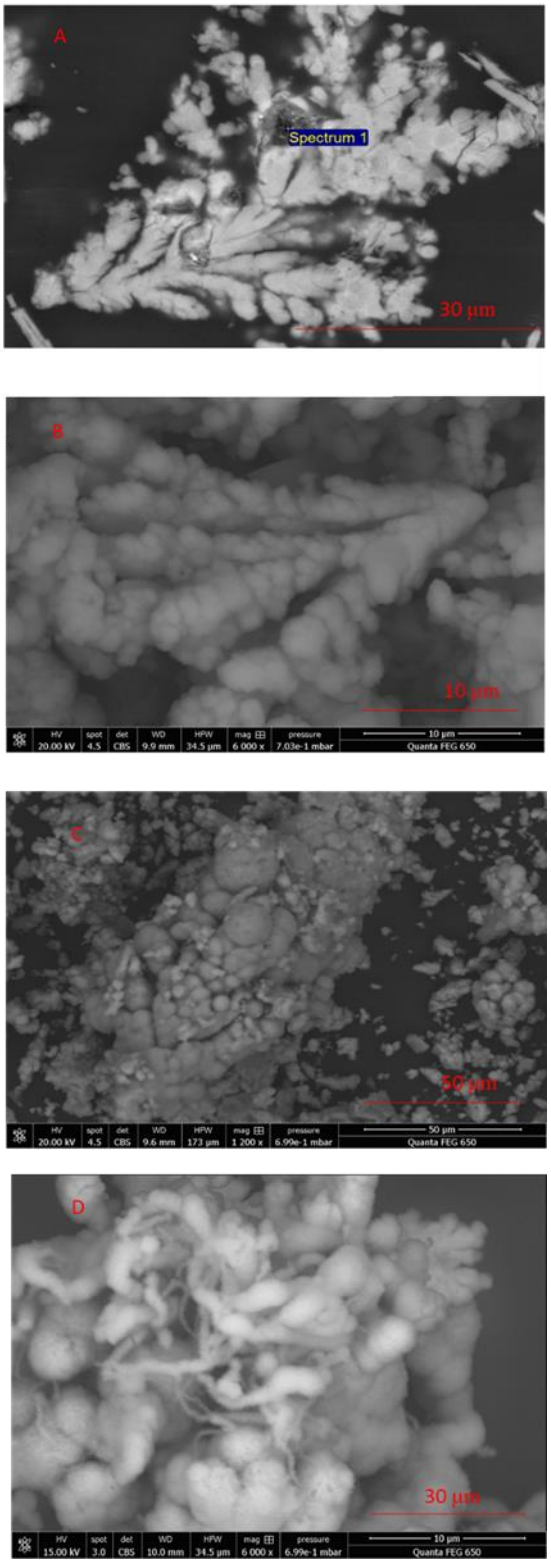

Fig.12: The bulk material of the YBS consists primarily of manganese and calcium in varying concentrations, but also a minor phase that includes fluorine. Within this manganese bulk, three different structures exist: dendritic or shrub-like (A and B), microspherolitic/botrydoidal (C) and wad-like material frequently covered by filaments of varying thickness (D).

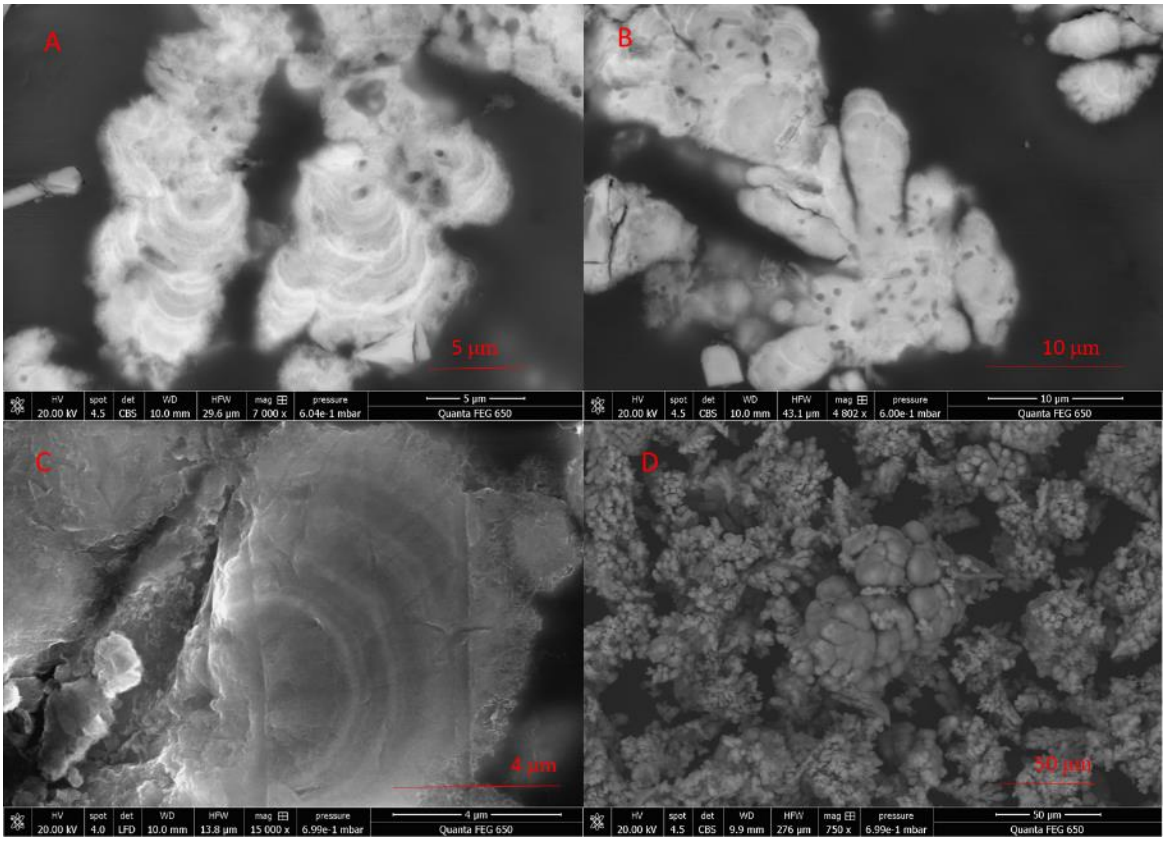

Fig.13: A & B) Scanning Electron Microscope (SEM) images showing polished thin sections of Mn oxide-hydroxide-rich laminated branches having a microstromatolitic structure. This is likely the internal structure of the microsperolitic/botryoidal morphology (Fig.12:C and Fig.13:D). A CBS detector was used to provide information about the composition of the deep layers of these microstructures. Analyses revealed that the alternating light and dark layers mainly express variation in Mn and Ca concentrations but also in the Mn/Ca ratio. The lower reflectance bands (darker grey) comprise higher concentrations of Mn and Ca than the higher reflectance bands (white- grey) and the higher reflectance bands show a consistent higher Mn/Ca ratio than the dark layers. C) Close-up of lamination using a LFD detector D) Image showing surface morphology of the microsperolitic/botryoidal component surrounded by shrub-like/dendritic components of the YBS.

Other less frequent Mn-Ca bearing structures are also bserved in the YBS. Images of these structures accompanied with a short text are presented next.

Fig.14: Scanning Electron Microscope (SEM) images showing polished thin sections of crust surrounding these tubes is enriched in fluoride. A) Tube manganese-calcium bearing tube structures. The structures attached to what resembles a honeycomb-shaped net of distorted possibly hexagonal cells. B) The darker spots in the image are likely transections of these tubes.

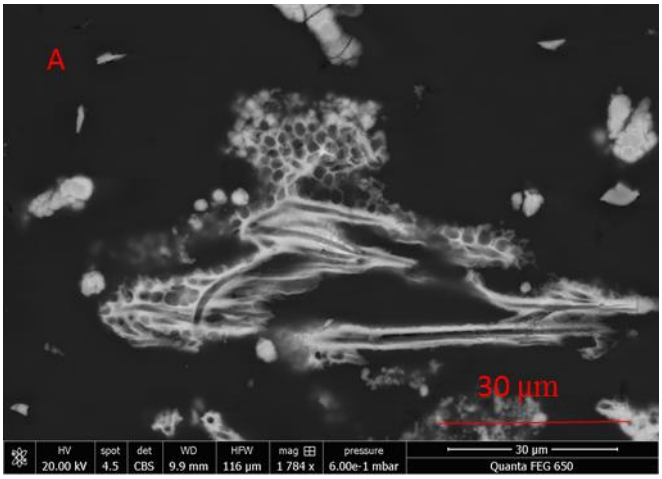

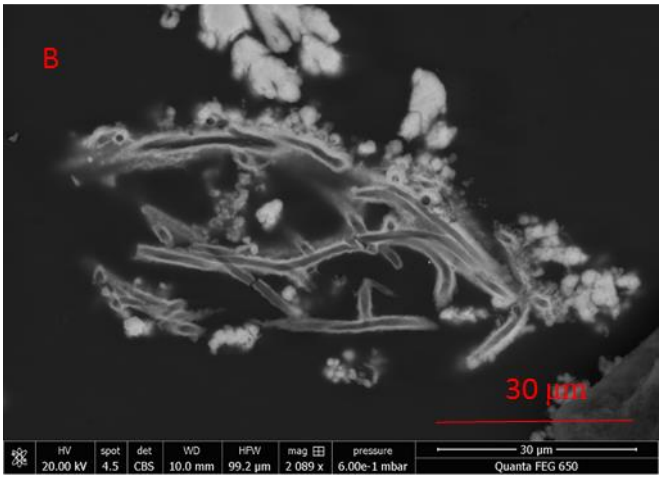

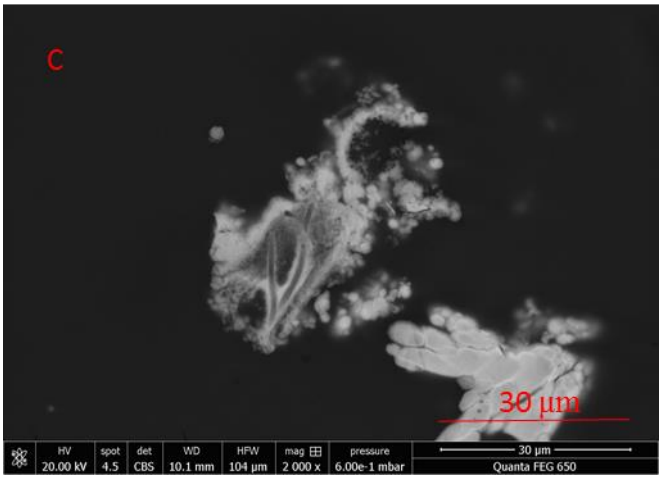

Figure 15: Scanning Electron Microscope (SEM) images (A & B) showing polished thin sections of a calcium-rich manganese oxide-hydroxide which also is a frequently observed microstructure in the YBS. It appears to grow from the center and outwards. Qualitative measurements of elemental concentrations show an increasing gradient of carbon concentrations towards the center of each micro-unit. This increase in carbon is accompanied with a consistent decrease in manganese (Mn) and calcium (Ca) concentrations but an increase in the Mn:Ca ratio. Fluorine is also present in minor amounts, but no pattern for its occurrences in this structure has been detected. A close-up of an isolated micro-unit is presented in image B. The dark areas show vague radial textures and appear to serve as nuclei for the more regularly laminated growth. An elemental mapping of the same compound is seen in the images below and visualizes the positive correlation between manganese and calcium concentrations characteristic for all structures in the YBS.

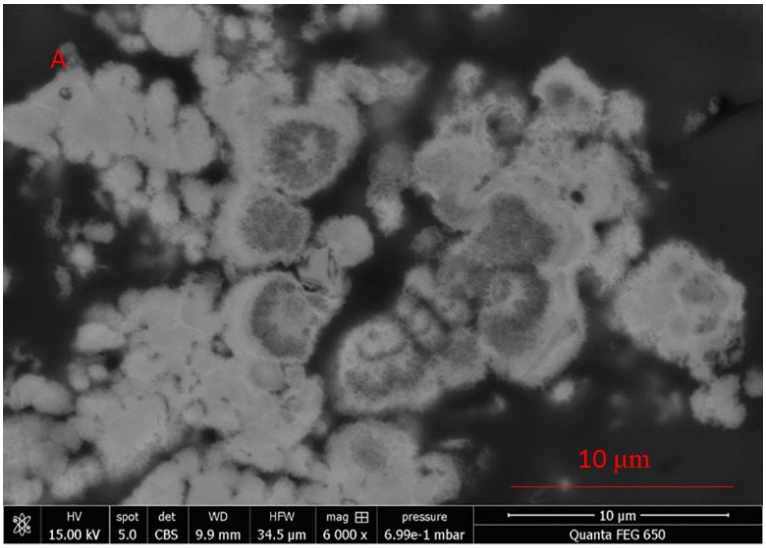

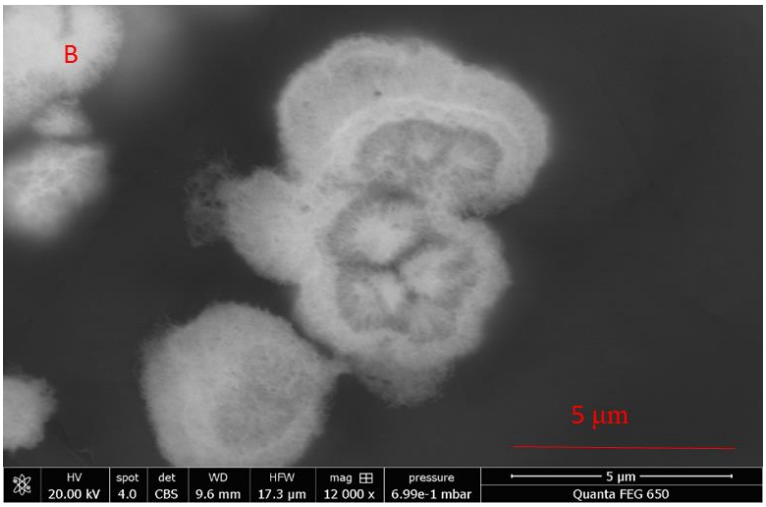

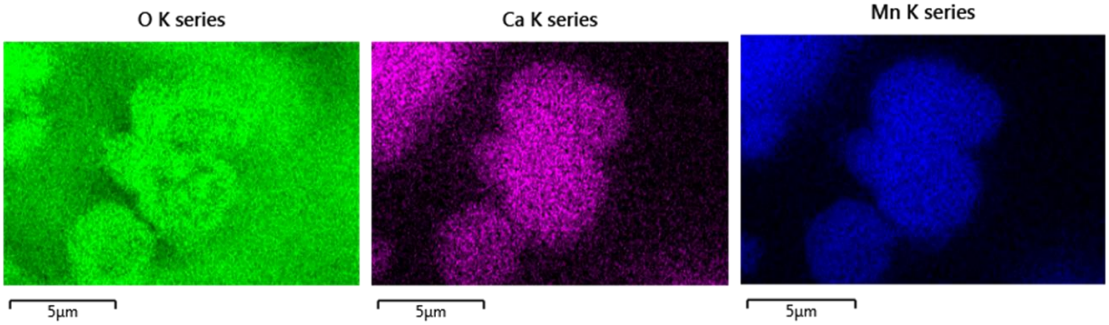

Figure 16: A) SEM image showing a silver-rich or possibly silver-coated microsphere and an organic capsule surrounded by shrub-like manganese bulk material. B) Close-up of a silver-rich or silver-coated microsphere. C) Close-up of an organic capsule where its circular contents is visible.

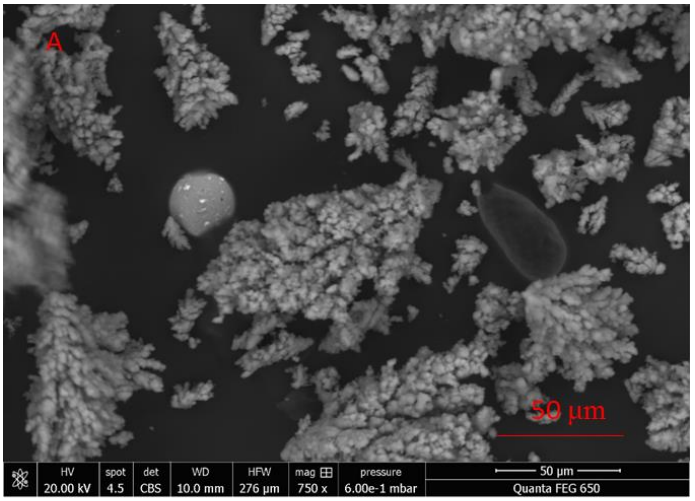

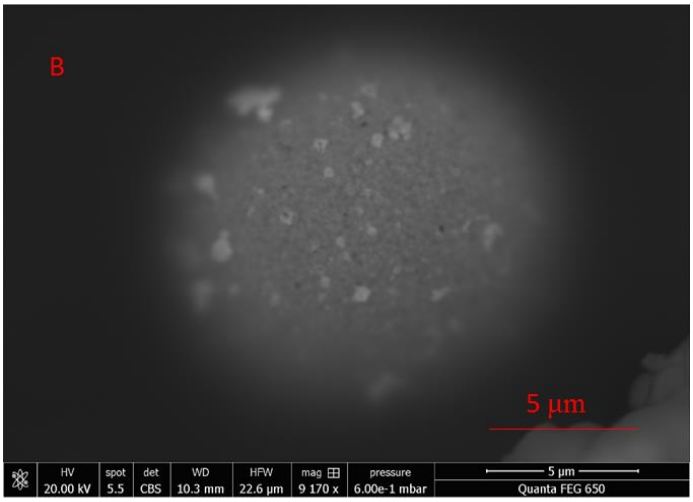

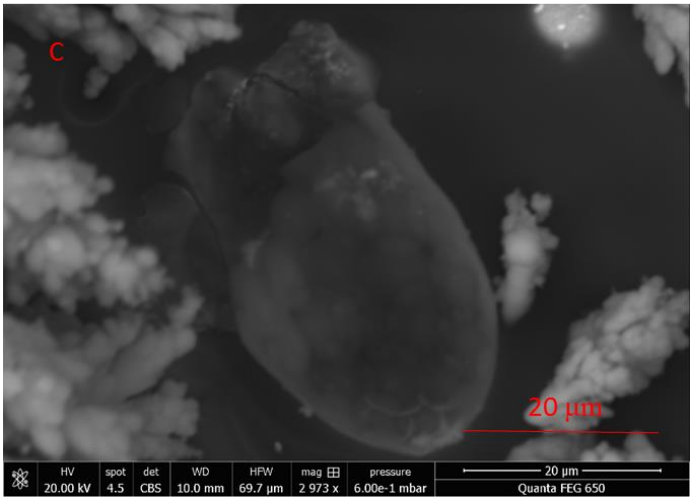

5.3.2. Fracture rocks

There are two different rock types bordering the investigated fracture: a metagranite (14-YB-01) and a relatively more mafic type (14-YB-03). The metagranite is dominated by quartz, plagioclase, chlorite, microcline and garnets. Within the garnet group substitution of Mg, Fe and Mn is common. Thus, this is possible manganese source in rocks adjacent to the YBS. The mafic rocks are dominated by amphibole, biotite, quartz and plagioclase. Manganese may be present in amphibole and biotite. Petrographic analyses verify that the 1-2 mm thick lithified layer covering the surface of the rocks is calcite. Between the calcite rim (Fig.17:A) and the metagranitic bedrock there is a cloudy,altered area of oxidation (Fig.17:B). Fluids from this area have filled fractures around and within other minerals present in the rock. Fe oxide has stained the groundmass which has a reddish rusty colour. Within this altered area there exist euhedral crystals of pyrite (FeS_2) and needle-shaped crystals of another iron sulphide mineral having a Fe:S atomic ratio of approximately 1:1. These needles (Fig.17:C) have a bright red/magenta colour in crossed polarized light and primarily occur as crack fillings (Fig.17:D). The presence of iron sulphides in this altered area is an indication of reducing conditions. The existence of both oxidized and reduced species in the same altered area is likely a result of previously reducing conditions in an area which is now fully oxidized.

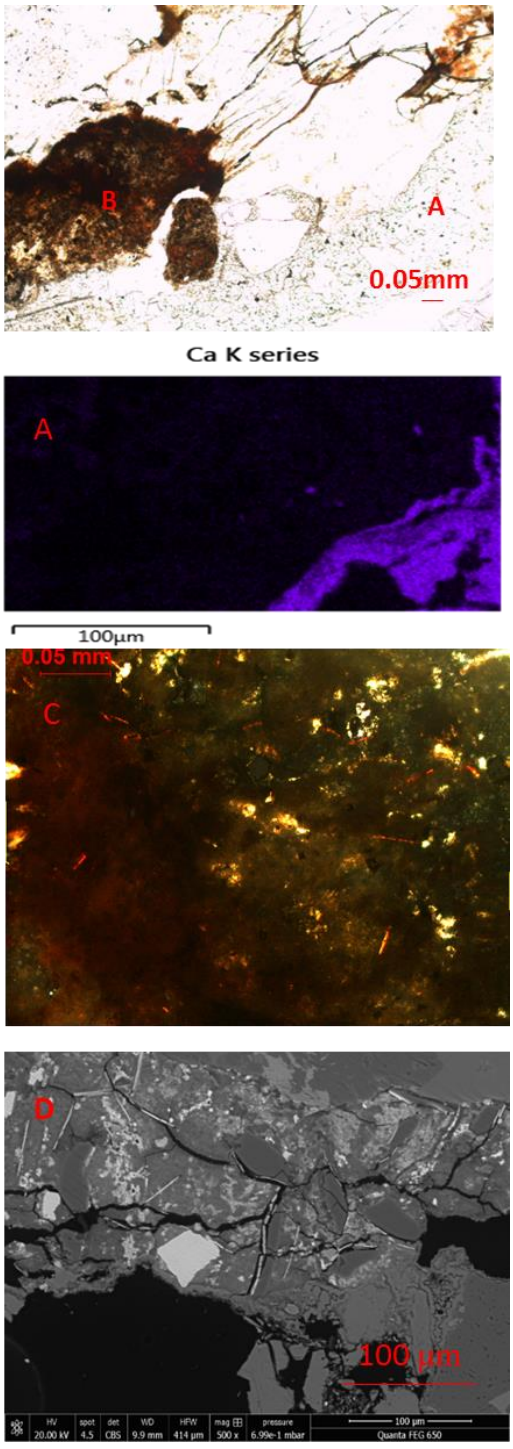

Figure 17: SEM images showing the rim of calcite (A) and the cloudy, altered area of oxidation (B). C) Microphogograph in crossed polarized light showing red-magenta coloured iron sulphide needles. D) SEM image showing these FeS-needles as crack filling. Euhedral pyrite (Fe2) crystal is also seen as a highly reflecting cube.

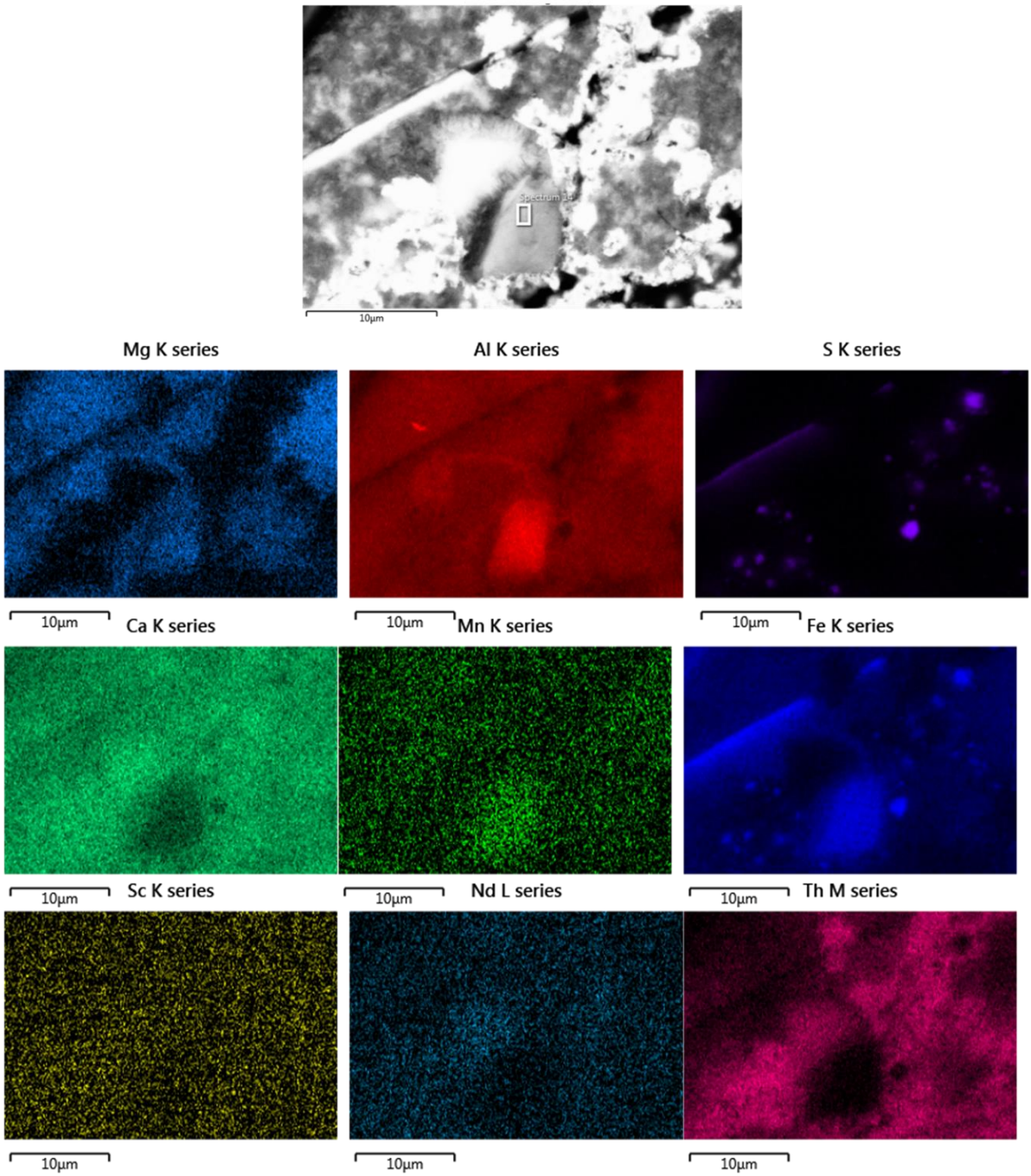

Figure 18: Elemental mapping of the altered area between the calcite rim and the metagranitic rock. These images show that presence of iron sulphides in the oxidized zone. The mineral marked in the top image Thorium (Th), scandium (Sc) and neodymium (Nd) are scattered over the whole area. Note the mineral marked in the top image. It consist mainly of Fe, Si and Al but also minor amounts of Mn and Ag.

5.4. X-ray powder diffraction pattern

The present data show that quartz is present in the sample and was recognized by its characteristic 3.34 Å peak, calcite is also present and is recognized by the peak around 3.03 Å and plagioclase is recognized by its 3.2 Å peak. The variability in relative intensity between reference minerals and the YBS is however significant and might have at least two different reasons; *i)* there is less of the particular mineral in the powder compared to the reference material and *ii)* peaks from different minerals overlap. Except for these minerals, it was difficult to identify distinct crystalline phases. However, data appear to fit diffraction patterns for a number of manganese oxides and hydrous oxides even though certain identification of specific mineral phases was not possible. A main reason for this is that these mixtures often are poorly crystalline and that many phases exhibit similar crystal structures and thus similar diffraction patterns (Post, 1999). Also, the broad diffraction peaks seen in the graphic readout (Fig.19) made it difficult to isolate each peak. This might be the result of considerable overlapping of peaks.

Approximate 2theta-and corresponding Å-values were used to understand which minerals could be present in the YBS. The reflection at 7Å might indicates the presence of phyllomanganates with one H_2O layer while the one at 10Å is characteristic of phyllomanganates incorporating two H_2O layers or of the tunnel structured oxides, also referred to as tectomanganates (Adams et al., 2008). The XRD diffraction pattern for the YBS appears to include one or several types of phyllomanganate minerals having their principal reflection either between 7.1 and 7.6Å or around 10Å (Kim, 1991). The varying reflections in this span are due to structural differences of interlayer cations and H_2O molecules, i.e. layers between MnO_6 octahedral layers (Kim, 1991). Further comparisons to diffraction patterns of manganese minerals did reveal that these phyllomanganates are likely to be poorly crystalline birnessite and/or vernadite. An additional XRD analysis was made using software to search for a birnessite XRD pattern in the YBS (Fig.20) and results clearly show that there is a match. Vernadite is a highly disordered manganese oxide which exists as both 7Å and a 10Å hydrates, incorporating one respectively two H_2O layers (Bodeï et al, 2007). Except for reflections at 7Å and 10Å and, both vernadite diffraction patterns are characterized by broad XRD lines at 2.46, 1.42 and occasionally a smaller one at 2.2 (Post, 1999). The reflection at 10Å may also belong to a todorokite which is a tunnel structured hydrous oxide. Moreover, the reflections around 3.1Å, 2.4Å and 1.6Å indicate the presence of pyrolusite which is a manganese dioxide which belongs to the tunnel structured minerals (Post, 1999). The XRD spectrum further suggests the presence of clay minerals in the YBS, but considering the low concentrations of aluminum identified by the chemical analysis, they are only present in minor quantities. Diffraction data are presented in the graphic readout (Fig.19) and matching peak information in Table 6.

During the pilot study in 2012, a Raman analysis using a LabRAM HR 800 instrument with an argon-ion laser at the Department of Geological Sciences, Stockholm University, was employed to identify a manganese oxide, Mn_3O_4 ($Mn^{2+}Mn_2^{3+)}$ present in the YBS. This oxide is known as the mineral Hausmannite. The principle reflections of Hausmannite (2.49Å, 2.77Å and 1.54Å) are not in the peak list, but could possibly correspond to peaks between peak 10 and 11 and 18 and 19 in the graphic readout.

The graphic readout from the X-ray detector (Fig.19) plots peak intensity as a function of the 2theta angle, i.e. the diffraction angle multiplied by two. The intensity-values given in the diffraction digital data are relative intensities, i.e. the ratio of the individual peak divided by the highest peak in the spectrum. Low angles correspond to large d-spacing and are thus situated to the right in the readout while high angles are related to small d-spacing and thus are found to the left.

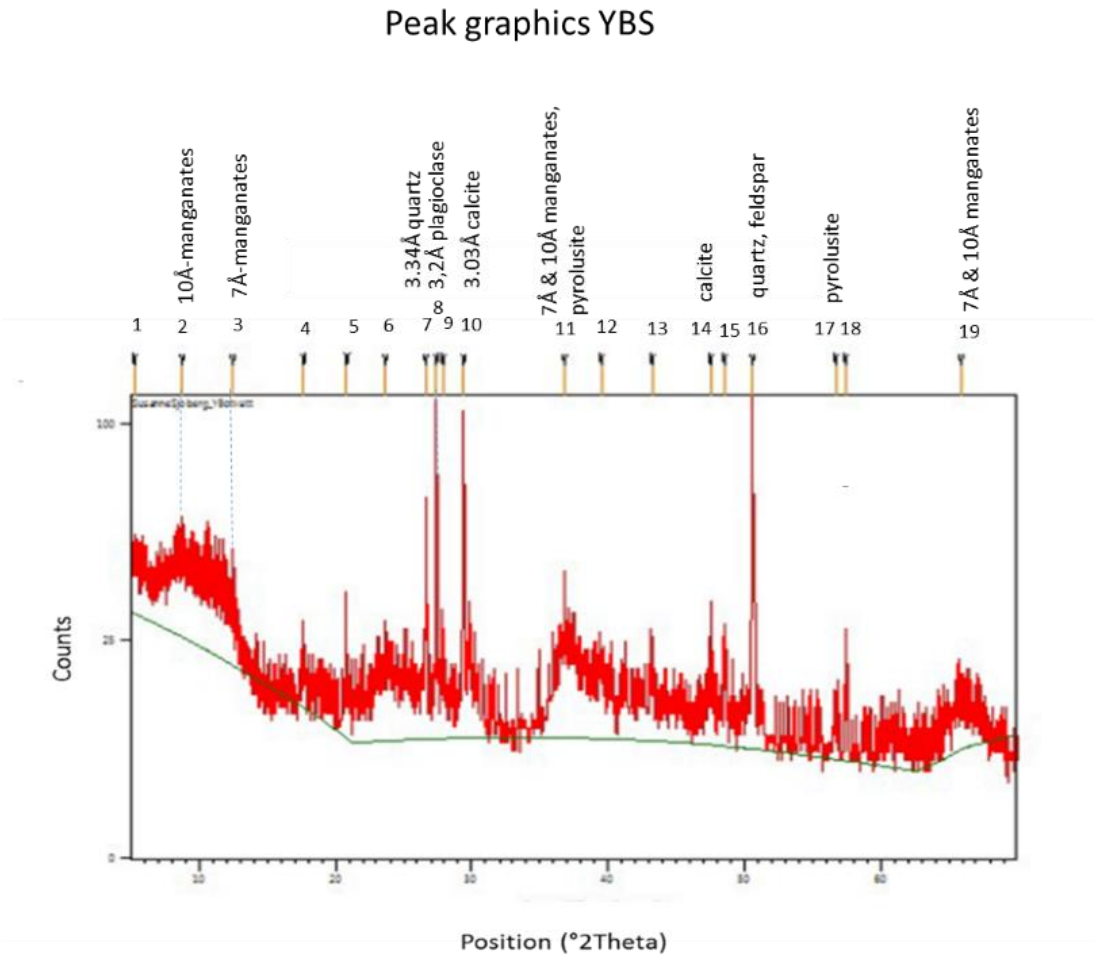

Fig. 19: X-ray diffraction peak graphics of the YBS. Peak positions are matched with peaks for suggested minerals but satisfactory criteria for certain identification (section 4.5) of phases is not fulfilled.

Digital Peak list:

Peak #	Position (°2Th)	Height (cts)	D-spacing (Å)	Relative Intensity (%)	Suggestions for mineral identification*
1	5.2210	13.52	16.92640	13.89	Smectite clay mineral or possibly Vermiculite clay mineral?
2	8.7522	22.22	10.10366	22.82	10Å manganates (vernadite, todorokite) and/or mica (possibly phlogopite)
3	12.4571	15.77	7.10575	16.20	7Å mangantes (the highest peak might correspond to the birnessite principal reflection while the broader peak area reflects a mixture of other 7Å-manganates)
4	17.6558	6.11	5.02346	6.28	10Å vernadite, Mica, possibly phlogopite
5	20.8264	14.81	4.26532	15.21	Quartz
6	23.6297	11.28	3.76527	11.58	Plagioclase, probably Ca-rich (anorthitic)
7	26.6277	49.55	3.34775	50.90	Quartz principal reflection
8	27.3930	77.28	3.25593	79.38	Propably a potassic feldspar
9	27.8689	15.55	3.20141	15.97	Plagioclase, probably Ca-rich (anorthitic)
10	29.4057	93.01	3.03751	95.54	Calcite principal reflection, Vernadite principal reflection, Phlogopite minor reflection?
11	36.7761	19.64	2.44392	20.17	7Å manganate (birnessite second strongest reflection), vernadite (δMnO2), pyrolusite, vermiculite?
12	39.4759	13.84	2.28278	14.21	Calcite second strongest reflection, possibly influenced by vernadite, manganite third strongest reflection.
13	43.2007	14.55	2.09420	14.95	Plagioclase
14	47.5102	20.56	1.91381	21.12	Calcite fourth strongest reflection
15	48.5377	15.34	1.87567	15.76	Calcite third strongest reflection
16	50.5999	97.35	1.80247	100.00	Quartz , Microcline
17	56.6946	3.10	1.62366	3.19	Pyrolusite?
18	57.4120	19.21	1.60506	19.73	Pyrolusite? Minor vermiculite peak
19	65.8963	7.31	1.41748	7.51	7Å & 10Å manganates (birnessite vernadite)

Table 6: X-Ray diffraction digital peak list.

***** *Satisfactory criteria for certain identification of phases is not fulfilled. Ytterby peak positions are however matched with peaks for suggested minerals in any one of sources of references mentioned in section 4.6.*

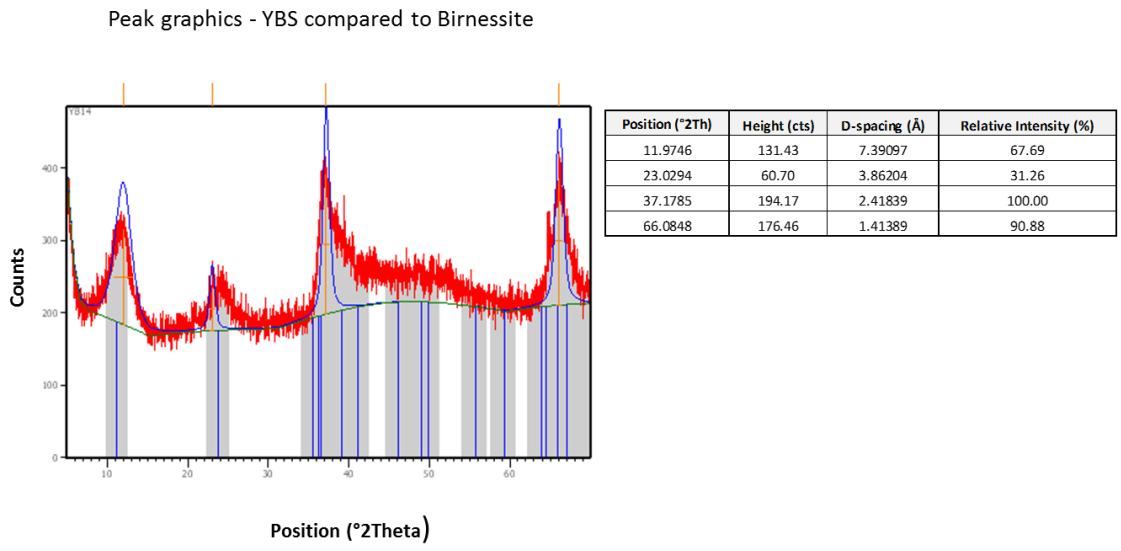

Position (°2Th)	Height (cts)	D-spacing (Å)	Relative Intensity (%)
11.9746	131.43	7.39097	67.69
23.0294	60.70	3.86204	31.26
37.1785	194.17	2.41839	100.00
66.0848	176.46	1.41389	90.88

Fig. 20: X-ray diffraction pattern of the YBS matched with reference spectrum of birnessite.*

* *Analysis made using highscore software, Swedish Museum of Natural History (2014).*

5.5. Infrared spectra (IR-Spectra)

The infrared spectrum consists of only one distinct peak (trough) at 1630 cm^{-1}. This is where C=O in carboxylic acid-groups as well as NH_2 in amides can occur (Lang et al., 1974). Although the peak is distinct, it is relatively small which confirms that the major part of the sample is not organic. Distinct C-H-peaks are missing. The peak around 3200 cm^{-1} is indicative of water and its moderate absorbance is surprisingly low considering that the LOI at 1050°C is determined to 27 wt.%. The major absorbance below 800 cm^{-1} increase in intensity at shorter wavelengths and is possibly caused by a metal oxide.

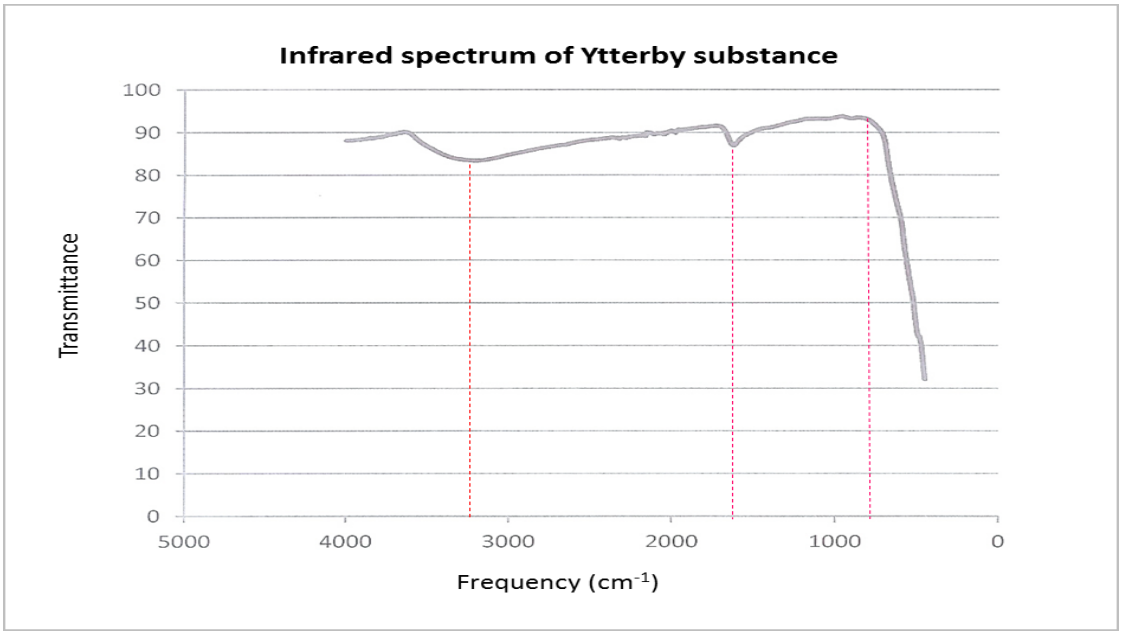

Fig.21: Infrared spectra of the YBS

5.6. Concentrations and isotopic signatures of C, N and S

Data of carbon, nitrogen and sulphur isotopic analyses are listed in Table 6.

Sample	$\delta^{13}C_{tot}$ vs PDB (‰)	$\%C_{tot}$	$\delta^{13}C_{org}$ vs PDB (‰)	$\%C_{org}$	$\delta^{15}N$ vs air (‰)	% N	$\delta^{34}S$ vs CDT (‰)	%S
Not washed YB 1	-18,21	1,82	-24,72	0,60	13,99	0,08	8,08	0,08
Not washed YB 2	-19,01	1,79	-24,75	0,58	13,98	0,10		
Averages	-18,61	1,81	-24,73	0,59	13,99	0,09		

Table 7: Concentrations and isotopic signatures of C, N and S

$\delta^{13}C$

Carbon isotopic analyses show that approximately 1.81 % of the dried YBS is carbon and that approximately one third of this 1.81% is organic carbon (0.59%). The $\delta^{13}C_{tot}$ is -18.21±0.15‰ and the corresponding value for the organic part is -24.73±0.15‰. The difference in $\delta^{13}C$ signatures between the two types of carbon analyses, without and with acid, confirms the presence of carbonates in the YBS. Consequently, the inorganic fraction of carbon is increasing the overall carbon signature and therefore the $\delta^{13}C_{org}$ of -24.73±0.15‰ should be used for determining the biogenic source of the organic matter in the YBS.

$\delta^{15}N$

The concentration of nitrogen in the YBS is 0.09% and the $\delta^{15}N$ value is 13.99±0.15‰. Thus the sample is enriched in ^{15}N compared to ^{14}N relative to air.

$\delta^{34}S$

The sulphur concentration of the Ytterby sample was determined to be 0.08% and the $\delta^{34}S$ value 8.08±0.2‰. Thus it is enriched in the heavier isotope.

5.7. Lipid analysis

The findings of molecular fragmentation patterns and recognizable mass spectra have provided valuable complementary information about the organic fraction of the YBS. A brief introduction to lipids as biomarkers and to chemical compounds relevant to this study is given in appendix 4. Even though most of the peaks are identified, a few remain unsolved due to the lack of reference mass spectra for comparison. This is particularly valid for the extended and irregular hopanoid compounds where documentation is still scarce (Peters et al., 2005). There is no significant difference between the duplicates, indicating that similar results would be obtained if the analysis is to be repeated. Thus, one of the series was chosen for analysis: the A-series which consists of fraction A:1 (Hexane), A:2 (Hexane/DCM 1:1) and A:3 (DCM/MeOH 1:1). Fractions are listed in order of increasing polarity. Results revealed a larger apolar fraction and a smaller mid- and polar one (Fig. 22).

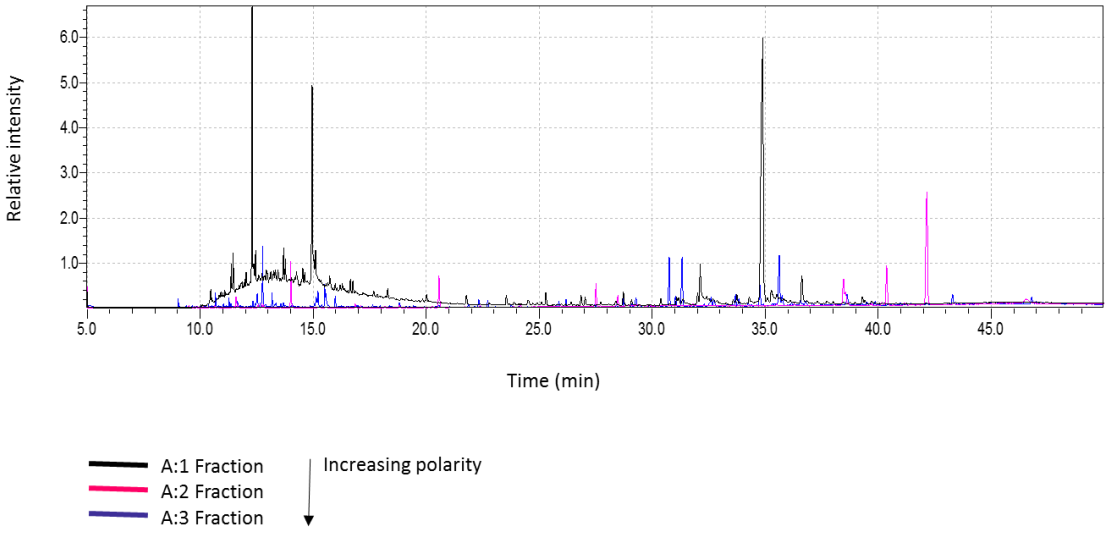

Fig. 22: Image showing the distribution of the total amount of lipids is the YBS.

The A:1 Fraction

This fraction (Fig.23) is dominated by a fan-shaped spectrum of processed and degraded hydrocarbons of varying shapes and structures. More recent material would correspond to longer chain alkanes and thus higher boiling fractions, coming out at the right end of the spectrum. However, within this hump of ancient hydrocarbons, there are two major peaks both corresponding to long chain alcohols. The pronounced peak further to the right (33) has a pronounced 191 m/z which is diagnostic for pentacyclic triterpenoids (Gaines et al., 2009) and is further identified as diploptene which is a lipid associated with bacterial communities. It is part of the hopane family of triterpenoids which are used as biomarkers for eubacteria (Gaines et al., 2009), resins and a few higher plants such as ferns, lichens (Hunt, 1995), mosses and fungi (see complete list of sources in Peter et al., 2005). In particular, diploptene has been observed as a major constituent in cyanobacteria (see complete list of sources in Peter et al., 2005). Data listed in Table 8 show that diploptene accounts for 40% of the total amount of lipids in this fraction, alcohols for another 30% while the remainder 30% correspond to ancient hydrocarbons.

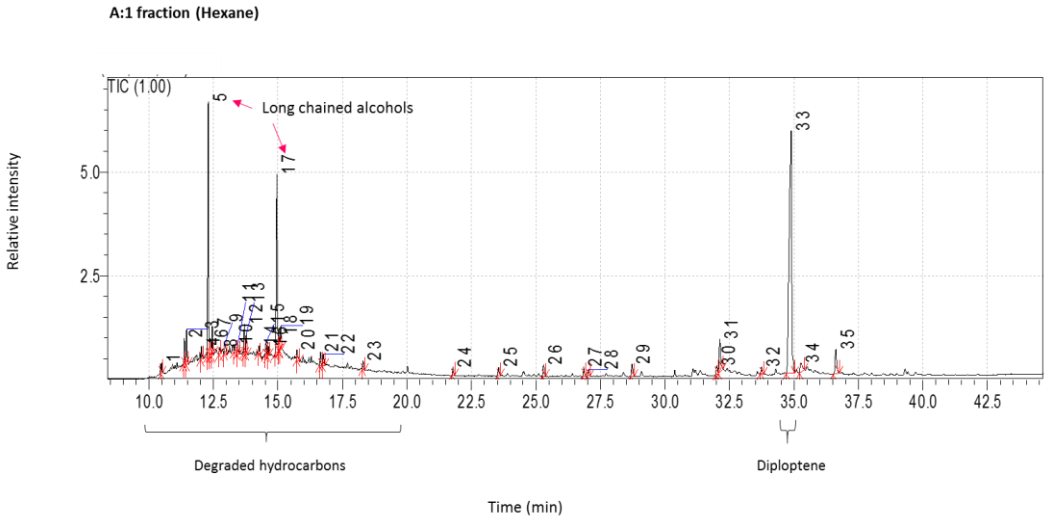

Fig. 23: The A:1 fraction is dominated by a fan-shaped spectra at the left end typical for degraded and processed hydrocarbons. Within this hump of ancient hydrocarbons, there are two major peaks both corresponding to long chain alcohols. The pronounced peak further to the right in the spectrum (33) is identified as diploptene which is a lipid associated with bacterial communities.

Peak #	Identified lipid	Comment	Area %
1	Pentadecane	$C_{15}H_{32}$, Alkane	0.41
2	Octadecane	$C_{18}H_{38}$, Alkane	1.10
3	Tetramethylhexadecane	$C_{20}H_{42}$	1.91
4	?		0.77
5	1-Hexadecanol	$C_{16}H_{34}O$, aliphatic alcohol	13.92
6	Degradation product of Squalene?		1.36
7	Hexacosane	$C_{26}H_{54}$	1.55
8	2-methylhexacosane-like compound		0.38
9	*Heptafluorobutyric acid, hexadecyl ester*		*1.11*
10	*3-methylnonadecane*	*$C_{20}H_{42}$*	*0.55*
11	*1-Dodecanol, 2-octyl-*		*0.85*
12	Hexacosane	$C_{26}H_{54}$	1.53
13	*5,5-Diethylheptadecane*		*1.06*
14	*Sulfurous acid, octadecyl pentyl ester*		*0.56*
15	*3,3-Diethylheptadecane*		*0.92*
16	*1-Cyclopentyleicosane*		*0.47*

17	*n-Nonadecanol-1*	*$C_{19}H_{40}O$, fatty alcohol*	*12.45*
18	*Tetrapentacontane, 1,54-dibromo-*		*0.67*
19	*Octacosane*	*$C_{28}H_{58}$*	*1.71*
20	*Octadecyl trifluoroacetate*	*$C_{20}H_{37}F_3O_2$*	*0.90*
21	*Octacosane*	*$C_{28}H_{58}$*	*0.86*
22	*5,5-Diethylheptadecane*		*0.72*
23	*Pentacosane*	*$C_{25}H_{52}$*	*0.55*
24	*Pentacosane*	*$C_{25}H_{52}$*	*0.63*
25	*Tetracontane*	*$C_{40}H_{82}$*	*0.72*
26	*Octacosane*	*$C_{28}H_{58}$*	*0.90*
27	*2-Buten-1-one, 1-(2,6,6-trimethyl-3-cyclohexen-1-yl)-*		*0.72*
28	*Heneicosane*	*$C_{21}H_{44}$*	*0.53*
29	*Tetratetracontane*		*1.05*
30	*Pentacosane*	*$C_{25}H_{52}$*	*0.76*
31	*Octacosanol*	*$C_{28}H_{58}O$*	*3.14*
32	?		0.54
33	Diploptene	The simplest C_{30} hopanoid.	40.58
34	*Octacosanol*	*$C_{28}H_{58}O$, fatty alcohol*	*1.35*
35	*Cholesta-3,5-dien-7-one*		*2.77*

Table 8: Peak identification fraction A:1

The A:2 Fraction

The left part of the A:2 fraction (Fig.24) is dominated by aldehydes. Squalene (peak 6) which is seen surrounded by the aldehydes and ketones, is the precursor for synthesis of the hopane skeleton (AOCS Lipid Library website, 2014). The right side of the spectrum is dominated by peaks identified as hopanoids or hopanoid-like structures. A few of these peaks do not match any reference spectra for comparison but they do appear to fit the pattern where the D-E ring fragments of hopanes increase by 14 mass units for the addition of each CH_2 group (Gaines el al., 2009). This means that the characteristic 191 mass units for the C_{30} hopanoid is increased by 14 to 205 mass units for the C_{31} compound, another 14 to 219 mass units for the C_{32} compound and so forth. The presence of these extended hopanoids is a distinct sign of bacterial presence in the depositional environment. They also have this quality of being hydrophobic at one end and hydrophilic at the other. A characteristic which make them indecisive of which fraction to join and thus often come out somewhere in between. (Gaines et al., 2009). This indecisiveness is confirmed in the Ytterby sample where they are found in this middle fraction.

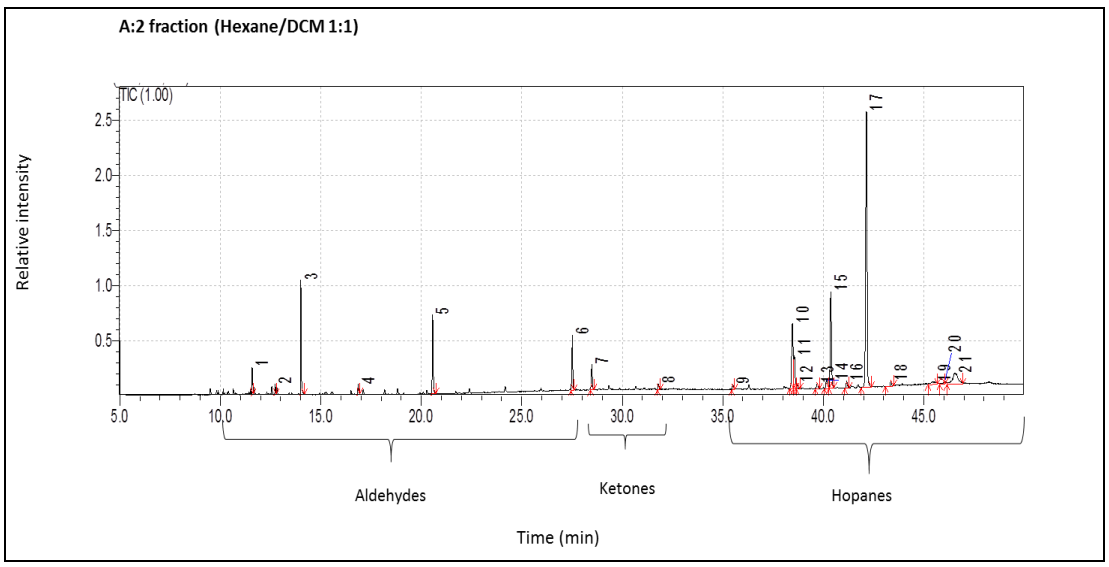

Fig. 24: The A:2 fraction is dominated by aldehydes and hopanes.

Peak #	Identified lipid	Comment	Area %
1	Tetradecanal	Aldehyde, $C_{14}H_{28}O$	1.76
2	Octadecanal	Aldehyde, $C_{18}H_{36}O$	0.70
3	Octadecanal	Aldehyde, $C_{18}H_{36}O$	6.94
4	1-Docosanol, acetate	Aldehyde, $C_{24}H_{48}O_2$	0.77
5	Octadecanal	Aldehyde, $C_{18}H_{36}O$	6.95
6	Squalene*	Isoprenoid, $C_{30}H_{50}$	4.44
7	10-Nonadecanone	Ketone, $C_{19}H_{38}O$	2.31
8	10-Nonadecanone	Ketone, $C_{19}H_{38}O$	0.64
9	17α-hopane	17α-hopane, 30-hopane	0.71
10	17α21β –hopane (C31H54)		8.46
11	17β21β –hopane (C31H54)		4.49
12	Discarded	Too much noise in the signal.	0.66
13	Hopanoid-like structure		0.73
14	Hopanoid	189 m/z**	1.23
15	C_{32} –hopane (mixed signal)	Also Trisnorhopane (C29H50)?	10.87
16	Hopanoid	189 m/z**	1.00
17	C_{33} -hopane (mixed signal)		38.53
18	Hopanoid-like structure***		0.63
19	β, α-Neogammacer-13(18)ene	Unsaturated Hopane II ($C_{30}H_{50}$), 189 m/z	1.52
20	Hopanoid-like structure	C31-hopane?	0.63
21	Hopene II	Saturated Hopane II ($C_{30}H_{50}$), 191 m/z	6.03

Table 9: Peak identification fraction A:2

**Isoprenoid hydrocarbon common in bacteria and zooplankton (Hunt, 1995).*
*** 189 m/z is an indication of unsaturation at the C_6 in the A-ring (Talbot et al., 2007).*
****Major fragments of hopanoid have been identified (191 m/Z), exact masses have not been found in literature.*

The A:3 Fraction

The most intense peak in this fraction (33) is identified as C_{29} β-Sitosterol which is a compound associated with terrestrial higher plants or diatoms (Gaines et al., 2009) and the second most intense peak (26) is attributed to diatoms or bacterial presence. There is a predominance of even numbered compounds up to C_{26}, both saturated and unsaturated. The unsaturated even carbon numbered fatty acids ranging from C_{14} to C_{20} are common in most organisms (Gaines et al., 2009) while the saturated fats are more common in animals than in plants (White, 2013).

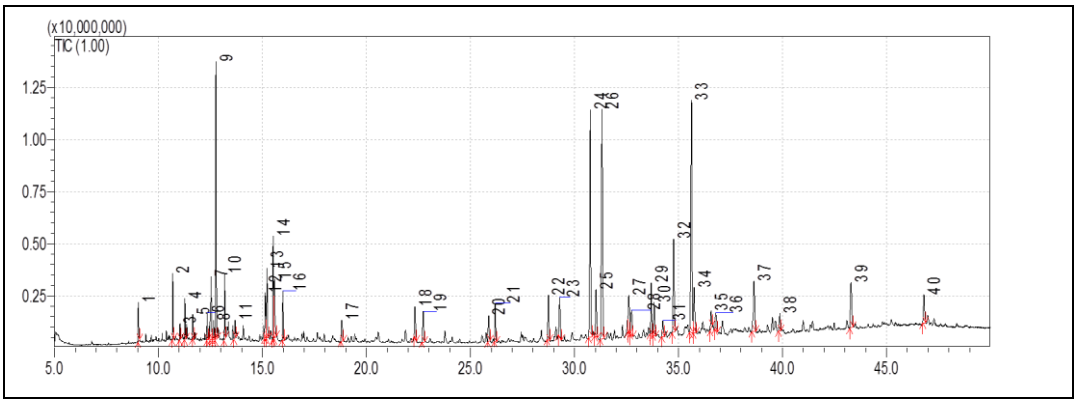

Fig. 25: The A:3 fraction is composed of two parts corresponding to fatty acids and plant material and/or algae. The further to the right in the spectrum, the longer the chains.

Peak #	Identified lipid	Comment	Area%
1	C_{12} FA	Straight chain fatty acid	0.92
2	C_{14} FA	Straight chain fatty acid	1.36
3	C_{16} TMS (TriMethylSilyl)	Straight chain fatty acid,	0.33
4	C_{15}	Straight chain fatty acid, saturated	0.86
5	C_{17}	Anteiso? (Values skewed +1)	0.62

6	C_{16}	Anteiso	0.68
7	$C_{16:1}$	A C_{16} with a double bond.	2.69
8	$C_{16:1}$	A C_{16} with a double bond.	0.64
9	C_{16}	Straight chain fatty acid	7.10
10	C_{16}-OH	Hydroxy fatty acid, very reactive.	1.61
11	?	A branched fatty acid?	0.51
12	$C_{18:1}$ FAME (FA Methyl Ester)	Monounsaturated	1.91
13	$C_{18:1}$ FAME (FA Methyl Ester)	Monounsaturated	2.59
14	C_{18}	Straight chain FA (unsaturated)	3.29
15	β-OH C_{16} FAME		2.32
16	C_{18} n-OH		1.55
17	?	A branched fatty acid?	1.06
18	C_{22} FAME	Fatty Acid Methyl Ester	1.37
19	C_{22} OH + ?	With something else in there.	1.41
20	C_{24} FAME	Fatty Acid Methyl Ester	1.14
21	C_{24} OH	?	1.42
22	?	?	1.74
23	C_{26} FA	Fatty Acid	2.07
24	Diol?	Maybe C_{24} β-O OH_3-acid?	9.49
25	?	?	2.26
26	Hop-17(21)-ene	$C_{30}H_{50}$, Bacterial or diatom.	11.57
27	$C_{27:1}$*	Cholesterol, a four ring alcohol**	1.81
28	C_{27}*	Cholestanol, a sterane	1.59
29	C_{26} (ω-1)OH-FAME	C_{26}(gamma-1)OH-FAME	1.99
30	Diol?	?	1.42
31	Delta 5 $C_{28:1}$ Camposterol*	24-methylcholest-5-en-3B-ol	0.90
32	$C_{29:2}$ Sterol		4.37
33	C_{29} β-Sitosterol*		12.84
34	C_{29} Sitostanol		2.80
35	?		0.83
36	?		1.04
37	Tetrahymanol (TMS ether)	Microorganisms (not plant derived)	3.08
38	Diol?		0.79
39	Hopanoid?		2.57
40	Ring structure?		1.46

Table 10: Peak identification fraction A:3

** Reference material is from a study on diatoms*

*** With or without branch group attached to the C-24 positon? With= common in algae and fungi, without= all sorts of organisms (Gaines et al., 2009)*

****Anteiso are fatty acids with a methyl group attached to the third carbon atom from the end, identified as lipids of heterotrophic bacteria (Gaines et al., 2009)*

5.8. Electron paramagnetic resonance (EPR) analysis

The EPR technique was used to obtain structural information about the manganese complexes in the YBS sample and more specifically in an attempt to determine whether the manganese oxides-hydroxides are biotically and abiotically precipitated compounds. Biogenic precipitated manganese minerals produce narrow EPR spectral linewidths (~500 G) while the abiogenic equivalences produce markedly broader linewidths, ranging from 1200 to 3000 G (Kim et al., 2011). The reason for these differences in EPR linewidths are primarily the different causes for the negative charge characteristic for most manganese oxides (Kim et al., 2011). In biogenic precipitates the crystal structure includes layer site vacancies whereas the reason for negative charge of abiogenic manganese oxides is due to an exchange of higher valence manganese ions for lower valence ions (Kim et al., 2011; Villalobos et al., 2003). Results show a multicomponent EPR spectrum which is a superposition of two or possibly three components. One component having a linewidth of 1800 G and one having 600 G. The multicomponent character of the spectrum is likely due to the content of both biogenic and abiogenic manganese compounds in the YBS.

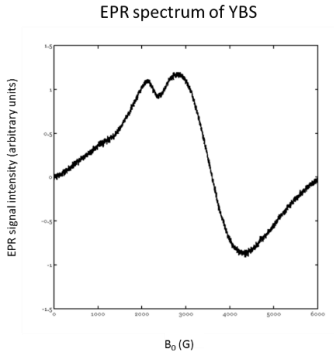

Fig.26: A multicomponent electron paramagnetic resonance (EPR) spectrum of the YBS showing superposition of two or possibly three components.

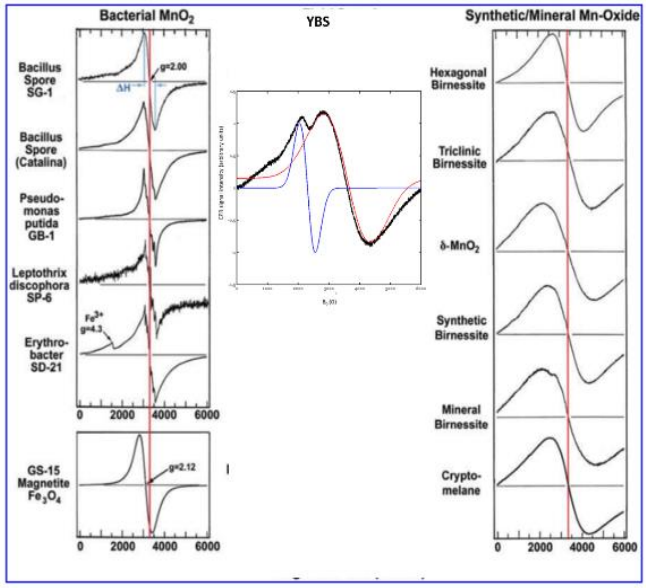

Fig.27: Left: EPR spectra of biogenic manganese oxides characterized by narrow spectral linewidths (~500 G). Middle: Multicomponent EPR spectrum of YBS, likely consisting of one biogenic component having a spectral width of 600 G (blue line) and one abiotic component having a spectral width of 1800 G (red line). Right: EPR spectra of synthetic or abiotic precipitated manganese oxides characterized by broader spectral linewidths (~1200-3000 G). Modified after Kim et al., (2011).

6. DISCUSSION

Chemical composition

Results from loss on ignition show that that the sample is rich in varying degrees of loosely attached water. It can thus be concluded that the material has hygroscopic properties and appear to attract water from its surroundings. It also readily suspends in water when agitated, and the fine particles stay floating for hours until they finally settle. This could be an indication of a high content of crystalline water. The carbon content of the YBS is very low (C_{tot} 1.81wt.%) relative to samples of carbonaceous matter investigated in previous studies where concentrations range from 46 to 86wt.% (Sandström et al., 2006). Clearly this is not a carbonaceous matter in the sense that carbon is the major constituent of the sample. Results also show losses on ignition of 14 and 27wt.% at 450°C and 1050°C respectively (expressed as weight percent of the dry substance). Knowing that these percentages only consist of a small fraction of carbon, it is plausible that the remaining loss mainly correspond to crystalline water and possibly conversion of hydroxides to oxides.

Geochemical analyses in combination with data from electron scanning microscopy show that the bulk of the YBS primarily consists of manganese-calcium oxides-hydroxides and a minor phase that includes fluorine. Given the relatively low concentrations of carbon (1.81wt.%), nitrogen (0.09wt.%) and sulphur (0.08wt.%), it seems likely that the dominating anion is the hydroxyl ion (OH^-) and to a minor extent carbon, nitrogen, sulphur and fluorine complexes. The dominating cations are clearly manganese and calcium. Results for most of the major elements differ between the rinsed and sieved YBS sample and the unrinsed and sieved sample. SiO_2 is almost completely absent in the former and only half of the calcium is left. This indicates that a large percentage of these elements are weathering products from the bedrock and the calcium carbonate blanket and exist as particles larger than the bulk of the sample and thus as separate phases. These results are also supported by the XRD analysis where the three major peaks most probably correspond to quartz, feldspar and calcite. The presence of carbonates in the sample is also confirmed by the difference in concentration between C_{tot} and C_{org}. Results also confirm that REEs are present in substantial concentrations in the YBS.

Mineralogy and microstructures

The XRD spectrum of the YBS illustrates the low crystallinity of the sample; there are few distinct peaks and most of the refractions are gathered as clusters of small peaks creating humps in the spectra. The three clearly identifiable phases, quartz, calcite and plagioclase most probably reflect the content of the calcium carbonate cover and the underlying rock. XRD results further suggest that there is a mixture of primarily tetravalent manganese phases present in the Ytterby sample. It is likely that these phases are poorly crystalline birnessite $(Na,Ca)Mn_7O_{14}*2.8H_20$, vernadite ($\delta MnO_2$) MnO_2*nH_2O, pyrolusite MnO_2 and possibly todorokite $(Ca,Na,K)_X(Mn^{4+},Mn^{3+})_6O_{12}*3,5H_2O$. Considering the results of the chemical analyses of the Ytterby sample and data given by SEM sessions, it is likely that the dominant phases in this material incorporate both manganese and calcium in their mineral structure. Both the birnessite-group of hydrous manganese oxides and todorokite have chemical formulas including calcium while vernadite is reported to frequently contain minor amounts of this element (Post, 1999). In addition both todorokite and vernadite often contain high concentrations of Co, Ni, Cu and metals such as REEs (Glasby, 2006). Further comparisons to XRD spectra imply that the poorly crystalline birnessite in the YBS has hexagonal unit cell symmetry as opposed to triclinic symmetry of more ordered birnessite (Villalobos et al., 2003). Moreover, considering the results of the chemical analysis, SEM analysis and X-ray diffraction analysis, it is highly likely that the major absorbance below 800 cm^{-1} in the infrared spectrum reflects the existence of these manganese oxides-hydroxides. Previous results of infrared spectra of tetravalent manganese oxides show that some of these phases have absorbances at similar wavelengths as the Ytterby sample (Potter and Rossman, 1979). However, the fine resolution

of these reference minerals was not possible to obtain on the Ytterby sample which once again tells that this is an ill-defined compound.

SEM-analyses revealed that mainly three different Mn microstructures exist in the YBS: dendritic or shrub-like, microspherolitic/botryoidal and wad-like spheres frequently covered by filaments of varying thickness. The internal structure of the microsherolitic/botryoidal morphology shows lamination which implies an iterative change in production. This is also the case for the shrub-like structures but in these the lamination occurs more randomly. The alternating light and dark layers mainly express variation in Mn and Ca concentrations but also in the Mn/Ca ratios. In contrast to other Mn accumulations reported about, the Fe content of the YBS is very low. Concentrations of 1300 ppm in the YBS can be compared to concentrations of 321 000 ppm reported for ferromanganese concretions in the Baltic Sea (Ingri, 1985).

The fact that the mineral assemblage suggested to be present in the YBS appear to coincide with the dominant phases, birnessite, todorokite and vernadite, (See complete list of sources in Post, 1999) present in manganese nodules is interesting. This similarity made me think that the YBS perhaps was a suspended analogue to lithified manganese nodules. Further observations revealed nodular outgrowths or flattened crusts attached to the tunnel walls or sitting in rock crevices. These outgrowths are approximately 2-10 mm in diameter and located in a previously water-filled tunnel next to the mine shaft in contrast to the YBS which is located in a dry tunnel further away from the shaft which has never been water-filled (Fig.3). Initial SEM-analyses revealed a bulk material rather different from the YBS. The main constituent of these outgrowths is carbon and to a minor extent silica, oxygen and sulphur. However, the silver-rich or possibly silver-coated microspheres which exist as separate components in the YBS (Fig.16) are also present in these outgrowths which provides a possible link between the two materials. Moreover, the SEM-analyses revealed two seemingly organic microstructures rich in carbon and zink. For more information and images of these outgrowths and its constituents, the reader should consult appendix 5.

Isotopic signatures of C, N and S in the YBS

Results show that approximately 0.6% of the dried matter is organically derived carbon. The origin of this organic matter can be traced using the concentrations and isotopic signatures of C, N and S combined with the information retrieved from the lipid analysis.

The average $\delta^{13}C$ signature for C_3 terrestrial plants is -27‰ to -26‰ while the corresponding value for marine plants is approximately -20‰ (Sharp, 2007). Thus, values for freshwater lakes are usually found somewhere in between the marine and terrestrial signatures. In accordance with the typical values described above, a recent study on the Stockholm archipelago sediments concluded that the $\delta^{13}C$ signature increased along a freshwater-brackish gradient with values from -28.2±0.6‰ in Lake Mälaren to -23.6±0.3‰ in the outer archipelago (Jönsson et al., 2005). From this I can conclude that the $\delta^{13}C$ signature of the YBS (-24.73±0.15‰) is similar to values reported for sediments in the inner Stockholm archipelago (-25.4±1.0‰) but slightly more marine. This vague marine signal is strengthened by a C:N molar ratio of 7.6 which is very close to the Redfield ratio of ~6.6. Even though the influence of terrestrial material is expected to be high in a location such as the Ytterby mine tunnels, the $\delta^{13}C$ signature primarily appears to reflect the proximity to the brackish Baltic water.

Present data show a very high $\delta^{15}N$-value of 13.99±0.15‰ which indicates that the sample is enriched in the heavy isotope relative to the standard. Activities that involve large fractionation of nitrogen include different microbial soil processes such as nitrification and denitrification (Fry, 2006). Denitrification enriches the soil in the heavy isotope through the loss of light nitrogen to the atmosphere (Sharp, 2007). Suggested source materials having $\delta^{15}N$ signals as high as 13.99‰ are organic fertilizers (Sharp, 2007) and sewage (Heaton, 1986). However, from these data it is not possible to conclude why the YBS carries such a high $\delta^{15}N$

signature, but it is likely an indicator of possible anthropogenic nitrogen input or extensive microbial activity.

A $\delta^{34}S$ signature of 8.8±0.2‰ is relatively close to precipitation values in Sweden the last 50 years (~5-6). A pure marine signal would have been around 17‰ to 21‰ while the corresponding values for terrestrial vegetation range from 2‰ to 6‰ (Fry, 2006). The C:S molar ratio is 19.7. This could be interpreted as a marine signal mixed with pyrite or some other sulphide mineral.

Lipid analysis

The search for molecular fragmentation patterns and recognizable mass spectra has provided valuable complementary information about the organic fraction of the YBS. Results revealed a larger apolar fraction and a smaller mid- and polar one. The hydrocarbon part of the apolar fraction is degraded and more processed than the polar one and thus corresponds to ancient organic matter while the polar one indicates more recent material. Each fraction is discussed in more detail below.

A:1 fraction
The left part of the spectrum is dominated by degraded and processed hydrocarbons of varying shapes and structures. The biological origin of these compounds is no longer traceable but it appears likely that sedimentary vestiges in rock crevices are the source. Among the ancient hydrocarbons, there are two major peaks both corresponding to long chain alcohols. These compounds are not part of the ancient material but rather contemporary biological markers which are difficult to contribute to a specific source (Peters et al., 2005). The Diploptene peak corresponds to approximately 40% of this fraction and is therefore a major component of the material. Diploptene belongs to the hopanoid group of compounds and is the simplest C_{30}-hopane. Considering the intensity of the peak, it is highly unlikely that it has been transported far and we strongly suspect that it has been produced in situ. If it had been transported, the peak would have been degraded. Since we know that hopanoids are made by eubacteria and that this is a dark environment where no photosynthesis occurs, we can exclude photosynthetic eubacteria from possible bacteria present in the YBS.

A:2 fraction
The middle fraction is divided in two main sections; a group of aldehydes and ketones at the left side of the spectra and hopanoid compounds on the right. Hopanoids, which is a very interesting group of biomarkers associated with bacterial communities, are recurrent in all three fractions but primarily so in the mid-fraction where they occur as both simple and extended hopanes. The presence of the C_{31} to C_{35} extended side chain species of hopanes is a distinct sign of bacterial presence in the depositional environment. The relative distributon of the 17β21β –hopanes and 17α21β –hopanes allows for an estimation of the maturity of the organic matter. The 17β21β –hopanes transform with time to the more stable 17α21β –hopanes which means that the higher the percentage of the α-version relative to the β-version, the more mature the organic matter is (Gaines et al., 2005). In the YBS there is a predominance of the α-version and thus of ancient organic matter. However, a source of ambiguity is that the spectra of these compounds are based on a very small amount of organic matter which makes conclusions less reliable. The other very exciting aspect of the lipid identification is the search for what type of bacteria that produce the identified hopanes. It is known that hopanes appear to be limited to eubacteria and are often found in methanotrophs, cyanobacteria and organisms belonging to the α-proteobacteria such as the nitrogen-fixing eubacteria (see complete list of sources in Peters et al., 2005). It is also known that they are frequent in bacterial species living in stressful environments where they are thought to provide rigidity and adjustable permeability to the cell membrane (see complete list of sources in Peters el al., 2005). The really interesting question is what type of eubacteria that produce the identified hopanes. When time allows, it may well be rewarding to dig deeper into this field and try to identify the precise strains of these extended

hopanes. From these data it is not possible to determine whether this is a living or fossilized community of microorganisms. However, based on the predominance of 17α21β- over 17β21β -hopanes the bacterial remains appear to consist of fossilized mature matter while in contrast, the intensity of a number of peaks strongly suggest that it has been produced in situ. These results fit well the overall signature of the organic part as being a mixture of ancient and contemporary marine and terrestrial matter.

A:3 fraction
This fraction is dominated by compounds associated with terrestrial higher plants or diatoms (Gaines et al., 2009) and to a minor extent by components indicating bacterial presence.

Origin, transport and deposition

The Ytterby mine is located along the Baltic coastline and the marine influence on the YBS is visible in the $\delta^{13}C$ signature, the relative concentrations of organic carbon and nitrogen and to a certain extent the identified lipids. However, chemical and mineralogical data clearly show that calcium concentrations are high in both groundwaters and the YBS, which rather suggests a dominating terrestrial influence. Information derived from the identified lipid biomarkers reflects the highly variable content of the organic matter. This is a mixture of ancient and contemporary matter of both terrestrial and marine origin and within this organic mixture there are clear signs of bacterial presence. Considering the clean peaks in the lipid spectra, this is likely to be a living community of microorganisms. I have not been able to identify a sedimentary source rock in the close environment but through geologic history these Svecofennian rocks have been covered by sediments now eroded away. The ancient part of the organic matter is likely sedimentary detritus once caught in these rock fractures and now released or possibly remains of the previously stored petroleum products. This mixture of organic matter has been transported by groundwater to the present mine location.

The fact that the mineral assemblage suggested to be present in the YBS appear to coincide with the dominant phases, birnessite, todorokite and vernadite, (See complete list of sources in Post, 1999) present in manganese nodules is interesting. However, these three minerals are also common in oxidized terrestrial environments (Post, 1999) and of particular interest in groundwater systems or in similar surface environments (Tuhela, 1997). Terrestrial phyllomanganates are typically rich in calcium. If they were marine then they would be enriched in magnesium. The reason is that the relatively higher concentrations of magnesium compared to calcium in seawater while the opposite conditions prevail in freshwater (see complete list of sources in Bodeï et al, 2007). This suggests that these hydrous manganese oxides have precipitated from groundwater in the Ytterby area. This suggestion is also strengthened by the chemical results showing higher manganese concentrations in fracture groundwater compared to the mine and water shaft samples. Furthermore, the absence of manganese in the water separated from the YBS suggest that both dissolved and suspended manganese precipitated when water left the crack, creating the bulk of the YBS. It appears as two different phases precipitate from the fracture groundwater; the lithified layer of $CaCO_3$ and the YBS. Whether or not these two phases have interacted is not known but it seems likely. Soils in this area are rich in calcium carbonate which originates from sedimentary rocks in the Baltic Sea. The high calcium concentrations in the groundwater samples are probably a result of the presence of these soils. This is an area where groundwaters reflect both the composition of brackish-marine water and fresh meteoric water.

Accumulations of fine-grained masses of manganese oxides like the YBS commonly occur as weathering and alteration products of primary manganese carbonate, silicate or oxide minerals or of other minerals where manganese substitutes for elements like iron or magnesium (Nesse, 2000). Despite the well documented mineralogy of the Ytterby pegmatite, there are no manganese minerals except from garnets (may be of the manganese type) reported from the area. The YBS therefore likely represents the first manganese minerals detected in this historic

location. However, there are a number of minerals in which manganese likely constitutes a minor component. It is possible that small particles, colloids, resulting from manganese weathering have become suspended in groundwaters in the Ytterby mine area and thus have started to move along fractures and are now circulating in the groundwater system. Manganese oxides are commonly negatively charged and therefore readily attract and adsorb various cationic species and thus work as metal traps (Tuhela, 1997; Tebo et al., 2004).This characteristic combined with the fact that Ytterby is the type locality for a number of REEs provides a plausible explanation for the high REE concentrations measured in the YBS. I therefore suggest that these manganese complexes are likely to contribute to the mobility of the REEs and that the YBS thus acts as a sink for heavy metals and particularly so for REEs in the Ytterby mine area.

The REE behaviour in Ytterby is of particular interest considering its history as the type locality for yttrium and six REEs and concentrations in the YBS are one to two orders of magnitude higher compared to concentrations in local rocks. Previous results show that the REE occurrences are highly localized in the quarry pegmatite and that local W-E trending vertical faults, displacing the contact between the amphibolite and the pegmatite in the quarry area, appear to have locally controlled the distribution of REEs (Sjöberg, 2012). These findings are consistent with the description in Almström (1925) of how the rare minerals were clustered close to the ground surface in the ESE corner of the quarry. In the mine tunnels there are a number of pegmatite veins of varying size. Whether the rare minerals are as frequent in the tunnel pegmatites as in the quarry pegmatite is not known, but their absence in the neighbouring rocks suggest that they have been trapped in this manganese rich fluid and transported through cracks in the rocks until deposited at this location. From this I conclude that the YBS is most likely a secondary deposit where REEs from a primary deposit such as the adjacent pegmatites are concentrated by sedimentary processes and weathering. However, the chondrite normalised pattern of the YBS is almost identical to the neighbouring metagranite, showing enrichment in LREEs and pronounced negative Eu anomalies. Apparantly this is a pattern often seen in granitic and metagranitic rocks (Sandström et al., 2008) which suggests that the REE concentrations in the YBS originates from the adjacent metagranites and not the Ytterby pegmatites which in contrast are enriched in the HREEs. Data also show that concentrations of all REEs except Eu (in the more mafic rock) are higher in the altered fracture rocks compared to fresh rocks of similar types. This suggest that there is a substance-rock exchange where the rocks are affected by the YBS and not the other way around. This transport might have occurred through microcracks which also would explain why samples collected close to the fracture contained thorium and REE enriched fluids. However, given the compositional differences between the YBS and the fluid detected in the rock, it is also possible that these two substances are not related at all.

Even though the organic carbon content is low, the influence of microorganisms in the accumulation of manganese oxides may still be important. Inorganic oxidation of Mn^{2+} to Mn^{3+} and Mn^{4+} is a slow process that takes years to complete in environments with pH up to 8.5 (Tebo et al., 2004). Biologically catalyzed oxidation is more rapid and a substantial number of scientific reports argue that biotic precipitation is responsible for the majority of manganese accumulations (Tebo et al, 2004). This is commonly made by various types of bacteria and fungi (Tebo et al., 2004) and apparently it is sufficient with a rather small community to guarantee that the initial production is dominated by biological activity (see complete lists of sources in Konhauser, 2007). In the Ytterby substance, lipid biomarkers show distinct signs of bacterial presence and also suggest that that this presence is caused by eubacteria or possibly fungi. Moreover, since there is no sunlight in the tunnels, these bacteria have to be light independent. Considering the mine's history as a fuel deposit, the previously stored petroleum products may have provided a major source of carbon in the area and combined with the seeping fracture-water created favourable growth conditions for microorganisms. SEM-images also revealed structures which appear to have a biological origin, i.e. capsules, biofilm and what may be tunnels that bacteria left behind. Apparently, microorganisms living in manganese- or iron-rich

environments are often encrusted in the precipitates (Tuhela, 1997). Recently, a new technique based on electron paramagnetic resonance (EPR) has been used to distinguish abiotically and biotically precipitated manganese. (Kim et al., 2011). I had the opportunity to run such a test on the Ytterby sample and results indicate a two or multiple component substance where one part is likely to be biotically precipitated and the other one abiotically precipitated.

7. CONCLUSIONS AND FUTURE RESEARCH

This study identifies the YBS as a Mn- and Ca-bearing substance highly enriched in yttrium (Y) and rare earth elements (REE). A minor phase that includes fluorine is also present. The organic content is low. The mineral assemblage is suggested to primarily consist of poorly crystalline birnessite, vernadite and pyrolusite and the observed internal lamination of one of these manganese oxides-hydroxides implies an iterative change in production. The high calcium concentration indicates a terrestrial origin. Previous results show that the REE occurrences in Ytterby are found in the quarry pegmatite and that they are highly localized within it. It is therefore suggested that manganese colloids, suspended in the local groundwater, work as metal traps and likely contribute to the mobility of the REEs. The black substance acts thus as a sink for these metals in the Ytterby mine area. Oxidizing conditions in a previously anoxic environment has induced changes in biogeochemical processes and even though the organic content is low the influence of microorganisms in the accumulation of these manganese oxides appears to be important. Lipid biomarkers provide evidence of bacterial presenceand also suggest that this presence is caused by *in situ* production of light independent eubacteria. Results imply that the YBS is a two, or multiple, component substance where at least one part has a biogenic signature.

I would like to conclude this thesis by suggesting a number of areas for future research:

The redistribution of REEs in the Ytterby mine area.
An extended evaluation and discussion of the observed chondrite normalized REE-pattern of the YBS is necessary for determining the source of the REEs. Further studies are also suggested to identify redistribution mechanisms for the REEs. A comparison with reported values of REEs in secondary minerals may indicate that the accumulation in the YBS is among the highest observed.

Establish the chemistry of the secondary REE-bearing phases.
A sequential extraction procedure may give information on the nature of the Mn-REE association, and possibly the reason for the low content of Fe. Successive SEM and XRD-analyses, after controlled extraction/leaching, may possibly indicate what mineral components, if any, are active in the REE accumulation process.

Evaluation of the composition of the organic matter in the YBS –
Characterization of the microbial community -
The detailed analysis of the organic fraction of the YBS (identified organic compounds as well as stable isotopes of C, N, S) is the basis for further evaluation. To help identify the most complex lipid signals, a $\delta^{13}C$ analysis should be made on the extracted lipids. A future study combining these data with a characterization of the microbial community present in the YBS would provide information about the source of the YBS and about the current accumulation processes. An analysis of the observed gas bubbles will be included in this study.

Groundwater and mine water chemistry
At present there is a lack of analytical data on the anions in recorded water compositions. This largely prevents a detailed evaluation of the origin of the water in e.g. the fractures with YBS. Existing compositional data of the water systems should therefore be complemented with new analyses (major an- and cations, trace elements, DOC and so forth) for all relevant waters, i.e.

groundwater, surface water, fracture water and water from the mine shaft. These data should thereafter be compiled and evaluated.

The mineralogy of the Ytterby mine

At least 50 minerals have been identified in the Ytterby mine and approximately 15 of these minerals include REEs. There are no manganese minerals except from garnets (may be of the manganese type) reported from the area. The YBS therefore likely represents the first manganese minerals detected in this historic location and it would therefore be of interest to identify all minerals present.

ACKNOWLEDGEMENTS

I thank my supervisors Alasdair Skelton (Stockholm University) and Bert Allard (Örebro University) for valuable discussions during this work, Jayne Rattray (Stockholm University) for her expert guidance through the lipid analysis, Martin Lundmark (The Swedish Fortifications Agency) and P-O Lindgren (The Swedish Defence) for their generosity of letting me visit the Ytterby mine as often as necessary and for sharing data on this unique locality, Dan Zetterberg for his fine work making thin sections, Marianne Ahlbom, Heike Siegmund and Malin Söderman (Stockholm University) for their assistance with ESEM and isotope analysis, respectively, Eve Arnold (Stockholm University) for guidance on the interpretation of XRD-spectra, Magnus Mörth (Stocholm University) for valuable discussions, Joakim Mansfeld (Stockholm University) for advice and input on rocks in the Ytterby area, Curt Broman (Stockholm University) for the Raman analysis, Anders Engqvist (Royal Institute of Technology, Stockholm) for review, Anna Neubeck who introduced me into the fascinating world of microbes, Håkan Gustafsson (University of Linköping) and Magnus Ivarsson (Swedish Museum of Natural History) for performing the EPR analysis and for providing valuable knowledge in this field, respectively.

REFERENCES

Books

Bertini, I. and Rosato, A., (2010), *The role of metals*, Handbook of Hydrocarbon and Lipid Microbiology, Springer-Verlag, Berlin, Heidelberg.

Blatt, H. et al., (2006), *Petrology-Igneous, Sedimentary and Metamorphic*, 3rd ed., W. H. Freeman, New York. USA

Boss, C.B. and Fredeen, K.J., (1997), Concepts, Instrumentation and Techniques in Inductively Coupled Plasma Optical Emission Spectrometry, second edition, Perkin Elmer, USA

Boynton, W.V., (1984), *Cosmochemistry of the rare earth elements: meteorite studies*, Developments in geochemistry, 2:63-114

Brindley, G.W. and Brown, G. (1980) , *Crystal Structures of Clay Minerals and their x-ray identification*, Mineralogical Society, Monogragph No.5, London, pp 495

Bydén, S. et al., (2003), *Mäta vatten – Undersökningar av sött och salt vatten*, tredje upplagan, Institutionen för miljövetenskap och kulturvård Göteborgs Universitet

Fersman, A.E., (1931), *Les pegmatites-leur importance scientifique et pratique, tome III, les pegmatites granitiques*, Academie des sciences de L'U.R.S.S.

Fry, B., (2006), *Stable Isotope Ecology*, Springer New York

Gaines, S. M., Eglinton, G. and Rullkötter, J., (2009), *Echoes of life, what fossil molecules reveal about Earth history*, Oxford University Press

Hunt, J., M., (1995), *Petroleum Geochemistry and Geology, Second Edition*, W.H. Freeman and Company, United States of America

Lang, L., Holly, S. and Sohar, P (Eds), (1974), *Absorbtion spectra in the infrared region. Vol.1.Theoretical and technical introduction.* Academiai Kiado, Budapest.

Lindqvist, B., (1989), *Stockholms skärgård i periodiska systemet*, naturen berättar, utveckling och forskning vid Naturhistoriska rikdmuséet, p.89

London, D., (2008), *Pegmatites*, the Canadian mineralogist, special publication 10, the mineralogical association of Canada

Nelson Eby, G., (2004), *Principles of Environmental Geochemistry*, Brooks/Cole, Cengage Learning, USA

Nesse, W.D., (2000), *Introduction to mineralogy*, Oxford University Press

Peters, K.E. et al., (2005), *The Biomarker Guide, volume 1, Biomarkers and isotopes in the environment and human history*, Cambridge University Press

Peters, K.E. et al., (2005), *The Biomarker Guide, volume 2, Biomarkers and isotopes in petroleum exploration and earth history*, Cambridge University Press

Rouessac, F. and Rouessac A., (2007), *Chemical Analysis - Modern Instrumentation Methods and Techniques*, Second Edition, John Wiley & Sons Ltd

Schlesinger, W.H. and Bernhardt, E.S., (2012), *Biogeochemistry, an analysis of global change, third edition*, Elsevier

Sharp, Z., (2007), *Principles of Stable Isotope Geochemistry*, 1st editon, Pearson Education Inc

White, W. M., (2013), *Geochemistry*, John Wiley & Sons

Articles and Papers

Adams, J.P. et al., (2008), *Mn-oxides and sequestration of heavy metals in a suburban catchment basin of the Chesapeake Bay watershed*, Environ Geology, 58:1269-1280

Aliferis, K.A. and Jabaji, S., (2010), *Metabolite composition and bioactivity of Rhizoctonia solani sclerotial exudates*, J. Agric. Food Chem, 58:7604-7615

Bengtson, S. and M. Ivarsson et al., (2014), *Deep-biosphere consortium of fungi and prokaryotes in Eocene subseafloor basalts*, Geobiology,12:6:489-496

Bodeï, S. et al., (2007), *Formation of todorokite from vernadite in Ni-rich hemipelagic sediments*, Geochimica et Cosmochimica Acta, 71:5698-5716

Černý, P., (1992), Geochemical and petrogenetic features of mineralization in rare-element granitic pegmatites in the light of current research, Department of geological sciences, University of Manitoba, Canada

Černý, P. and Ercit, T. S., (2005), *Classification of granitic pegmatites revisited*, Can. Mineral., 43:2005-2026

Chafetz, H.S. and Guidry S.A., (1999), *Bacterial shrubs, crystal shrubs, and ray-drystal shrubs: bacterial vs. abiotic precipitation,* Sedimentary Geology, 126:57-74

Chukanov, N.V. et al., (2009), *Carbonaceous matter in pegmatites of different genetic types and their role in formation of mineral associations*, New data on minerals. M., 44

Cooke, M. et al., (2009), *Bacteriohopanepolyol biomarker composition of organic matter exported to the Arctic Ocean by seven of the major Arctic rivers*, Organic Geochemistry, 40:11:1151-1159

Frondel, C., (1953), *New manganese oxides – Hydrohausmannite and Woodruffite*, American Mineralogist, 38:9-10

Grant, J.A., (1986), *The Isocon diagram – a simple solution to Gresen's equation for metasomatic alteration*, Econ.Geol, 81:1976-1982

Heaton, T. H. E., (1986), *Isotopic studies of nitrogen pollution in the hydrosphere and antomsphere: a review*, Chemical Geology, 59:87-102

Heiri, O. et al., (2001), *Loss on ignition as a method for estimating organic and carbonate contenet in sediments: reproducibility and comparability of results*, Journal of Paleolimnology 25: 101-110

Ingri, J., (1985), *Geochemistry of ferromanganese concretions in the Barents Sea*, Marine Geology, 67:101-119

Jönsson, A., (2005), *Evalutation of the Stockholm Archipelago sediments, northwestern Baltic Sea Proper, as a trap for freshwater runoff organic carbon*, Journal of marine systems, 56:167-178

Kim, S.J., (1991), *New characterization of takanelite*, American Mineralogist, 76:1426-1430

Kim, S. S., (2011), *Searching for Biosignatures using Electron Paramagnetic Resonance (EPR) Analysis of Manganese Oxides*, Astrobiology, 11:8:2011

Lööf, E., (1981), *Ytterby gruva*, Hembygdsskrift Nr 2 kap 3, Österåkers Hembygds- och fornminnesförening, Österåker, Sweden

McClelland, J.W. and Valiela, I., (1998), *Linking nitrogen in estuarine producers to land-derived sources*, Limnology and Oceanography, 43:577-585

Nordenskiöld, N., (1893), 677-678

Nordenskjöld, I., (1904), *Ytterby Fältspatbrott*, Skandinavisk Tidskrift för Lervaru- och Stenindustri, Organ för tegel, cement, beton, kalk, sten och byggnadsmaterialier, N:o 6 & 7, Stockholm, Sweden

Piper, D. Z. and Williamson M. E, (1981), *Mineralogy and composition of concentric layers within a manganese nodule from the north pacific ocean*, Marine Geology, 40: 255-268

Post, J. E., (1999), *Manganese oxide minerals: Crystal structures and economic and environmental significance*, PNAS (Proceedings of the National Academy of Sciences of the United States of America), 96:7:3447-3454

Potter, R.M. and Rossman, G.R., (1979), *The tetravalent manganese oxides: identification, hydration, and structural relationships by infrared spectroscopy*, American Mineralogist, 64:199-1218

Rossi, C. et al., (2010), *Manganese stromatolites in caves: El Soplaou (Cantabria, Spain)*, Geology, 38:1119-1122

Rönnback, P. et al., (2008), *Comparison of the behaviour of rare earth elements in surface waters, overburden waters and bedrock groundwaters in two granitoidic settings, Eastern Sweden*, Applied Geochemistry, 23:1862-1880

Sadegi, M. et al., (2013), *Rare earth element distribution and mineralization in Sweden: An application of principal component analysis to FOREGS soil geochemistry*, Journal of Geochemical Exploration, 133:160-175

Sandström, B. et al. (2006), *The occurrence and potential origin of asphaltite in bedrock fractures, Forsmark, central Sweden*, GFF, 128:3:233-242

Sandström, B., Annersten, H. and Tullborg, E-L., (2008*), Fracture-related hydrothermal alteration of metagranitic rock and associated changes in mineralogy, geochemistry and degree of oxidation: a case study at Forsmark, central Sweden*, International Journal of Earth Sciences, 99:1-25

Simoneit, B.R.I., (2002), *Molecular indicators (Biomarkers) of past life*, The Anatomical Record, 268: 186-195

Sundius, N., (1948), *Beskrivning till Berggrundskarta över Stockholmstrakten*, Sveriges Geologiska Undersökning, Ser. Ba, N:o 13, Kungl. Boktryckeriet, P.A. Norstedt & Söner, Stockholm, Sweden

Sundius, N., (1948), *Berggrundskarta över Stockholmstrakten*, Skala 1:50 000, Sveriges Geologiska Undersökning, Ser. Ba, N:o 13, Generalstabens Litografiska Anstalt, Stockholm, Sweden

Simmons, Wm. B. and Webber, K. L, (2008), *Pegmatite genesis: state of the art*, Eur. J. Mineral, 20:421-438

Talbot, H.M. et al., (2007), *Structural characterization of unsaturated bacterial hopaoids of atmospheric pressure chemical ionization liquid chromatography/ion trap mass spectrometry, Rapid Communications in mass spectrometry*, 21:1613-1622

Tebo et al., (2004), *Biogenic Manganese Oxides: Properties and Mechanisms of Formation, Annual Reviews*, Earth and Planetary Sciences, 32:287-328

Tuhela, L., et al., (1997), *Biogeochemical transformation of Fe and Mn in oxic groundwater and well water environments*, Journal of Environmental Science and Health, A34, Environmental Science and Engineering and Toxicology, 32:2

Villalobos et al., (2003), *Characterization of the manganese oxide produced by Pseudomonas putida strain MnB1*, Geochimica et Cosmochimica Acta, 67:14:2649-2662

Voss. M. et al.,(2000), *Stable isotope signals of eutrophication in Baltic Seas sediments*, Journal of Marine Systems, 25:287-298

Welin, E., (1966), *The Occurrence of Asphaltite and Thucholite in the Precambrian Bedrock of Sweden*, Geologiska Föreningen i Stockholm Förhandlingar, 87:4:509-526

Other published sources

Geological Survey of Sweden (SGU), (2013*), Bedömningsgrunder för grundvatten*, SGU-rapport 2013:01

J&W Energi och Miljö, Kemakta Konsult AB, (2001), Fortifikationsverket, *Miljökonsekvensutredning för avveckling av Fortifikationsverkets oljelagringsanläggning i Ytterby, Vaxholms kommun*

Rattray, J.E., (2008*), Ladderane lipids in anammos bacteria: occurrence, biosynthesis and application as environmental markers*, Dissertation, no. 288, Faculteit Geowetenschappen Universiteit Utrecht

World Health Organization, WHO (2011), *Guidelines for drinking-water quality, fourth edition*, Geneva

Unpublished sources

Fortifikationsverket, (2012), *Utredningsprogram Ytterby, Vaxholms Kommun; 4:610, 4:564, 4:611, 4:9,* Rev A, 2012-04-10

Kungliga Fortifikationsförvaltningens ritning nr. M101, (1957).

Undocumented interviews

Lindgren, P-O, (2014), FD Drivmedelsinspektör, Försvarsmaktens Logistik, FM LOG

Lundmark, M, (2014), Skyddsinspektör, Fortifikationsverket

Internet

http://www.actlabs.com/ (June 30, 2014)

http://www.doitpoms.ac.uk/tlplib/xray-diffraction/index.php (July 3, 2014)

http://lipidlibrary.aocs.org/ (September 27, 2014)

http://mee-inc.com/index.html (November, 2014)

http://www.mindat.org/ (June 30, 2014)

http://rruff.geo.arizona.edu/AMS/amcsd.php (July 3, 2014)

http://www.vanpetro.com/ (June 12, 2014)

http://webmineral.com/ (September 20, 2014)

Appendix 1

Minerals found in Ytterby

The Ytterby pegmatite which is situated in the south-eastern corner of Resarö island mainly consists of large crystals of quartz and feldspar but there is also a considerable amount of other minerals. The Swedish Museum of Natural History, Stockholm has made an account for them all. Chemical formulas are taken from mindat.org (2012), Blatt, H et al, (2006). To note is that radioactive trace elements are not included in the chemical formulas.

albite – $NaAlSi_3O_8$
allanite - $(CaY)(Al_2Fe^{2+})(Si_2O_7)(SiO4)O(OH)$
anderbergite - (Zr, Ca, Si, O, H, REE) (also contains Th_2O_5, see Nordenskjöld, 1908 for a complete analysis)
apatite – $Ca_5(PO_4)_3(F,OH,Cl)$
arrhenite - (Y, Er, Ca, Zr, Ta, Si,O),
bastnäsit(Ce) – $(Ce,La)(CO_3)F$
bertrandite – $Be_4(Si_2O_7)(OH)_2$
beryl – $Be_3Al_2(Si_6O_{18})$
Biotite – $K(Fe,Mg)_3AlSi_3O_{10}(OH)_4$
bismuth – Bi
calcite – $(CaCO_3)$
Chlorite – $(Mg,Fe)_5Al_2Si_3O_{10}(OH)_8$
chrysoberyl- $(BeAl_2O_4)$
cordierite – (Fe,Mg)2Al4Si5O18, At low P in peraluminous rocks
cyrtolite – $Zr((SiO_4),(OH)_4)$
epidote – $Ca_2Al_2Fe^{3+}SiO_4Si_2O_7(O,OH)$
Fergusonite – $(Y,Ce,La,Nd,Y)NbO_4$ (also contains UO_3, see Nordenskjöld, 1908 for a complete analysis)
fluorite – CaF_2
Gadolinite – $Y_2Fe^{2+}Be_2Si_2O_{10}$ (also contains ThO_2 and Ce_2O_3, see Nordenskjöld, 1908 for a complete analysis)
Galena –PbS
Garnet -
Hisingerite- $Fe^{3+}{}_2(Si_2O_5)(OH)_4*2H_2O$
keiviite-(Y) – $(Y,Yb)_2(Si_2O_7)$
Kimuraite-(Y) – $Ca(Y,Nd)_2(CO_3)_4*6H_2O$
Lanthanite – $(La,Ce)_2(CO_3)_3*8H_2O$
Lokkait-(Y) – $Ca(Y,Gd,Nd,Dy)_4(CO_3)_7*9H_2O$
Magnetite – $Fe^{2+}Fe^{3+}{}_2O_4$
Microcline – $KAlSi_3O_8$
Microclinperthite – Mixture of Albite-Anorthite series, K-feldspar
Milarite – $K_2Ca_4Al_2Be_4Si_{24}O_{60}\cdot H_2O$
Molybdenite – MoS_2
Monazite – $CePO_4$ – Typical high content of LREEs Th and U
Muscovite – $KAl_3Si_3O_{10}(OH)_2$
Oligoclas – $(Na,Ca)(Al(Si,Al)Si_2O_8$
Orthoclase – $KAlSi_3O_8$
Plagioclase – $NaAlSi_3O_8$-$CaAl_2Si_2O_8$
Polycrase – $(Y,U)(Ti,NB)_2O_6$
Prehnite – $Ca_2Al_2Si_3O_{12}(OH)$
Pyrite – FeS_2
Pyrrhotite – $Fe_{1-X}S(X=0$ to $0.17)$
Quartz – SiO_2

Tengerite – $Y_2(CO_3)_3$*2-3H_2O
Thortvelite – $(Sc, Y)_2Si_2O_7$
Titanomagnetite – titanium rich magnetite
Wasit – a variety of allanite
Xenotime – $(Yb, Y, HREE)(PO_4)$
Yftisite-(Y) – $(Y,Dy,Er)_4(Ti,Sn)(SiO_4)_2O(F,OH)_6$
Yttrotantalite – $(Y,Ca,U^{4+},F^{2+})_2(Ta,Nb)_2O_8$ (also contains other REE, see Nordenskjöld, 1908 for a complete analysis)
Zircon – $ZrSiO_4$

Appendix 2

Chemical results of YBS and rocks

Analyte Symbol	Unit Symbol	Det. Limit	Analysis Method	14-YB-RINSED	14-YB-UNRINSED	14-YB-R01	14-YB-R02A	14-YB-R02B	14-YB-R03A	14-YB-R03B
SiO2	%	0.01	FUS-ICP	0.94	12.31	75.97	75.7	76.08	59.19	58.95
Al2O3	%	0.01	FUS-ICP	0.25	3.24	13.02	12.68	12.08	18.84	18.76
Fe2O3(T)	%	0.01	FUS-ICP	0.13	1.23	1	2.12	2.06	6.6	6.23
MnO	%	0.001	FUS-ICP	58.47	36.55	0.046	0.034	0.032	0.114	0.108
MgO	%	0.01	FUS-ICP	0.62	0.77	0.09	0.23	0.22	1.45	1.38
CaO	%	0.01	FUS-ICP	8.6	15.07	1.25	0.74	0.44	5.54	5.44
Na2O	%	0.01	FUS-ICP	0.06	0.82	2.92	2.74	2.88	4.64	4.57
K2O	%	0.01	FUS-ICP	0.1	0.53	4.97	5.25	5.12	1.49	1.38
TiO2	%	0.001	FUS-ICP	0.012	0.125	0.04	0.174	0.163	0.486	0.458
P205	%	0.01	FUS-ICP	0.07	0.08	<0.01	0.03	0.03	0.23	0.24
LOI	%		FUS-ICP	27.84	27.26	0.9	0.96	1.87	1.46	1.36
Total	%	0.01	FUS-ICP	97.08	97.98	100.2	100.7	101	100	98.87
Sc	ppm	1	FUS-ICP	2	4	2	3	3	12	11
Be	ppm	1	FUS-ICP	<1	1	4	2	2	3	2
V	ppm	5	FUS-ICP	587	368	26	33	33	71	68
Cr	ppm	20	FUS-MS	<20	20	390	360	370	270	190
Co	ppm	1	FUS-MS	174	119	2	3	3	11	11
Ni	ppm	20	FUS-MS	50	50	<20	<20	<20	<20	<20
Cu	ppm	10	FUS-MS	1540	1630	<10	<10	<10	<10	10
Zn	ppm	30	FUS-MS	410	630	<30	30	<30	90	90
Ga	ppm	1	FUS-MS	50	40	28	21	16	26	25
Ge	ppm	0.5	FUS-MS	5.3	4.4	2.4	1.9	1.6	2.1	2.1
As	ppm	5	FUS-MS	18	12	<5	<5	<5	<5	<5
Rb	ppm	1	FUS-MS	3	23	198	213	231	99	89
Sr	ppm	2	FUS-ICP	654	533	160	137	83	568	560
Y	ppm	0.5	FUS-MS	1010	883	47	18.9	16.2	28.6	24
Zr	ppm	1	FUS-ICP	31	41	74	147	130	79	75
Nb	ppm	0.2	FUS-MS	17.8	13.2	8.5	8.1	7.6	9.6	9.1
Mo	ppm	2	FUS-MS	98	24	27	25	25	19	13
Ag	ppm	0.5	FUS-MS	<0.5	<0.5	<0.5	1	0.8	<0.5	<0.5
In	ppm	0.1	FUS-MS	<0.1	<0.1	<0.1	<0.1	<0.1	<0.1	<0.1
Sn	ppm	1	FUS-MS	<1	<1	<1	2	2	1	1
Sb	ppm	0.2	FUS-MS	1.5	1.4	0.4	0.4	0.4	0.4	0.4
Cs	ppm	0.1	FUS-MS	<0.1	0.4	1.6	1.9	1.4	3.4	2.9
Ba	ppm	3	FUS-ICP	2007	1299	732	542	677	589	543
La	ppm	0.05	FUS-MS	1960	1280	14.3	33.7	30.2	48.5	45.1
Ce	ppm	0.05	FUS-MS	>3000	2160	31.6	82.3	57.3	99.1	89.8
Pr	ppm	0.01	FUS-MS	401	264	4.2	9.79	6.64	11.4	10.1
Nd	ppm	0.05	FUS-MS	1660	1140	17.9	36.5	24.8	42.9	38
Sm	ppm	0.01	FUS-MS	328	253	6.04	5.66	4.33	8.11	6.92
Eu	ppm	0.005	FUS-MS	31.1	21.1	0.65	0.711	0.589	2.46	2.37
Gd	ppm	0.01	FUS-MS	322	263	6.16	4.08	3.25	6.02	5.14
Tb	ppm	0.01	FUS-MS	45.5	38.9	1.27	0.58	0.51	0.9	0.78
Dy	ppm	0.01	FUS-MS	230	202	7.92	3.07	2.87	4.98	4.18
Ho	ppm	0.01	FUS-MS	40.3	38.2	1.7	0.61	0.57	0.99	0.85
Er	ppm	0.01	FUS-MS	111	97.6	5.36	1.82	1.65	2.82	2.48
Tm	ppm	0.005	FUS-MS	13.4	12.6	0.989	0.281	0.263	0.433	0.375
Yb	ppm	0.01	FUS-MS	73.5	69.2	6.77	1.81	1.73	2.86	2.4
Lu	ppm	0.002	FUS-MS	10.6	9.76	1.11	0.249	0.255	0.44	0.372
Hf	ppm	0.1	FUS-MS	2	2.5	2.5	3.8	3.6	2.2	1.9
Ta	ppm	0.01	FUS-MS	<0.01	<0.01	3.5	0.75	0.76	1.23	1.01
W	ppm	0.5	FUS-MS	418	94.8	5	4.4	3.7	2.3	2.1
Tl	ppm	0.05	FUS-MS	2.05	1.11	0.85	0.98	1.22	0.57	0.5
Pb	ppm	5	FUS-MS	110	90	51	27	25	20	18
Bi	ppm	0.1	FUS-MS	<0.1	<0.1	<0.1	<0.1	<0.1	<0.1	<0.1
Th	ppm	0.05	FUS-MS	5.94	6.61	49.6	32	30.8	15.3	12.3
U	ppm	0.01	FUS-MS	6.12	7.63	23.9	3.9	5.07	10.5	7.99

Analyte Symbol	Unit Symbol	Det. Limit	Analysis Method	14-YB-R04	14-YB-R06	14-YB-R09	14-YB-R12	14-YB-R15
SiO2	%	0.01	FUS-ICP	77.94	48.45	38.64	54.96	52.97
Al2O3	%	0.01	FUS-ICP	11.22	17.42	15.55	15.13	16.19
Fe2O3(T)	%	0.01	FUS-ICP	2.13	10.09	7.64	8.95	11.16
MnO	%	0.001	FUS-ICP	0.035	0.156	0.161	0.131	0.167
MgO	%	0.01	FUS-ICP	0.27	2.99	3.46	4.34	2.38
CaO	%	0.01	FUS-ICP	1.02	13.13	18.06	9.05	9.68
Na2O	%	0.01	FUS-ICP	4.55	0.83	1.71	2.73	0.96
K2O	%	0.01	FUS-ICP	0.97	0.42	0.82	1.15	1.61
TiO2	%	0.001	FUS-ICP	0.042	0.913	0.885	0.779	1.643
P205	%	0.01	FUS-ICP	0.02	0.29	0.29	0.08	0.28
LOI	%		FUS-ICP	1.19	5.71	12.7	2.2	3.06
Total	%	0.01	FUS-ICP	99.39	100.4	99.92	99.51	100.1
Sc	ppm	1	FUS-ICP	5	21	19	35	35
Be	ppm	1	FUS-ICP	4	6	5	2	2
V	ppm	5	FUS-ICP	35	148	142	333	355
Cr	ppm	20	FUS-MS	510	220	170	180	140
Co	ppm	1	FUS-MS	9	16	16	28	21
Ni	ppm	20	FUS-MS	<20	30	30	<20	<20
Cu	ppm	10	FUS-MS	20	20	<10	20	<10
Zn	ppm	30	FUS-MS	<30	80	70	80	110
Ga	ppm	1	FUS-MS	21	42	27	19	31
Ge	ppm	0.5	FUS-MS	1.8	8.4	6.1	3.2	4.6
As	ppm	5	FUS-MS	<5	<5	<5	<5	<5
Rb	ppm	1	FUS-MS	52	21	37	64	69
Sr	ppm	2	FUS-ICP	122	580	140	533	738
Y	ppm	0.5	FUS-MS	47.1	33.7	35.5	17.8	40.6
Zr	ppm	1	FUS-ICP	47	94	72	66	247
Nb	ppm	0.2	FUS-MS	57.7	10.6	5.9	2.6	11
Mo	ppm	2	FUS-MS	35	12	6	10	9
Ag	ppm	0.5	FUS-MS	<0.5	<0.5	<0.5	<0.5	1.6
In	ppm	0.1	FUS-MS	<0.1	<0.1	<0.1	<0.1	<0.1
Sn	ppm	1	FUS-MS	2	8	2	3	3
Sb	ppm	0.2	FUS-MS	0.5	0.5	0.5	0.4	0.5
Cs	ppm	0.1	FUS-MS	0.4	4.8	7.5	0.6	0.8
Ba	ppm	3	FUS-ICP	79	34	95	234	336
La	ppm	0.05	FUS-MS	3.87	46.8	35.8	17.1	43.2
Ce	ppm	0.05	FUS-MS	3.66	82.5	65.6	33.9	98.1
Pr	ppm	0.01	FUS-MS	0.5	9.59	7.78	4.04	12.2
Nd	ppm	0.05	FUS-MS	2.9	38.2	32.1	16.3	48.5
Sm	ppm	0.01	FUS-MS	2.3	7.83	6.61	3.72	10.5
Eu	ppm	0.005	FUS-MS	0.213	2.53	1.62	1.01	2.31
Gd	ppm	0.01	FUS-MS	4.41	6.26	6.26	3.08	8.14
Tb	ppm	0.01	FUS-MS	1.1	0.94	0.86	0.53	1.31
Dy	ppm	0.01	FUS-MS	7.89	5.04	4.69	3.13	7.34
Ho	ppm	0.01	FUS-MS	1.67	1.04	0.9	0.63	1.42
Er	ppm	0.01	FUS-MS	5	3.15	2.65	1.87	4.1
Tm	ppm	0.005	FUS-MS	0.823	0.521	0.39	0.311	0.623
Yb	ppm	0.01	FUS-MS	5.21	3.5	2.54	2.07	3.97
Lu	ppm	0.002	FUS-MS	0.774	0.552	0.403	0.306	0.59
Hf	ppm	0.1	FUS-MS	2.2	2.2	1.6	1.8	5.6
Ta	ppm	0.01	FUS-MS	3.27	1.03	0.53	0.88	1.02
W	ppm	0.5	FUS-MS	3.4	4.4	5.8	2.6	3.6
Tl	ppm	0.05	FUS-MS	0.31	0.17	0.21	0.38	0.33
Pb	ppm	5	FUS-MS	46	8	7	9	8
Bi	ppm	0.1	FUS-MS	<0.1	0.2	<0.1	<0.1	<0.1
Th	ppm	0.05	FUS-MS	11.2	4.9	2.31	14.6	7.27
U	ppm	0.01	FUS-MS	27.4	4.18	4.82	3.31	3.74

Analyte Symbol	Unit Symbol	Det. Limit	Analysis Method	14-YB-R100	14-YB-R101	14-YB-R102	14-YB-R200	14-YB-R201	14-YB-R202
SiO2	%	0.01	FUS-ICP	75.05	74.19	74.99	60.21	59.97	59.65
Al2O3	%	0.01	FUS-ICP	13.24	12.61	12.91	19.19	18.81	18.14
Fe2O3(T)	%	0.01	FUS-ICP	2.45	2.29	0.97	6.31	6.41	6.34
MnO	%	0.001	FUS-ICP	0.035	0.036	0.011	0.116	0.109	0.118
MgO	%	0.01	FUS-ICP	0.31	0.24	0.06	1.39	1.42	1.42
CaO	%	0.01	FUS-ICP	1.58	0.91	0.73	5.52	5.56	5.68
Na2O	%	0.01	FUS-ICP	3.43	2.58	3.14	4.89	4.61	4.37
K2O	%	0.01	FUS-ICP	3.55	5.12	5.76	1.14	1.25	1.71
TiO2	%	0.001	FUS-ICP	0.169	0.189	0.179	0.408	0.464	0.437
P205	%	0.01	FUS-ICP	0.04	0.03	0.02	0.21	0.21	0.23
LOI	%		FUS-ICP	1.08	0.76	0.39	1.51	1.2	1.56
Total	%	0.01	FUS-ICP	100.9	98.96	99.15	100.9	100	99.66
Sc	ppm	1	FUS-ICP	5	4	3	12	11	11
Be	ppm	1	FUS-ICP	4	2	1	4	2	2
V	ppm	5	FUS-ICP	34	30	25	47	55	57
Cr	ppm	20	FUS-MS	350	330	360	240	230	180
Co	ppm	1	FUS-MS	3	3	1	9	10	9
Ni	ppm	20	FUS-MS	< 20	< 20	< 20	< 20	< 20	< 20
Cu	ppm	10	FUS-MS	< 10	< 10	< 10	< 10	20	10
Zn	ppm	30	FUS-MS	40	30	< 30	80	90	90
Ga	ppm	1	FUS-MS	15	15	13	24	24	23
Ge	ppm	0.5	FUS-MS	1.3	1.3	< 0.5	1.4	1.3	1.3
As	ppm	5	FUS-MS	< 5	< 5	< 5	< 5	< 5	< 5
Rb	ppm	1	FUS-MS	155	198	262	62	72	102
Sr	ppm	2	FUS-ICP	226	158	109	570	571	553
Y	ppm	0.5	FUS-MS	34.1	21	21.1	57	24.6	30.4
Zr	ppm	1	FUS-ICP	130	127	134	88	91	89
Nb	ppm	0.2	FUS-MS	10.6	10.3	12	16.8	11.7	12.3
Mo	ppm	2	FUS-MS	25	24	70	17	16	13
Ag	ppm	0.5	FUS-MS	< 0.5	0.5	0.7	< 0.5	< 0.5	< 0.5
In	ppm	0.1	FUS-MS	< 0.1	< 0.1	< 0.1	< 0.1	< 0.1	< 0.1
Sn	ppm	1	FUS-MS	3	3	2	2	2	1
Sb	ppm	0.2	FUS-MS	0.4	0.4	0.3	0.4	0.4	0.4
Cs	ppm	0.1	FUS-MS	1.7	2.2	1.6	2.1	2.9	2.2
Ba	ppm	3	FUS-ICP	692	773	648	396	488	550
La	ppm	0.05	FUS-MS	35.4	29.6	28.2	45.1	38.8	40.3
Ce	ppm	0.05	FUS-MS	84.2	56.4	62.2	99.5	76.1	81.6
Pr	ppm	0.01	FUS-MS	9.87	6.29	6.96	12.2	8.64	9.56
Nd	ppm	0.05	FUS-MS	34.5	21.4	23.7	45.2	32.3	36.9
Sm	ppm	0.01	FUS-MS	6.64	3.65	4.56	10.3	5.99	6.49
Eu	ppm	0.005	FUS-MS	0.81	0.74	0.605	2.25	2.38	2.4
Gd	ppm	0.01	FUS-MS	5.61	3.08	3.72	9.23	4.7	5.6
Tb	ppm	0.01	FUS-MS	0.9	0.51	0.56	1.45	0.66	0.82
Dy	ppm	0.01	FUS-MS	5.66	3.25	3.21	8.6	3.85	4.86
Ho	ppm	0.01	FUS-MS	1.12	0.67	0.63	1.71	0.76	1
Er	ppm	0.01	FUS-MS	3.01	2.16	1.88	5.17	2.31	3
Tm	ppm	0.005	FUS-MS	0.405	0.358	0.299	0.745	0.343	0.455
Yb	ppm	0.01	FUS-MS	2.33	2.38	1.95	4.76	2.31	2.86
Lu	ppm	0.002	FUS-MS	0.345	0.35	0.274	0.701	0.337	0.439
Hf	ppm	0.1	FUS-MS	3.4	3.4	4.7	2.2	2.3	2.3
Ta	ppm	0.01	FUS-MS	2.49	1.73	0.77	2.15	0.82	0.94
W	ppm	0.5	FUS-MS	2.4	2.5	2.6	2.1	1.7	1.6
Tl	ppm	0.05	FUS-MS	0.74	0.93	1.23	0.37	0.41	0.5
Pb	ppm	5	FUS-MS	34	27	16	22	18	20
Bi	ppm	0.1	FUS-MS	< 0.1	< 0.1	< 0.1	0.2	0.1	0.2
Th	ppm	0.05	FUS-MS	32.2	11.8	28.4	12.7	12.1	10.5
U	ppm	0.01	FUS-MS	11.8	3.68	5.11	9.28	6.94	6.64

Appendix 3

Chemical results of water samples

14-YB-W01 – Water feeding the fracture
14-YB-W02 – Water separated from YBS by centrifugation
14-YB-W03 – Mine shaft at 1.3m depth
14-YB-W04 – Mine shaft at 0.5m depth
14-YB-W05 - Water shaft at 1.0m depth

	µg/L					
	Detection limit	**14-YB-W01**	**14-YB-W02**	**14-YB-W03**	**14-YB-W04**	**14-YB-W05**
Ph		~8	~8	7.02	7.06	8.23
T C°				7.4	7.4	8.2
Cond. (mS/m)				1932	1932	446.3
Redox				69.9	51.7	123.5
Al	**0,18**	0,5688	4,445	141	147,4	11,5
As	**0,47**	1,602	1,617	1,642	1,975	1,301
B_	**2,76**	45,01	529,9	49,76	36,33	50,19
Ba	**0,18**	3,226	69,71	13,27	16,17	7,281
Ca	**0,08**	46920	67900	56330	44190	57900
Cd	**0,02**	<DL	0,0624	0,1409	0,1563	0,0457
Ce	**1,92**	<DL	<DL	<DL	<DL	<DL
Co	**0,06**	0,2165	0,3071	0,6686	0,9445	0,2116
Cr	**0,18**	<DL	0,4597	<DL	<DL	0,473
Cu	**0,09**	1,569	14,56	10,74	12,36	3,982
Dy	**0,22**	0,9297	2,696	5,216	4,015	2,072
Er	**0,83**	<DL	<DL	2,648	1,324	<DL
Eu	**0,11**	<DL	<DL	<DL	<DL	<DL
Fe	**0,5**	<DL	2,241	229,6	243,5	8,641
Gd	**0,66**	<DL	<DL	<DL	<DL	<DL
Ho	**0,35**	<DL	<DL	<DL	<DL	<DL
K_	**1,09**	1567	3203	3693	3141	5239
La	**0,29**	<DL	<DL	0,6946	<DL	<DL
Li	**0,06**	3,592	17,99	3,1	2,437	3,81
Lu	**0,03**	<DL	<DL	0,6811	0,378	<DL
Lu	**0,22**	<DL	<DL	<DL	<DL	<DL
Mg	**0,07**	6582	7221	5798	4107	9593
Mn	**0,35**	147	<DL	23,61	19,35	<DL
Mo	**2,41**	1,059	2,222	5,737	3,845	1,622
Na	**0,48**	24760	33740	39940	30210	30260
Nd	**1,39**	4,137	8,707	7,243	5,234	0,296
Ni	**0,14**	<DL	<DL	1,882	2,064	<DL
P_	**20**	<DL	22,59	21,13	<DL	<DL
Pb	**1,12**	<DL	<DL	1,463	1,92	<DL
Pr	**1,12**	<DL	<DL	<DL	<DL	<DL
Rb	**9,8**	<DL	<DL	<DL	<DL	<DL
S_	**13,2**	8033	12400	20600	15860	11730
Sc	**0,24**	<DL	<DL	0,8546	0,9668	<DL
Se	**14,8**	<DL	<DL	<DL	<DL	<DL
Si	**4,16**	6898	10300	6328	5715	6211
Sm	**1,17**	7,654	7,961	9,624	10,58	11,14
Sr	**0,07**	208,6	544,4	193,3	150,2	162,8
Tb	**1,4**	<DL	<DL	<DL	<DL	1,899
Ti	**1,07**	5,668	8	8,321	8,926	7,097
Tm	**0,18**	<DL	<DL	<DL	<DL	<DL
U_	**2,49**	<DL	<DL	<DL	<DL	<DL
V_	**2,29**	<DL	<DL	<DL	<DL	<DL
Y_	**0,09**	5,912	4,377	46,18	28,74	<DL
Yb	**0,04**	0,55	0,71	4,67	2,87	0,2
Zn	**0,86**	<DL	2,238	314,3	500	50,64
Zr	**1,7**	<DL	<DL	<DL	<DL	<DL

Appendix 4

Lipid biomarkers and associated chemical compounds

Lipid biomarkers

Biomarkers are the fingerprints of nature. A biomarker has to be unique to its original material and resistant to degradation (Gaines et al., 2009). Because of their relatively high resistance to decomposition over long time compared to other major components of life, lipids are suitable for use as biomarkers (Simoneit, 2002). Lipids are not defined by their structure but rather their characteristics of being water insoluble organic substances (White, 2013). They are essential components of cell membranes and include compounds such as fats, oils, waxes and steroids (White, 1998). The range and variety of lipid functions is wide and include involvement in photosynthesis and digestion to protection of the cell (White, 2013).

Hydrocarbons

Hydrocarbons consist of only carbon and hydrogen atoms and constitute the basic structure in organic chemistry to which functional groups can be attached to form other compounds (White, 2013). The source of oil is not only the degraded matter from what was once various plants and algae, but also the remains of the bacteria living off these buried remains (Gaines el al., 2009). Different hydrocarbon structures include the alkanes (paraffins) which are straight chains of single bonded carbon atoms, the alkenes (olefins) which contain one or more double bonds and are liquids (Hunt, 1995), the cycloalkanes and cycloarenes (aromatics*)* which contain one or more benzene rings. Long-chain saturated hydrocarbons are solids (waxes) while the short-chain are liquids (Hunt, 1995).

Fatty acids and alcohols

Fats and oils are important for energy storage and are usually a combination of fatty acids and alcohols. *Fatty acids* are alkanes, commonly even numbered in the range C_{12} to C_{36}, with a carboxyl group (-COOH) at the end while *alcohols* instead have a hydroxyl (-OH) group attached to the alkane. Carboxyl groups are highly acidic which means that these compounds readily give up its hydrogen atoms (White, 2013). If also one or more hydrogen atoms are substituted by a hydroxyl group (-OH) it becomes a hydroxy acid which is very reactive (White, 2013). Fatty acids are divided into common-, iso- and anteiso fatty acids (Gaines, Eglinton and Rullkötter, 2009). Common ones are straight chains while the iso- and anteiso are branched chains. Anteiso means bacteria (Source). Long chained alcohols, i.e. fatty alcohols, of high molecular weight commonly occur as even numbered carbon chains just like the fatty acids (White, 1998). By combining the straight chained fatty acids and the fatty alcohols which both typically range from C_{24} to C_{28}, wax esters are formed.

Terpenoids and Hopanoids

One major biosynthetic pathway involves polymerization of the isoprene unit, C_5, forming branched and cyclic isoprenoids in multiples of five carbon atoms, i.e. C5, C10 and so forth (Hunt, 1995). These structures of combined isoprene units are called *terpenoids* and occur as both saturated and unsaturated compounds (White, 2013). Squalene is a triterpenoid ($C_{30}H_{50}$) found in both plants and animals and the precursor to a class of compounds called steroids (White,2013). *Hopanoids* are C_{27} to C_{35} pentacyclic triterpenoids which occur in cell membranes of prokaryotic organisms, resins and in a few higher plants such as ferns, lichens (Hunt, 1995), mosses and fungi (see complete list of sources in Peter et al., 2005). However, the C_{31} to C_{35} extended side chain hopanoids are a distinct biomarker for bacteria (Peters et al., 2005). The presence of hopanoids in microorganisms are limited to eubacteria and often found in methanotrophs, cyanobacteria and organisms belonging to the α-proteobacteria such as the nitrogen-fixing eubacteria (see complete list of sources in Peters et al., 2005). Hopanes are also frequent in bacterial species living in stressful environments where they are thought to provide rigidity and adjustable permeability to the cell membrane (see complete list of sources in Peters el al., 2005). The hopanes have not yet been detected in archaea nor in animals (Peters et al.,

2005). They are thought to be the bacterial equivalent to sterols in eukaryotes (Gaines et al., 2009). The molecular structure of the hopanoids is very robust and therefore relatively well preserved in sediments. Thus, their use as biomarkers for certain species is therefore valuable.

Appendix 5

Outgrowths in previously water-filled tunnel

Field observations during the work with this project revealed nodular outgrowths or flattened crusts attached to the tunnel wall or sitting in rock crevices. These outgrowths are approximately 2-10 mm in diameter and located in a previously water-filled tunnel next to the mine shaft in contrast to the YBS which is located in a dry tunnel further away from the shaft which has never been water-filled (Fig.3). Initial SEM-analyses revealed a bulk material rather different from the YBS. The main constituent of these outgrowths is carbon and to a minor extent silica (Si), oxygen and sulphur. However, the silver-rich or possibly silver-coated microspheres which exist as separate components in the YBS (Fig.X) are also present in these outgrowths which provides a possible link between the two materials. For future research it would be interesting to see if there is any way of determining if these microspheres (20-40 um) are anthropogenic or some natural precipitates from groundwater. Moreover, the SEM-analyses revealed a number of seemingly organic microstructures which are described in the images below.

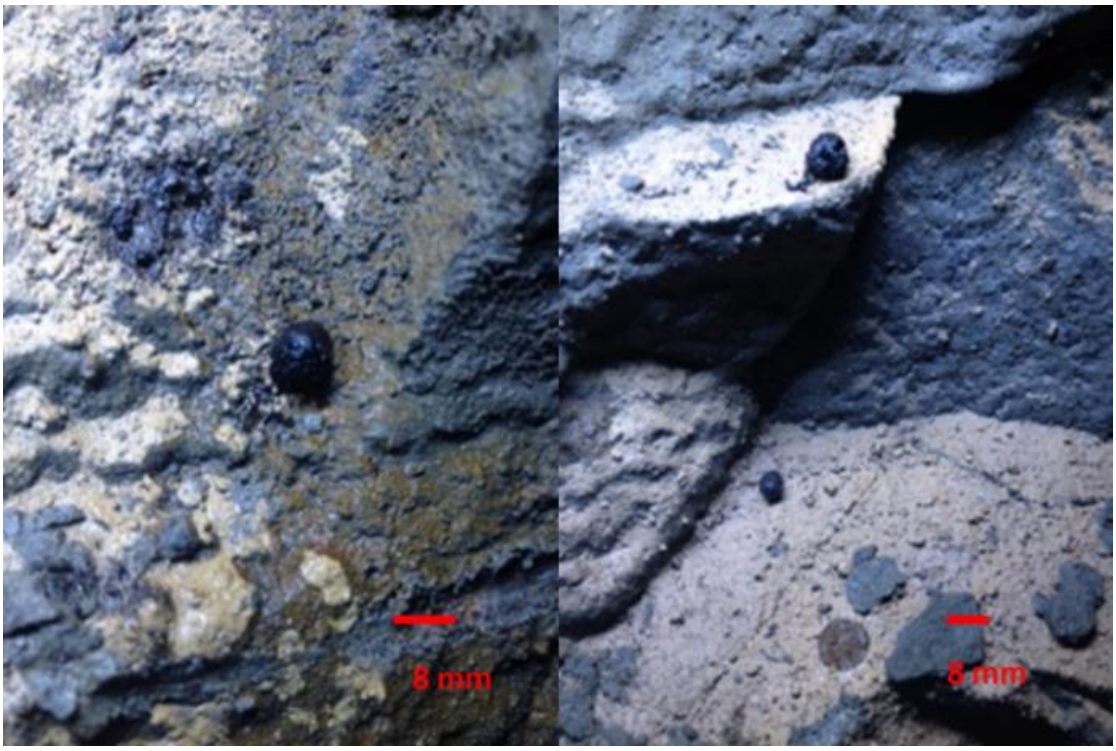

Fig 5:1: Nodular outgrowths sitting on the silty-clayey rock wall in the previously water-filled tunnel adjacent to the mine shaft (see Fig.X for location).

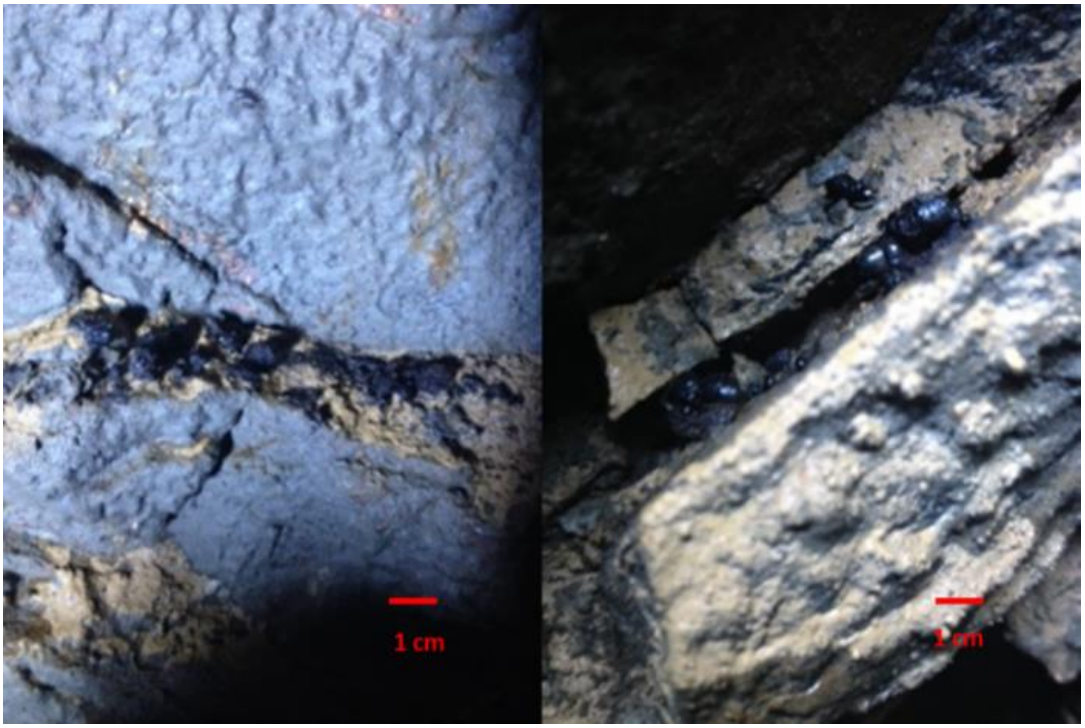

Fig 5:2: Cluster of nodular outgrowhts and flattened crusts sitting in silty-clayey rock shelves and crevices.

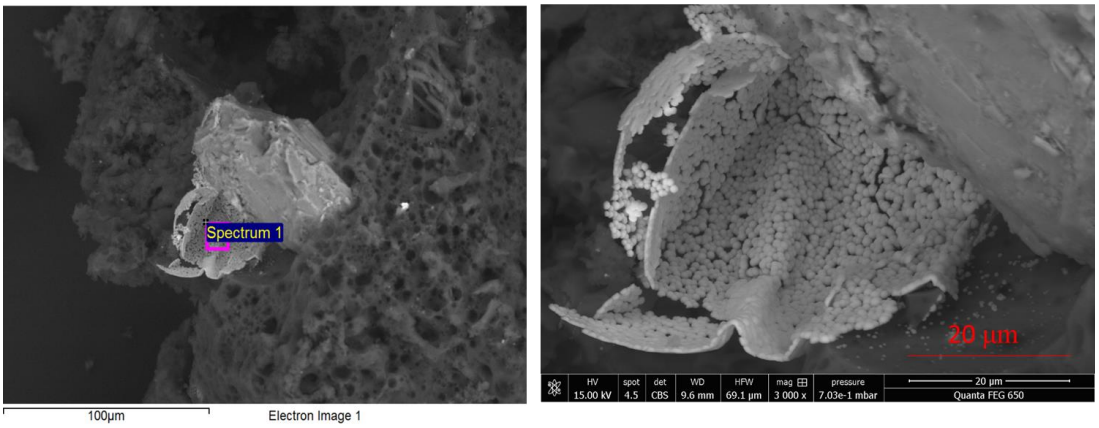

Fig.5:3: This crust-like structure mainly consist of carbon and zink and minor constituents are iron, calcium and silica. Oxygen concentrations are low. The mineral to which the crust-like structure is attached to is mainly composed of carbon and iron with minor concentrations of zink, calcium, silica, magnesium, aluminum and sulphur. Oxygen concentrations appear to be slightly higher compared to the crust-like structure. The darker shaded material is the bulk material of the outgrowths and consist mainly of carbon and minor amounts of oxygen and silica.

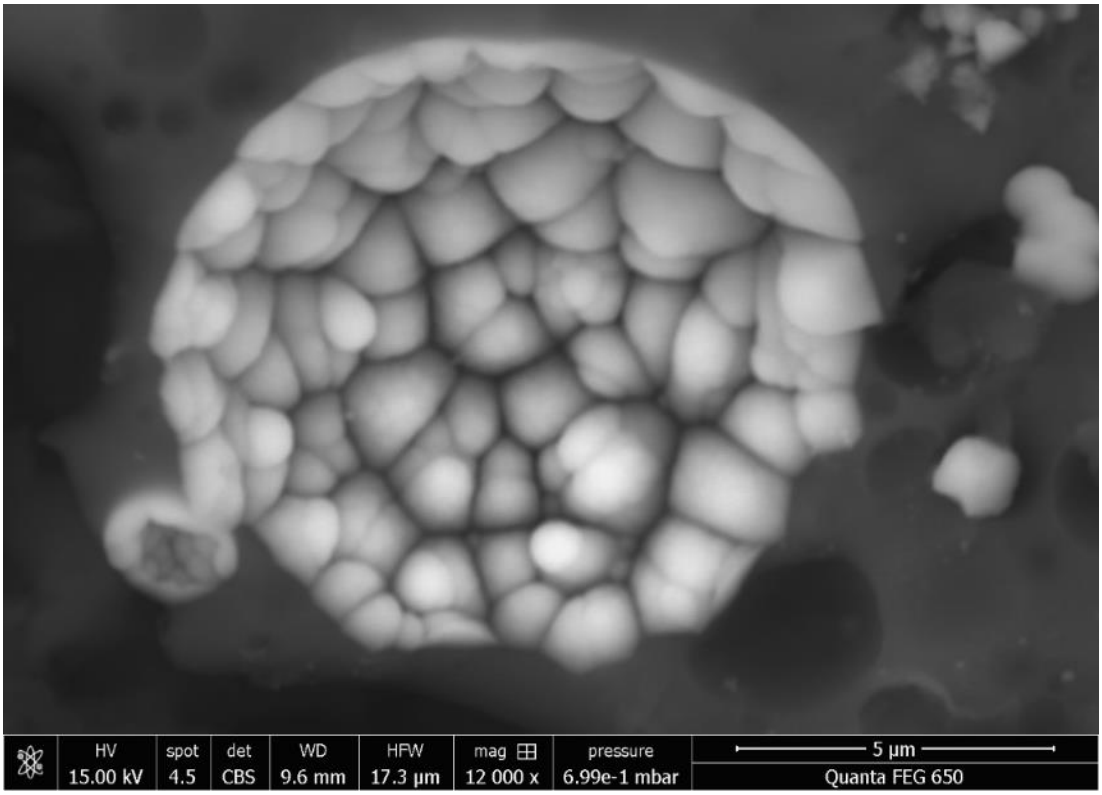

Fig.5:4: This fascinating microstructure is imbedded in the carbon bulk material and mainly consist of carbon and zink while sulphur and oxygen are present in lower concentrations. Traces of silica are also noted.

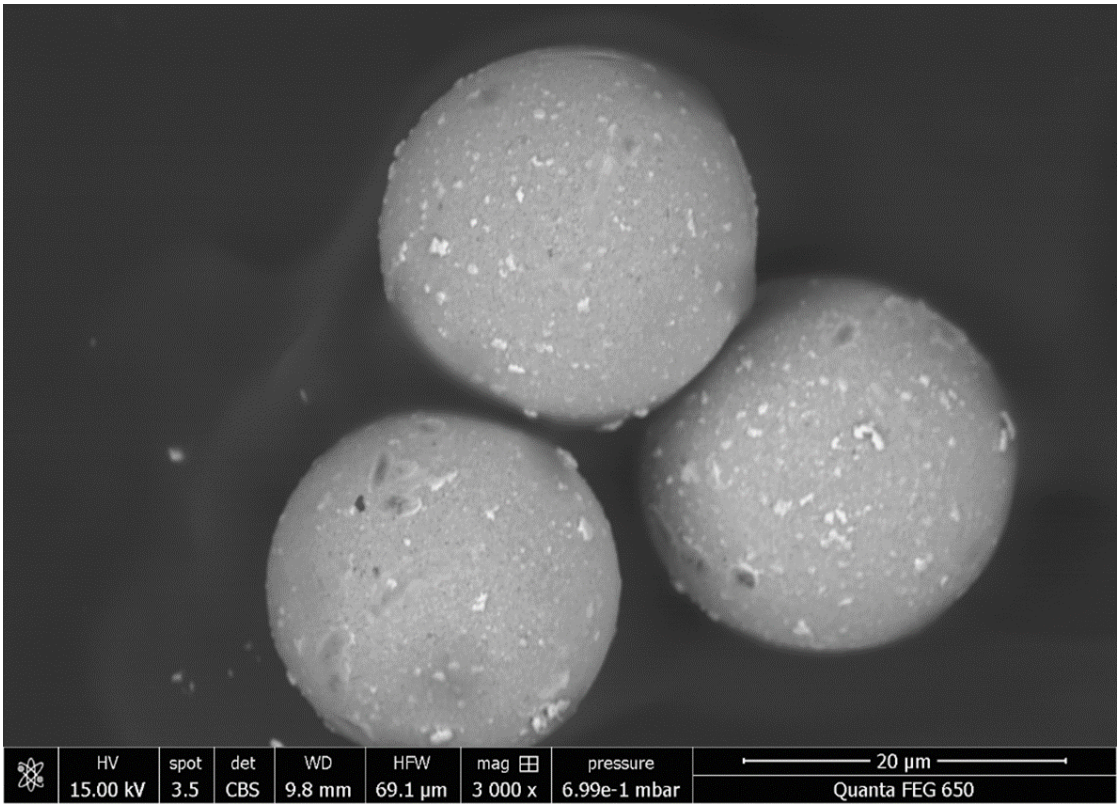

Fig 5:5: Silver-rich or possibly silver-coated microspheres which exist as separate components in these outgrowths. The fact that these microspheres are the same spheres as observed in the YBS (Fig.X) provides a possible link between the two materials.

Appendix 5

Permission granted by the County Administrative Board of Stockholm (Länsstyrelsen) – Ytterby natural monument

The grading facility at the Ytterby pegmatite quarry (Lööf, E., (1981)

Länsstyrelsen
Stockholm

Datum
2014-08-05

Beteckning
5213-14556-2014
0187-04-002

Enheten för naturvård
Elin Deremar

Delgivningskvitto

Susanne Sjöberg
Kullasundsvägen 21
185 37 Vaxholm

Provtagning inom naturminnet Ytterby varphögar i Vaxholms kommun

(2 bilagor)

Beslut

Länsstyrelsen medger med stöd av 7 kap 7 § samt 7 kap 10 § miljöbalken (1998:808) Susanne Sjöberg dispens från föreskrifterna för insamling av bergprover från naturminnet Ytterby varphögar, fastigheten Ytterby 4:610 i Vaxholms kommun.

Som villkor för beslutet gäller att:

1. Maximalt får 10 prover tas.
2. Dispensen gäller under 2014.
3. Vid provtagning ska detta beslut samt legitimation medföras.
4. Resultatet av undersökningarna ska delges Länsstyrelsen.

Detta beslut kan överklagas hos mark- och miljödomstolen vid Nacka tingsrätt, se bilaga 2.

Bakgrund

Susanne Sjöberg har ansökt om dispens från föreskrifterna för insamling av bergprover från naturminnet Ytterby varphögar i Vaxholms kommun, se bilaga 1. Provtagningen ska ske i samband med sökandens magisteruppsats vid Institutionen för geologiska vetenskaper, Stockholms universitet. Syftet är att undersöka och karaktärisera en svart sörja som under en tidigare studie upptäckts läcka fram ur bergsprickor inne i gruvtunnlarna. Sörjan är bl.a. anrikad på sällsynta jordartsmetaller i kombination med organiskt material.

Mellan 5-10 prover tas nära bergets yta genom att knacka loss små bitar (ca 3-4×3-4 cm) av berget, samt eventuellt från varphögen. Proverna analyseras som tunnslip i mikroskop samt genom en elektronsondalalys (EMPA) för att bestämma ämnessammansättning i olika delar av enskilda mineral.

Ytterby gruva på Resarö är internationellt känd eftersom flera nya grundämnen har upptäckts i mineral från gruvan. Gruvdriften lades ned år 1933. Inom gruvområdet ligger en större och en mindre varphög som bl.a. innehåller intressanta mineraler.

Datum
2014-08-05

Beteckning
5213-14556-2014
0187-04-002

Området är skyddat som naturminne genom Länsstyrelsens beslut 1976-09-27 (diarienummer 11.122-236-76). Syftet med skyddet är att bevara varphögarna ur vetenskaplig och kulturell synpunkt. För att trygga ändamålet med naturminnet är det bl.a. förbjudet för markägare, andra sakägare samt allmänheten att bortföra bergart eller mineral.

Området är av riksintresse för naturvården och omfattas av 100 meter strandskydd.

Länsstyrelsens bedömning

Länsstyrelsen bedömer att provtagning i vetenskapligt forskningssyfte är ett särskilt skäl, i miljöbalkens mening, och att åtgärden inte strider mot syftet med naturminnet. Länsstyrelsen bedömer att intrånget i naturminnet är begränsat och anser därmed att dispens från föreskrifterna för naturminnet kan medges.

Länsstyrelsen bedömer att åtgärden inte kräver dispens från strandskydds-bestämmelserna, eftersom åtgärden inte påverkar allmänhetens tillgänglighet och heller inte bedöms påverka växt- och djurlivet i området.

I handläggningen av detta ärende har deltagit tf enhetschef Britt Forsén, beslutande samt miljöhandläggare Elin Deremar, föredragande.

Britt Forsén

Elin Deremar

Bilagor:
1. Karta
2. Hur man överklagar

Sändlista:
Vaxholm stad, kansliet@vaxholm.se
Naturvårdsverket, registrator@naturvardsverket.se
Havs- och vattenmyndigheten, havochvatten@havochvatten.se
Riksantikvarieämbetet, registrator@raa.se
akten

Bilaga 1
5213-14556-2014

Länsstyrelserna
IT-enheten

Naturminne Ytterby varphögar, Vaxholms kommun

Skala 1:4500